GEOHAZARD POTENTIAL OF RAINFALL INDUCED SLOPE FAILURE

ON EXPANSIVE CLAY

by

Jubair Hossain

Presented to the Faculty of Graduate School of

The University of Texas at Arlington in Partial Fulfillment

of the Requirements

for the Degree of

DOCTOR OF PHILOSOPHY

THE UNIVERSITY OF TEXAS AT ARLINGTON

November 2012

ACKNOWLEDGMENTS

ABSTRACT

GEO-HAZARD POTENTIAL OF RAINFALL INDUCED SLOPE FAILURE

ON EXPANSIVE CLAY

Jubair Hossain, PhD

The University of Texas at Arlington, 2012

Supervising Professor: MD. Sahadat Hossain

Each year, rain induced slope failures cause significant damages in highway infrastructures and environments, as well as tragic losses of human lives around the world. Rainfall-induced slope failure is a common problem in areas with slope constructed on high plasticity clays. These post failure costs can be significantly reduced if precautions are taken ahead of time. Development of an early hazard warning system based on weather forecast data can help identify potential slopes susceptible to failure due to rainfall. But development of such system will require a better understanding of the in situ behavior of soil due to rainwater infiltration as well as changes in shear strength characteristics of the soil.

Slope stability studies in different parts of the world have indicated that infiltration of rain water into the soil has an adverse effect on the stability of earth slopes. During the

infiltration process, the matric suction in the unsaturated soil slope decreases as the saturation increases with time, thereby reducing the shear strength of the soil. Therefore, it is important to identify the depth of moisture variation zone (i.e., active zone), along with field infiltration behavior, to accurately predict the response and stability of earth slopes constructed on expansive clay when exposed to a rainfall event.

The objectives of this research are to determine, 1) the active zone of expansive clayey soil, 2) changes in moisture content and matric suction of soil slopes constructed on expansive clay due to infiltration of rainwater, 3) effects of rainwater infiltration on soil shear strength, 4) modeling and determining geohazard potential of soil slopes due to rainwater infiltration and finally 5) recommendation for future study. A field instrumentation program was undertaken to determine the active zone and study the infiltration behavior of embankment slope constructed on high plasticity expansive clay. An experimental program was developed to study the soil water retention characteristics and associated shear strength for different suction values. The results from laboratory testing and field instrumentation was combined with numerical modeling to study the effect of rainfall infiltration and associated geohazard potential of slope constructed on expansive clay.

Results obtained from the field instrumentation, indicates that the variation in the moisture content and matric suction were different at different depth. The maximum variation often occurred near the ground surface (i.e. at 1.2 m depth) and the magnitude of variation decreased with increase in depth. Presence of cracks at the crest also accelerated the ingress of water into the slope during rainfall events. The depth of active zone up to which moisture variation occurs was observed to be 3.6 m. Therefore, reduction in soil shear strength due to

cyclic variation of weather condition is limited to a depth of 3.6 m which also matches close to the observed failure depth (3.04 m) on slopes constructed on high PI clay.

Laboratory results on soil water characteristic curve (SWCC) showed that, SWCC of expansive clay yields higher air entry value and lower desaturation rate when compared with no volume change assumption during SWCC determination. Specimens compacted wet of optimum do not strongly depend on the applied stress history due to identical micro-structure formation. On the other hand, SWCC of expansive clay, compacted dry of optimum water content shows a shift to the right with high net normal stresses which indicates increase in air entry value.

Results obtained from suction controlled ring shear tests indicate that both net normal stress and matric suction has significant influence on peak and residual strength of expansive clay. Both peak and residual strength increases with increase in net normal stress and matric suction. Results obtained from direct shear tests on saturated samples indicated that, shear strength of high PI expansive clay decreases when subjected to cycles of wetting and drying. The value of cohesion completely disappears due to wet dry cycles leading to shear strength condition at normally consolidated state.

Based on the numerical modeling using PLAXIS, low intensity long duration rainfall was found to be most critical for expansive clay under current study which is consistent with the results previously reported for soils with low permeability. Effect of rainfall return period was found to be insignificant for the current study. Stability analyses performed for different rainfall event showed that, use of fully softened strength for active zone can reduce the factor of safety as low as twice the value as compared to the as compacted strength.

TABLE OF CONTENTS

LIST OF ILLUSTRATIONS

LIST OF TABLES

CHAPTER 1

INTRODUCTION

1.1 Introduction

Each year, rain induced slope failures cause significant damages in highway infrastructures and environments, as well as tragic losses of human lives around the world. Rainfall-induced slope failure is a common problem in areas with slope constructed on high plasticity clays. Such slopes are stable within a certain range of water saturation and when the saturation exceeds a critical value, the slope becomes unstable leading to failure. Most of these failures involve shallow surface slides with depth less than 10 ft (Wright, 2005) and require periodic maintenance which can become costly for state and Federal Agencies. Such a slope failure along I 30 WB constructed on high PI clay is presented in Figure 1.1.

Figure 1.1 Slope failure along I 30 West Bound

These post failure costs can be significantly reduced if precautions are taken ahead of time. Development of an early hazard warning system based on weather forecast data can help identify potential slopes susceptible to failure due to rainfall. But development of such system will require a better understanding of the in situ behavior of soil due to rainwater infiltration as well as changes in shear strength characteristics of the soil. From this information, stability analyses of slope can be performed for a certain rainfall forecast to determine the geo-hazard potential of that slope.

Field scale investigations to study the effect of rainfall infiltration on stability of slope have been performed by Lim et al. (1996), Li et al. (2005), Ng et al. (2008) and Kim et al. (2010). Most of these earth fills or cut embankments were constructed on unsaturated soil. The magnitude of negative pore water pressure or matric suction plays an important contribution to additional shear strength of soil (Fredlund and Rahardjo 1993, Melinda et al. 2004). During rainfall, the matric suction of the soil reduces thereby reducing the shear strength of soil due to water infiltration (Gan et al. 1988, Fredelund et al. 1996, Jotisankasa et al. 2010). The extent of reduction in shear strength depends on the water infiltration, which in turn depends on rainfall duration and intensity. The reduction in shear strength may also cause instability of slopes. However, most of these field scale studies have been carried out on residual soils of nonexpansive behavior. An expansive soil with high plasticity indices often features significant amount of cracks and fissures at the upper soil layer due to wetting and drying. This crack rich expansive soil can often results in a complex process of rainfall infiltration and volume change.

Another important consideration for slopes constructed on high plasticity clay is the softening behavior for top soil due to wet-dry cycles. Skempton (1977) reported that over time

the strength of slopes in the highly plastic London Clay decreases, eventually reaching what Skempton termed a "fully-softened" strength. Rogers and Wright (1986) investigated the long term strength of highly plastic clay involved in the failure of a highway embankment in Houston, Texas. The authors concluded that during failure the strength of the high plasticity clay reached at fully-softened state due to repeated cycles of wetting and drying. Kayyal and Wright (1991) determined the strength of highly plastic Red Beaumont clay and Paris clay after repeated cycles of wetting and drying and observed a significant reduction in strength. Skempton (1977) indicated that fully-softened strength is comparable to the shear strength of the soil in a normally consolidated state. Stark and Duncan (1991) investigated the cause of a slide at the upstream slope of California's San Louis Dam which is supported by stiff and desiccated clay. They showed that shear strength of the clay decreases rapidly to the fully-softened strength when the clay is soaked. The top few feet of slope which is susceptible to moisture variation shows reduction in shear strength after a long period of its construction due to climatic changes. Zornberg et al. (2007) reported the depth of moisture variation for slopes constructed on high PI clay is 1.5 m based on the numerical simulation with 30 year weather data for Austin and Houston. Determination of this zone of moisture variation or active zone is also important to clearly identify up to which depth strength degradation occurs due to softening to accurately predict the geohazard potential of rainfall induced slope failure.

1.2 Problem Statement

Research in the area of slope stability has indicated that most slope failures are caused by the infiltration of rainwater into a slope. It would be advantageous to be able to accurately

predict change in soil moisture as well as matric suction profile due to rainfall infiltration into a slope and the corresponding change in the factor of safety.

Based on the existing literature, the changes in moisture content as well as soil suction due to rainfall infiltration in soil slopes constructed on expansive clay are not well documented. Most of these field scale studies have been carried out on residual soils of nonexpansive behavior to understand the field infiltration behavior. An expansive soil with high plasticity indices often features significant amount of cracks and fissures at the upper soil layer due to wetting and drying. This crack rich expansive soil can often results in a complex process of rainfall infiltration and volume change. Therefore, it is important to understand the field infiltration behavior of a slope constructed on high PI expansive clay through field instrumentation. Moreover, from previous study, it was identified that softening of surficial clay due to wet-dry cycle has a significant effect on the triggering of slope failure due to rainfall. However, the depth of this moisture variation zone or active zone is not well established. Zornberg et al. (2007) reported the depth of moisture fluctuation on a slope constructed on high plasticity clay ranges from 1 to 1.5 meters which was predicted from finite element modeling. However, no field study was conducted to determine the active zone.

Embankment slope involve the use of unsaturated soil as a construction material or constructed on unsaturated ground. However, soil is always assumed to be saturated and soil strength is determined accordingly. The shear strength of unsaturated soil has gained increasing attention by several researchers (Gan et al. 1988, Fredelund et al. 1996, Jotisankasa et al. 2010) over the last three decades. The shear strength of unsaturated soil is greatly enhanced by matric suction. During rainfall, the matric suction decreases due to water infiltration and thereby

4

reducing the shear strength of soil. In order to accurately predict the geohazard potential of slope failure for a particular rainfall event, it is also necessary to determine the shear strength characteristics of unsaturated expansive clay. To date, however, there is hardly a few experimental evidence on change in shear strength of unsaturated expansive clay due to change in moisture content or matric suction.

Such slope failures are addressed at the post failure stage when significant damage has already took place. These slope failures are often triggered during heavy rainfall. Therefore, in order to mitigate slope failure disasters, it is important to evaluate the potential of slope failure events. A complete system needs to be developed which will take into consideration the changes in soil moisture content as well as pore water pressure due to rainfall infiltration, changes in shear strength with changes in moisture content and associated changes in stability of the slope.

1.3 Research Objectives

The objectives of this research are to determine, 1) the active zone of expansive clayey soil, 2) changes in moisture content and matric suction of soil slopes constructed on expansive clay due to infiltration of rainwater, 3) effects of rainwater infiltration on soil shear strength, 4) modeling and determining geohazard potential of soil slopes due to rainwater infiltration and finally 5) recommendation for future study. A field instrumentation program was undertaken to determine the active zone and study the infiltration behavior of embankment slope constructed on high plasticity expansive clay. An experimental program was developed to study the soil water retention characteristics and associated shear strength for different suction values. The results from laboratory testing and field instrumentation was combined with numerical modeling

to study the effect of rainfall infiltration and associated geohazard potential of slope constructed on expansive clay. The specific tasks to achieve these objectives are:

1. Site investigation and sample collection from the highway embankment slope along US Hwy 287 S.

2. Determination of basic soil characteristics.

3. Determination of active zone and study the field infiltration behavior through extensive field instrumentation.

4. Development of an experimental program to,

a. Study the effect of net normal stress on soil water characteristic curve (SWCC) of expansive clay at different initial water content. This study also focuses on the effect of volume change behavior of expansive clay on SWCC.

b. Study the unsaturated shear strength of expansive clay using suction controlled ring shear testing.

c. Study the softening behavior of high plasticity expansive clay due to wetting and drying using direct shear testing.

5. Study the infiltration behavior through transient seepage analyses for different rainfall condition and making comparison with field infiltration results.

6. Finally, determining the geo-hazard potential of slope failure for different rainfall condition through slope stability analyses using finite element software PLAXIS.

1.4 Thesis Organization

The thesis is divided into six chapters that can be summarized as follows:

Chapter 1 provides an introduction and presents the problem statement and objective of the research.

Chapter 2 presents the fundamental concepts of soil water characteristics (SWCC) and permeability of unsaturated soil and also a brief discussion on the previous work in measuring SWCC and permeability functions. This chapter also includes a review of the field instrumentation results from previous studies to study the infiltration process into the slope. In addition, a brief description on the shear strength of unsaturated soil and different methods used to measure the shear strength of unsaturated soil is presented. Finally, this chapter also includes a brief description of the previous work done to study the effect of softening behavior of high plasticity clay.

Chapter 3 describes the details of field instrumentation program and experimental procedures followed to determine the effect of stress state, initial water content and volume change behavior on SWCC as well as permeability of unsaturated expansive clay. This chapter also includes the experimental procedures undertaken to determine the shear strength characteristics of unsaturated expansive clay and softening behavior due to wetting and drying.

Chapter 4 presents all the field instrumentation and experimental results, discussion on the results and comparison with existing literature.

Chapter 5 presents the modeling of infiltration behavior into the slope and also stability analyses due to different rainfall condition to identify the effect of different rainfall intensity and duration.

Chapter 6 summarizes the main conclusions from the current research and provides some recommendation for future work.

CHAPTER 2

LITERATURE REVIEW

2.1 Introduction

Slope failures in unsaturated soils constructed on expansive clay are often triggered by rainfall infiltration during the wet period. Infiltration of rain water into a soil slope causes instability by changing the soil moisture profile and associated change in matric suction. Unsaturated expansive clay experiences high matric suction during dry periods, which contributes to increase in shear strength of soil. During prolonged wet periods, the moisture content of the soil increases which in turn decrease the matric suction. The additional shear strength contributed by the matric suction decreases with increase in moisture content and causes slope to fail. Moreover, slopes constructed on high plasticity expansive clay are susceptible to strength degradation due to cycles of wetting and drying which is limited to top few meters of the slope. Therefore, it is important to identify this moisture variation zone or active zone, along with the field infiltration behavior and shear strength changes to accurately predict the response and stability of earth slopes constructed on expansive clay when exposed to a rainfall event. Over the last two decades, significant efforts have been made in understanding the field infiltration behavior and shear strength characteristics of unsaturated soil which will be discussed in this chapter.

2.2 Fundamental Concept

The mechanical behavior of a soil which includes volume change and shear strength behavior can be described in terms of the state of stress in the soil. The state of stress in a soil can be viewed as a certain combination of stress variables which can be defined as stress state variable. The stress state variable for a saturated soil has been called the effective stress $(\sigma - u_w)$ and is expressed as:

$$\sigma' = \sigma - u_w \qquad (2.1)$$

where,

$\sigma' =$ effective normal stress

$\sigma =$ total normal stress

$u_w =$ pore-water pressure

The effective stress concept is the fundamental basis for saturated soil mechanics and all the mechanical behavior such as volume change and shear strength is controlled by the change in effective stress. In saturated soil, the pore water pressure is positive and the changes in σ and u_w are equivalent. However, unlike saturated soil, unsaturated soil is commonly viewed as three phase system namely as solid, water and air. More recently, the air-water interface or the contractile skin has been introduced as a fourth and independent phase (Fredlund and Morgenstern, 1977). The contractile skin possesses a property called surface tension resulting from inter-molecular forces which are different from those that act on molecules in the interior of

water. The contractile skin is subjected to an air pressure, u_a, which is greater than water pressure, u_w in an unsaturated soil which is presented in Figure 2.1. The pressure difference
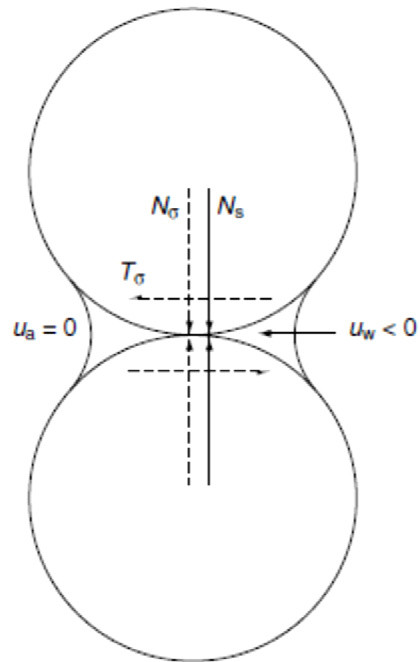
Figure 2.1 Influence of external stress and suction on inter-particle forces (Ng and Menzies, 2007)

gives rise to a stress component which is termed as matric suction ($u_a - u_w$). According to Burland and Ridley (1982), the changes in external stress, σ is not equivalent to changes in suction and the two stress systems give rise to entirely separate mechanical effects because of the fundamental differences in the way they are transmitted through the solid phase of the soil. The external stress which is applied to the boundary of a soil element produce both normal and tangential forces at particle contacts. On the other hand, the capillary effect arising from suction produces only an increase in the normal forces at particle contacts and provides an additional bonding force at the particle contacts.

However, all the proposed stress state variables for characterization of the mechanical behavior of unsaturated soil was primarily focused on single valued effective stress or one stress state variable for unsaturated soil. The most common single valued relationship was proposed by Bishop (1959):

$$\sigma^{'} = (\sigma - u_a) + \chi \, (u_a - u_w) \qquad (2.2)$$

Bishops equation relates net normal stress to matric suction through the incorporation of a soil property, χ which is related to water degree of saturation and ranging from 0 to 1. But the validity of the parameter χ has been questioned. Morgenstern (1979) reported that, the parameter χ, when determined for volume change behavior was found to differ when determined for shear strength. Jennings and Burland (1962) also suggested that Bishop's equation did not provide an adequate relationship between volume change and effective stress for most soils. However, considerable effort was made to establish a single valued effective stress variable for unsaturated soil by several researchers (Aitchison, 1961; Richards, 1966). In 1977, Fredlund and Morgenstern suggested the use of any two of three possible stress variables, $(\sigma - u_a)$, $(\sigma - u_w)$ and $(u_a - u_w)$ to describe the mechanical behavior of unsaturated soils. To date, the most common practice is to use net stress $(\sigma - u_a)$ and matric suction $(u_a - u_w)$ as the two independent stress variables.

In conventional slope stability analysis using limit equilibrium method of slices, shear strength contribution from matric suction is usually ignored which is reasonable if the slip surface is located below the ground water table. However, for situations where the failure is shallow or the ground water table is deep, matric suction plays a dominant role on the stability of

slope. Fredlund and Rahardjo (1993) proposed two methods to incorporate the matric suction into slope stability problems: total cohesion method and extended shear strength method.

Calculations for stability of slope are performed by dividing the soil mass above the slip surface into vertical slices. The forces acting on a slice within the soil mass are shown in Figure 2.2 for a circular slip surface and the variables are defined as,

W = the total weight of a slice of width b and height h,

N = the total normal force on the base of the slice,

S_m = the shear force mobilized on the base of each slice

E = the horizontal interslice normal forces

X = the vertical interslice shear forces

R = the radius for a circular slip surface

x = the horizontal distance from the centerline of each slice to the center of rotation or the to the center of moments

h = the vertical distance from the center of the base of each slice to the uppermost line in the geometry

a = the perpendicular distance from the resultant external water force to the center of rotation or to the center of moments

A = the resultant external water forces

α = the angle between the tangent to the center of the base of each slice and the horizontal

β = sloping distance across the base of a slice
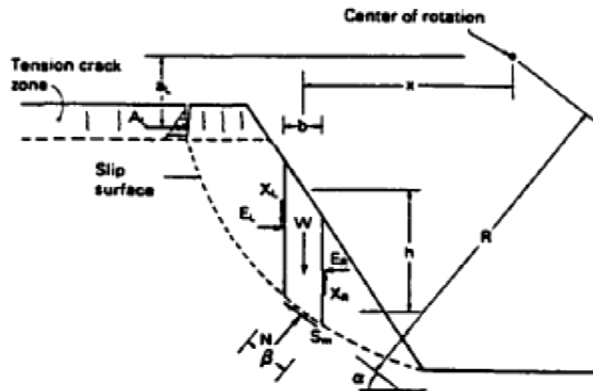
Figure 2.2 Forces acting on a slice through a sliding mass with a circular slip surface (Rahardjo and Fredlund, 1995)

The stability of a slope can be determined by comparing the resisting shear force (S_r) to the mobilized shear force (S_m) at the base of each slice. The ratio of resisting shear force and mobilized shear force is represented by factor of safety (F) which is defined as the factor by which the shear strength must be reduced in order to bring the soil mass into a state of limiting equilibrium along the assumed slip surface. The factor of safety can be written as,

$$F = \frac{S_r}{S_m} \qquad (2.3)$$

where, $S_r = \beta\{c' + (\sigma_n - u_a)tan\varphi' + (u_a - u_w)tan\varphi^b\}$

2.3 Field Infiltration Characteristic

Slopes that are initially unsaturated, the effect of rainfall at the slope surface will have a dramatically different effect. The pore water pressure that develops in the soil will occur as a

transient process as the infiltrating water moves downward in the soil profile (Collins et al, 2004). The flow of water in saturated soil is commonly described using Darcy's law which can also be incorporated for unsaturated soil (Richards, 1931; Fredlund and Rahardjo, 1993). However, there are two major differences between the water flows in saturated and unsaturated soils (Ng. et al, 2000). First, the ability of the unsaturated soils to retain water varies with soil suction which can be characterized by Soil Water Characteristic Curve (SWCC). Second, the coefficient of permeability is not constant in unsaturated soils but is a function of matric suction. Water flows through the pore space filled with water. As soil becomes unsaturated, air first replaces some of the water in large pores, and this causes the water to flow through the smaller pores to an increased tortuosity to the flow path (Ng and Menzies, 2007). A further increase in the matric suction of the soil leads to a further decrease in pore volume filled with water. As a result, the coefficient of permeability with respect to water phase decreases rapidly as the space available for water flow reduces. The above described phenomenon is presented in Figure 2.3.
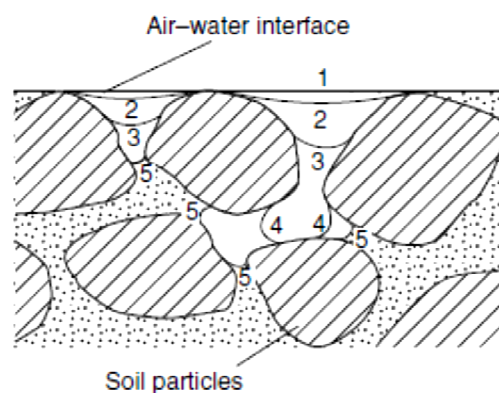
Figure 2.3 Development of an unsaturated soil by the withdrawal of the air-water interface at different stages of matric suction or degree of saturation (Ng and Menzies, 2007)

The governing partial differential equation (Fredlund and Rahardjo, 1993) for water flow through a two dimensional unsaturated soil element is given as follows:

15

$$\left\{ \frac{\partial}{\partial x}\left[k_x\frac{\partial h}{\partial x}\right] + \frac{\partial}{\partial y}\left[k_y\frac{\partial h}{\partial y}\right] + q(t) \right\} = m_1 \rho_w g \frac{\partial h}{\partial t} \qquad (2.4)$$

where, h = total hydraulic head; k_x and k_y = hydraulic conductivity in x and y- direction which is a function of matric suction; $q(t)$= applied boundary flux; m_1 = coefficient of water volume change with respect to a change in matric suction or the slope of the SWCC (Figure 2.3), ρ_w= density of water and g= gravitational acceleration.
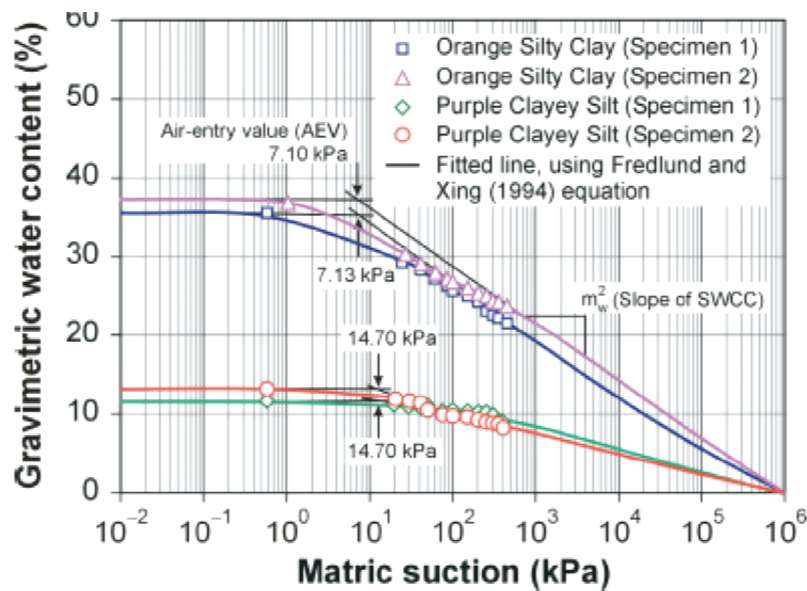
Figure 2.4 Soil-water characteristic curves (SWCC, drying phase) for the orange silty clay and purple clayey silt (Rahardjo et al., 2005)

From Eq, 2.4, it can be seen that, along with the hydraulic conductivity, soil water characteristic curve of unsaturated soils, plays an important role in controlling the flow of water into the soil.

2.3.1 Soil Water Characteristic Curve

Soil water characteristic curve (SWCC) defines the water holding capacity of soil at a particular suction state. The main features of a SWCC is presented in Figure 2.5 with two

characteristic points, A* and B*. Point A* represents the air-entry value which can be defined as the suction required to induce air to enter the larger pores of the soil and could be graphically estimated by the intersection of a line parallel to the suction axis at a degree of saturation of 100% and a line extending the linear slope portion of the curve. Point B* corresponds to the residual water content beyond which it becomes increasingly difficult to remove water from a specimen by drainage (Vanapalli et al., 1999). Prior to point A*, the soil is saturated or nearly saturated and it can be treated as a saturated soil with a compressible fluid due to existence of occluded air bubbles. Prior to point B*, as the water content is reduced further, tension in the pore water increases and eventually air is drawn into the soil matrix. At this stage, large reduction in water content are required to cause relatively small increases of soil suction which can be identified as the straight line portion of the SWCC between point A* and B*. There is little water present beyond point B* and the effect of water content or matric suction on soil behavior may be negligible (Zhan and Ng, 2004).
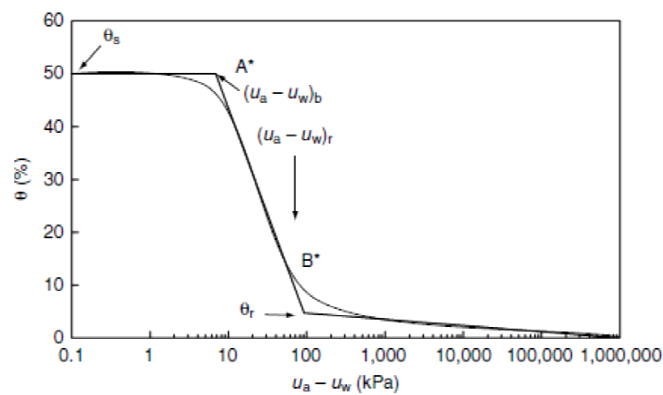
Figure 2.5 Idealized soil-water characteristic curve (Zhan and Ng, 2004)

According to Bao et al. (1998), the behavior of unsaturated soil is mostly governed by the stage between A* and B* where both air and water phases are continuous or partially continuous

and hence the soil properties are strongly related to its water content or matric suction. The linear part of the SWCC can be approximately represented with the air-entry value, the saturated and residual volumetric water content and the desaturation rate or the slope of the SWCC.

For saturated soil, the water coefficient of permeability is assumed to be constant but for unsaturated soil, coefficient of permeability depends on degree of saturation or matric suction. As matric suction increases, the volumetric water content of soil decreases which can be represented by SWCC. This affects the movement of water through soil because there are less water filled spaces available for water flow. As a result, with the increase in matric suction, the permeability of soil decreases. Therefore, the water coefficient of permeability for unsaturated soils with respect to matric suction bears a relationship to the SWCC. Estimates of the unsaturated water coefficient of permeability are difficult to obtain because measuring this parameter is time consuming and expensive. Several investigators, therefore, used models for calculating unsaturated water coefficient of permeability from the more easily measured soil-water characteristic curve (Brooks and Corey, 1964; Maulem 1976; Van Genuchten, 1980; Fredlund et al., 1994). Therefore, the water permeability function of unsaturated soils can be estimated in terms of saturated permeability, air-entry value, desaturation rate, saturated and residual volumetric contents (Zhan and Ng 2004).

The shape and magnitude of SWCC can vary significantly based on the soil type. Figure 2.6 presents the (a) SWCC and (b) relationship between water permeability and matric suction for high and low conductivity soils (Rahimi et al., 2011). From Figure 2.6 (a), it can be seen that, soils with greater fine content exhibit higher air-entry value. Soils with high air-entry value shows greater water retention ability at a given matric suction and the slope of the curve or

desaturation rate is more gradual. On the other hand, in a coarse grained soil, most of the pores are relatively large and once these larger pores are emptied at a given matric suction, only a small amount of water remains. From Figure 2.6 (b) it can be seen that, the coarse grained soil or high conductivity (HC) soil has high saturated permeability compared to the fine grained or low conductivity (LC) soil. However, the unsaturated permeability decreases more sharply and eventually becomes lower than the fine soil which is attributed due to the larger desaturation rate of the coarse soil.
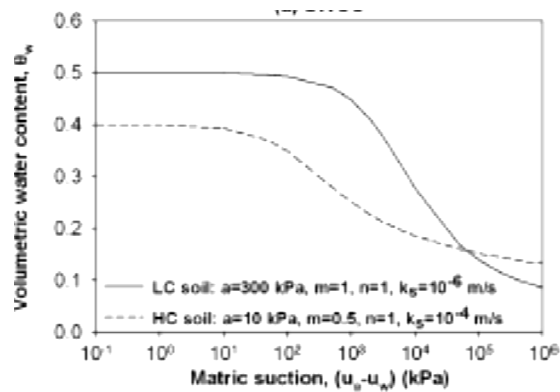
(a)
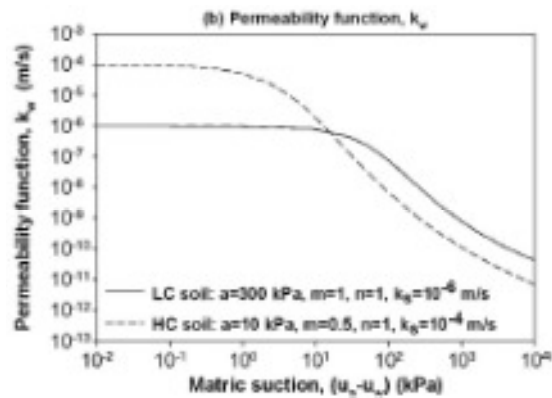
(b)

Figure 2.6 (a) Soil-water characteristic curve and (b) Unsaturated permeability function, k_w of the HC and LC soil (Rahimi et al., 2011)

The soil-water characteristic curve of a soil is conventionally measured by means of Tempe pressure cell and volumetric pressure plate extractor using axis translation technique. This technique was introduced to eliminate the cavitations of water under negative pressure (usually gauge pressure = -1 atm). Due to cavitations, the water phase becomes discontinuous and makes the measurement unreliable. Axis translation technique utilizes the fundamental definition of matric suction which is the pressure difference between the air-water interface ($u_a - u_w$), where u_a is the pore air pressure and u_w is the pore water pressure. In both the Tempe cell and pressure plate extractor, u_w is maintained constant, usually at the atmospheric pressure ($u_w = 0$) and u_a is increased to obtain the desired matric suction (Hilf 1956). A schematic diagram illustrating the axis translation technique is presented in Figure 2.7. The terminology "axis translation" refers to the technique where the origin of reference or axis for the matric suction variable is translated from the condition of atmospheric air pressure and negative water pressure to the condition of atmospheric water pressure and positive air pressure (Lu and Likes, 2004).

In the field

σ^1
u_a^1
$u_w^1 < 0$

Unsaturated soil

$\sigma^1 - u_a^1 = \sigma^2 - u_a^2$

$u_a^1 - u_w^1 = u_a^2 - u_w^2$

In the lab

σ^2
u_a^2
$u_w^2 > 0$
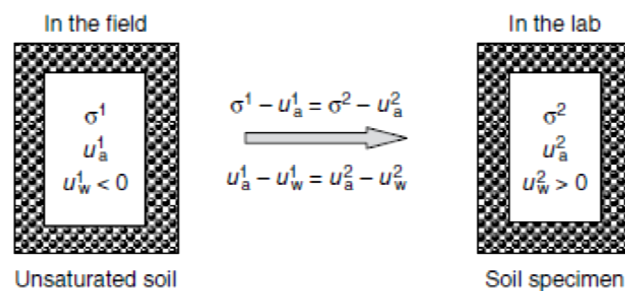
Soil specimen

Figure 2.7 Schematic diagrams illustrating the axis translation principle (Ng and Menzies, 2007)

In the conventional Tempe cell and volumetric pressure plate no vertical or confining stress is applied and volume change of the soil specimen is assumed to be zero. But, in the field, the soil is subjected to a certain stress. There are few experimental results available to date which

20

incorporates the effect of stress state on SWCC. Vanapalli et al. (1999) first reported the influence of the total stress state on SWCC of compacted sandy clay till through indirect procedure. The soil specimens were first loaded and then unloaded using a conventional consolidation apparatus to create a known stress history. Finally, the SWCC of the preloaded specimens were determined using a traditional pressure plate apparatus in which the change in water content due to the variation of soil suction was measured under zero-applied net normal stress (σ-u_a). It was observed that, the SWCC developed for the specimens compacted dry of optimum with equivalent pressures of 0, 25, 100 and 200 kPa showed high air-entry value with increasing equivalent pressure (Figure 2.8). Beyond the air-entry value of suction, the specimens
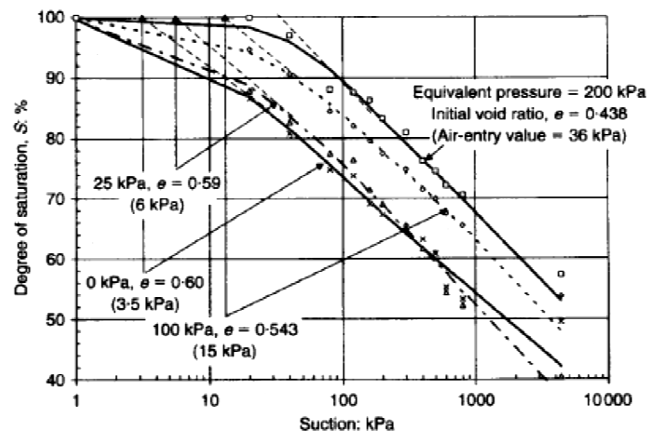
Figure 2.8 Soil-water characteristics for specimens compacted dry of optimum water content
(Vanapalli et al., 1999)

subjected to higher equivalent pressures have higher degrees of saturation. Figure 2.9 presents the SWCC for specimens compacted wet of optimum with different equivalent pressures.
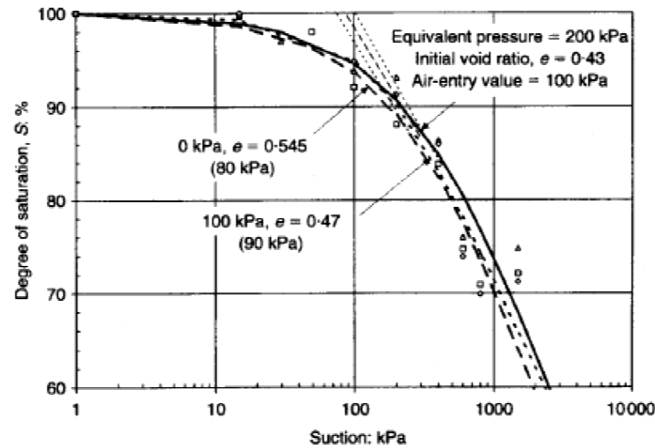
Figure 2.9 Soil-water characteristics for specimens compacted wet of optimum water content
(Vanapalli et al., 1999)

Vanapalli et al. (1999) reported that, though the specimens were subjected to different equivalent
pressures, the SWCC of the specimens with wet of optimum initial water content conditions
appear to be the same.

To investigate the influence of stress state on SWCC of completely decomposed volcanic
soil, Ng et al. (2000) modified volumetric pressure plate extractor in which total net normal
stress was controlled one-dimensionally and axial deformation was measured. The schematic
diagram of the modified apparatus is presented in Figure 2.10. An odometer ring equipped with a
high air entry ceramic plate at its base was located inside an airtight chamber. Vertical stress σ
was applied through loading frame to a soil specimen inside the ring. Dead weights via a loading
piston were used to apply the required vertical force. The total volume change of the specimen
was measured from the vertical displacement of the soil specimen using a dial gauge.

Three undisturbed soil specimens were used to determine the SWCC for three net normal
stresses of 0, 40 and 80 kPa. All the specimens were saturated prior to the test. The SWCC of all
the specimens were determined following both drying and wetting path and were limited to a

22

matric suction of 200 kPa. Figure 2.11 shows the results obtained by Ng et al. (2000) for three different net normal stress conditions. It can be seen that, higher the applied load on the specimen, the lower the rate of reduction in volumetric water content.
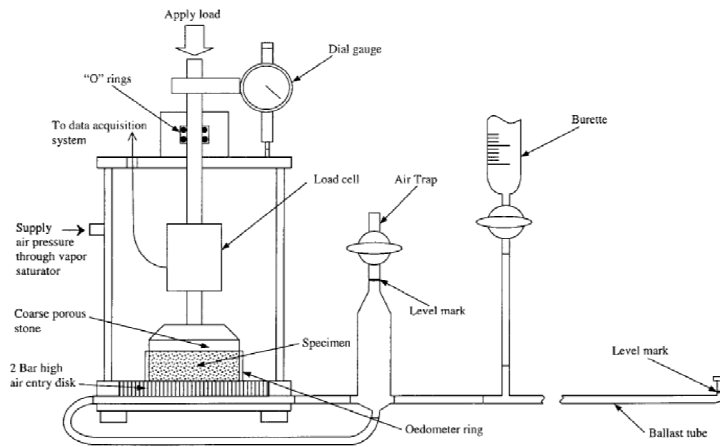
Figure 2.10 Schematic diagram of modified 1D volumetric pressure plate extractor
(Ng et al., 2000)
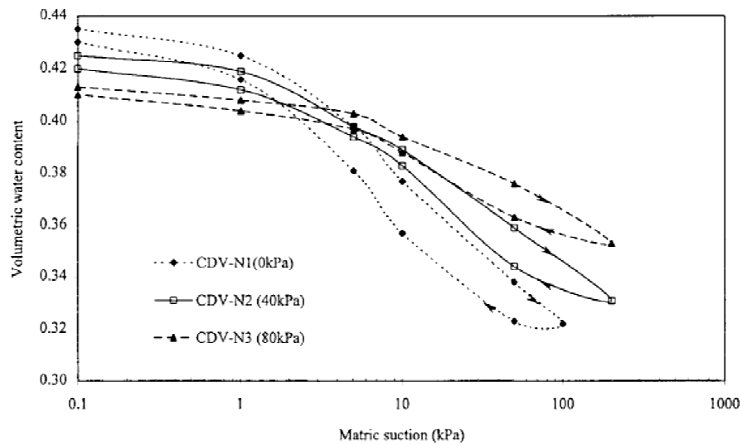
Figure 2.11 Effect of stress state on SWCC (Ng et al., 2000)

Ng et al. (2000) reported that, specimens subjected to higher stress, possess a larger air-entry value which may be due to the presence of smaller average pore size distribution in the soil specimen under the higher applied load.

Ng et al. (2000) also reported the permeability function that varies with matric suction for the above tested specimen. The SWCC for different stress state were fitted by a nonlinear equation proposed by Fredlund and Xing (1994) for obtaining the permeability function which is presented in Figure 2.12. From Figure, it can be seen that, soil specimen loaded to a higher net normal stress has a lower permeability function, because the applied net normal stress led to a smaller pore size distribution inside the soil specimen.
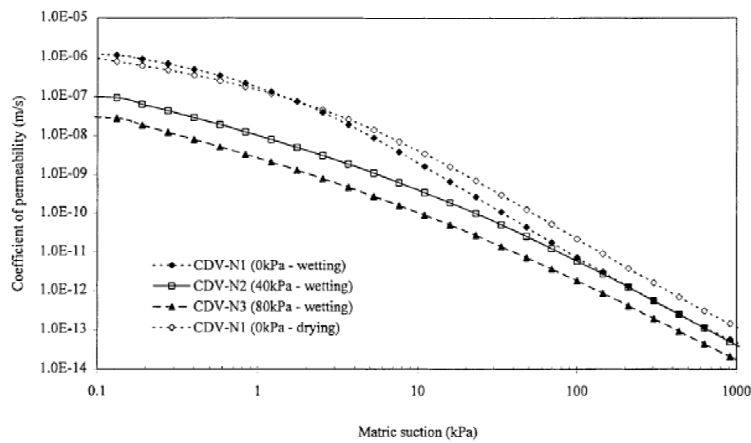
Figure 2.12 Permeability functions computed from measured soil-water characteristics

(Ng et al., 2000)

Vanapalli et al. (1999) reported the influence of initial compaction water content on the shape of the SWCC of sandy clay till. The specimens prepared on the dry of optimum water content exhibit a steeper soil water characteristic when compared with specimens compacted at optimum and wet of optimum water contents (Figure 2.13). The specimens compacter dry of optimum show the behavior of coarse-grained soil because of their highly aggregated macrostructure. On the other hand, microstructure governs the soil-water characteristic behavior of specimens compacted wet of optimum. Specimens compacted wet of optimum showed a

higher air-entry values and higher residual state of saturation than those compacted at optimum or dry of optimum water contents.
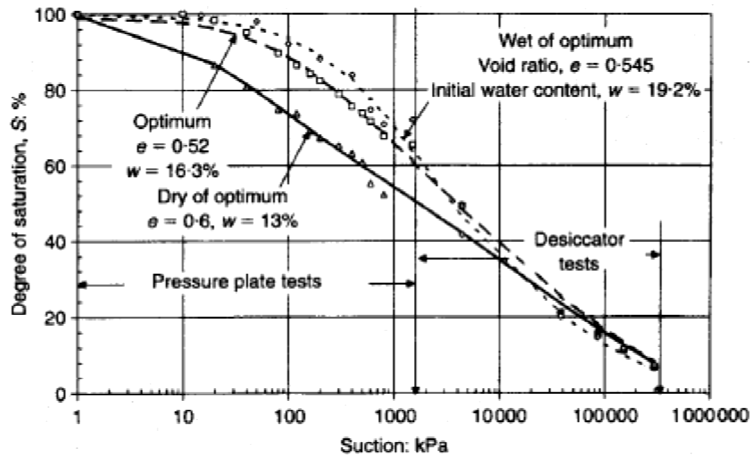
Figure 2.13 Soil-water characteristics of specimens compacted at different initial water content (Vanapalli et al., 1999)

Influence of initial water content on the SWCC of clay from Wisconsin river bank, has also been investigated by Tinjum et al. (1997). The author also reported that, increasing the compaction water content resulted in higher air-entry value and steeper slope of the SWCC (Figure 2.14). According to Tinjum et al., specimens compacted dry of optimum contains stiff clods that are not remolded during compaction. The presence of large interclod macrovoids resulted in lower air-entry value compared to the specimens compacted wet of optimum where the micropore dominates the structure.
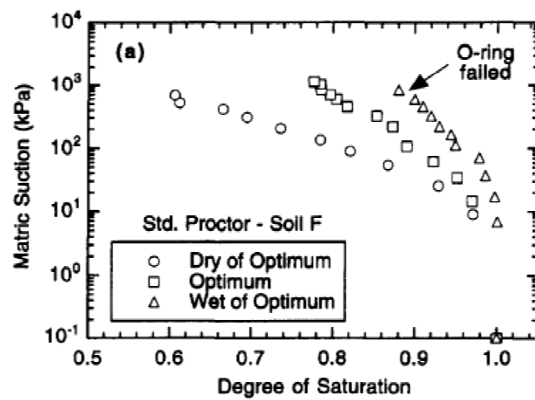
Figure 2.14 SWCCs dry of optimum, wet of optimum and at optimum water content using Standard Proctor Compaction (Tinjum et al., 1997)

Meerdink et al. (1996) reported the changes in unsaturated hydraulic conductivity function of clay for different compaction water content which is consistent with the changes in shape of SWCC. The unsaturated hydraulic conductivity of clay compacted dry of optimum showed a rapid decrease during desorption than for clay compacted wet of optimum (Figure 2.15). Specimens compacted dry of optimum have larger pores and a narrower pore-size distribution, which allow the pores to desaturate more readily.
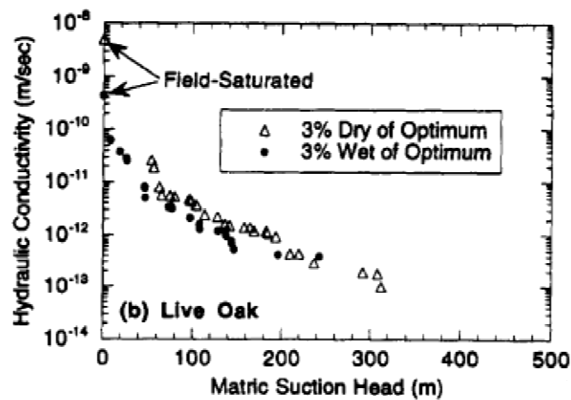
Figure 2.15 Unsaturated hydraulic conductivity at 3% dry or wet of optimum water content (Meerdink et al., 1996)

26

2.3.2 Previous Work on Field Infiltration Behavior

The application of seepage and slope stability analyses requires an understanding of the infiltration amount and its contribution to the water content and pore-water pressure changes in the slope. Therefore it is of primary importance to study through field instrumentations, the variation in infiltration, water content and pore water pressures due to different rainfall events.

Lim et al. (1996) reported results from field instrumentation program that was carried out in a residual soil slope in Singapore to show the variation in matric suction profiles using tensiometers in a canvas-covered grassed slope, grassed covered and a bare slope in response to rainfalls. The results from this field instrumentation indicates that the variation of the matric suction profile is less significant under the canvas covered section than under the grass-covered and the bare sections of the slope as shown in Figure 2.16. The author also reported higher coefficient of permeability ($1x10^{-6}$ m/s) at the crest of the slope during field permeability measurement as compared to the laboratory measurement ($1x10^{-9}$ m/s) which can be due to the presence of cracks near the ground surface.
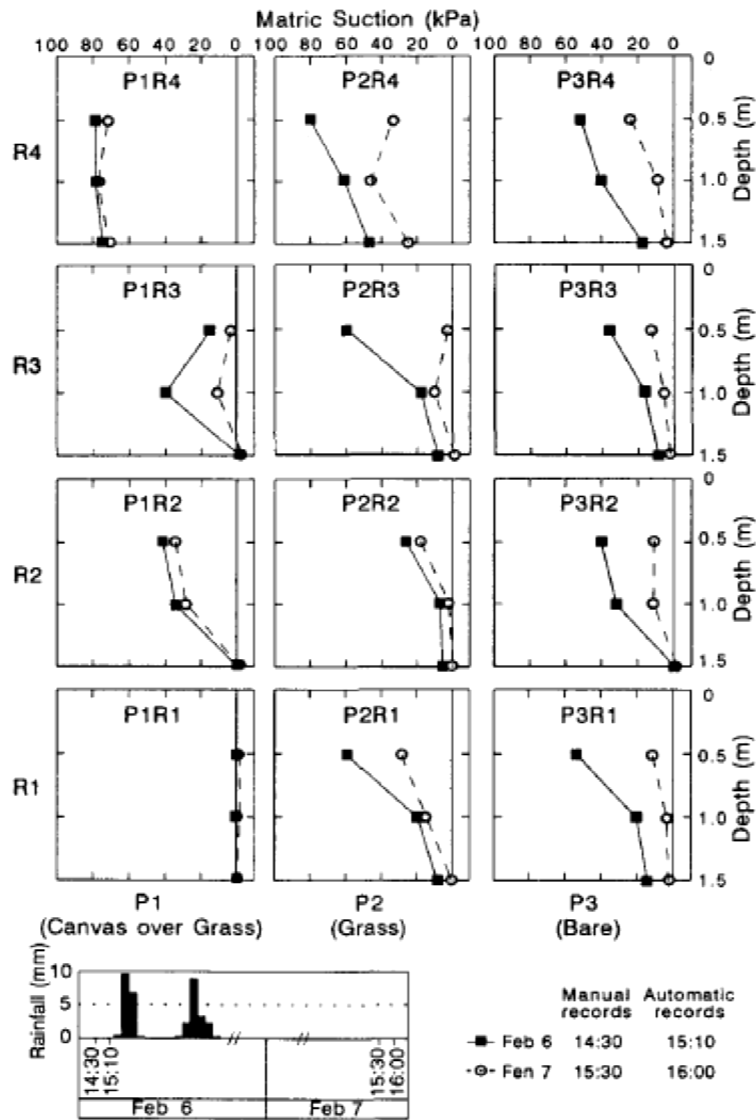
Figure 2.16 Changes of in situ matric suction profiles under three ground surface condition due to rainfall (Lim et al., 1996)

Zhang et al. (2000) reported results on the field instrumentation carried out by installing tensiometers in a residual soil slope in China which is limited up to 1.8 m depth. According to the author, the infiltration rate depends on the initial water content in the soil. The author also stated that, the infiltration pattern can be significantly disturbed by the presence of geological

discontinuities. Due to presence of the relic joint, lateral flow of water was observed which increased saturation up to top 80 cm depth, while the soil below remained unsaturated.

Based on the field instrumentation in a saprolite slope in Hong Kong, Li et al. (2005) reported that the infiltrated water during rainfall increased the soil moisture content of the soil at shallow depths. The author also reported that with the decrease in rainfall intensity, the infiltration rate increases. Similar results have also been reported by Rahardjo et al. (2005), for a residual soil slope in Singapore where the author observed a reduction in rainfall infiltration with the increase in total rainfall. According to the author, soil water contents tend to be higher near the toe of the slope than at the crest irrespective of rainfall events which indicates a subsurface movement of water in the down slope direction.

However most of these field scale investigation were conducted on residual soil slope with different weather condition as compared to Texas. Most of the slopes in Texas are constructed on high PI clay. Some of these high PI clay shows medium to high expansive behavior. In an attempt to understand the infiltration behavior through high PI clay Zornberg et al. (2007) performed a laboratory investigation to determine the unsaturated hydraulic characteristic of high PI clay.

The author conducted a series of evaporation and infiltration experiments to determine the effect of cracking on the hydraulic properties of unsaturated high PI clays by preparing a soil column and inserting HDU probes at elevations of 50, 100, 150 and 200 mm of the soil column. Testing of soil column included three stages (evaporation, infiltration and a second evaporation). A schematic representation of the sequences of evaporation, infiltration and second evaporation in soil column 3 is summarized in Figure 2.17.

		Stages			
I. Start 1st evaporation	II. End 1st evaporation	III. Start infiltration	IV. After 100 hours of infiltration	V. After 1000 hours of infiltration	VI. 2nd evaporation
Summary description					
A 25 cm high specimen was compacted 2% dry of optimum. A fan was then blown across the soil surface to start evaporation.	After 400 hours of evaporation the suction and water content at sensor levels C & D reached steady values constant. Small cracks were visible at the soils surface and the surface had settled 0.1 cm.	A constant head of 2.5 cm was applied at the upper boundary to start infiltration. The soil swelled from 24.9 cm in height to 27.7 cm in height during the first 18 hours of infiltration.	After 100 hours of infiltration an initial wetting front reached the base of the column and a second wetting front reached mid height.	After 260 hours of infiltration, the soil specimen swelled to the top of the infiltration collar at 32.5 cm elevation. Infiltration was continued until 1000 hours when no further downward movement of the second wetting front was observed.	The infiltration apparatus was removed and the soil above 25 cm elevation was removed. A fan was then used to start the 2nd evaporation phase. Significant cracking occurred during the second evaporation stage. After 1050 hours of evaporation testing was stopped.

Figure 2.17 Soil Column 3 time line (Zornberg et al., 2007)

From the presented data (Figure 2.18), it is evident that at a given level of suction, the measured volumetric water content is considerably lower for the second drying phase than for the first. At a particular volumetric water content, this shift would indicate a one to two order magnitude decrease in suction. Based on these results Zornberg et al. (2007) suggested that the soil moisture retention characteristics of the soil varies with depth and appropriate hydraulic conductivity should be adopted to accurately predict the stability of slope due to rainfall infiltration.
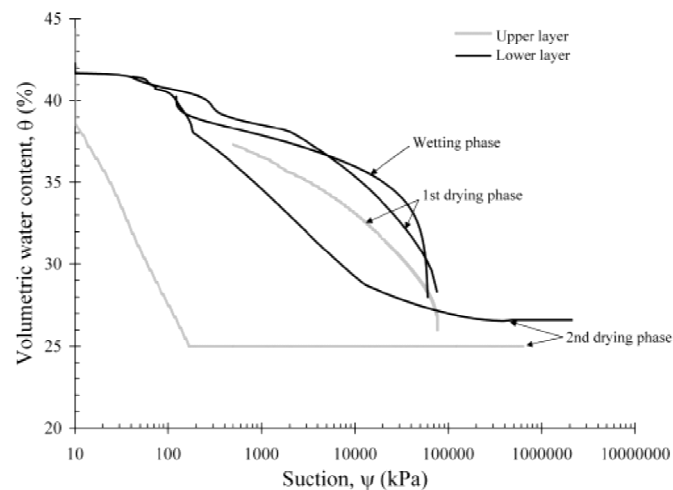
Figure 2.18 Soil water retention curves for soil column 4, soil compacted 2% wet of optimum (Zornberg et al., 2007)

The author also reported the depth of moisture variation for slopes constructed on high PI clay is 1.5 m based on the numerical simulation with 30 year weather data for Austin and Houston. However, experiences from previous slope failure on high PI expansive clay does not support the above conclusion. Therefore, it is necessary to identify the depth of this moisture variation zone through real time field data to accurately predict the potential for slope failure during rainfall events.

2.4 Unsaturated Shear Strength

The shear strength of soil is an important property which controls the stability of slope. Prediction of correct strength parameter is critical to identify the geohazard potential to slope failure due to rainfall infiltration. The effective stress variable, σ', proposed by Terzaghi (1936) has been used to predict the shear strength of saturated soil using Mohr-Coulomb failure criterion. The shear strength of saturated soils is generally expressed by the following equation,

$$\tau = c' + (\sigma_n - u_w)tan\varphi' \qquad (2.5)$$

Where,

τ = Shear Strength

$\sigma_n - u_w$ = Effective normal stress (σ')

c' = Effective cohesion

φ' = Effective friction angle

However, slopes constructed in arid and semi-arid region remain in unsaturated condition above the ground water table. To accurately predict the mechanical behavior of unsaturated soil, two stress state variables are required of which the most widely used, is the combination of net normal stress ($\sigma - u_a$) and matric suction ($u_a - u_w$). Based on these two stress state variables, Fredlund et al. (1978) proposed the following equation which is an extension of M-C theory to describe the shear strength of unsaturated soil:

$$\tau = c' + (\sigma - u_a)tan\varphi' + (u_a - u_w)tan\varphi^b \qquad (2.6)$$

32

Where,

$(\sigma - u_a)$ = net normal stress

$(u_a - u_w)$ = matric suction

φ' = angle of internal friction associated with the change in net normal stress

φ^b = angle representing the rate of change in shear strength relative to matric suction change

The first two terms on the right hand side in equation (2.5) describes the conventional M-C theory to determine the strength of saturated soil. The third term indicates the change in shear strength due to change in matric suction in unsaturated soil. The corresponding failure envelope for the extended M-C criterion is presented in three dimensional stress space in Figure 2.19.
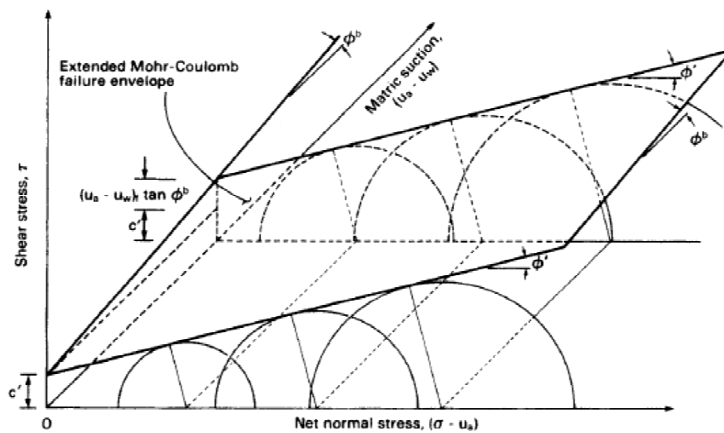
Figure 2.19 Extended Mohr-Coulomb failure envelope for unsaturated soils (Fredlund and Rahardjo, 1993)

Soils subjected to shearing under drained condition usually exhibit an increase in shear resistance with increasing displacement until a maximum resistance, a peak strength is reached which is presented in Figure 2.20. If the shearing is continued beyond this point, the resistance of

the soils starts to decrease until a minimum resistance, termed as residual strength is reached. The residual strength condition results from the reorientation of platy particles parallel to the direction of shear, which results in an increased face to face interaction of the particles (Skempton, 1985). This poor contact or bonding of the face to face particles results in reduction in shear strength. The author also suggested that residual strength is applicable to new and existing slopes that contain a pre-existing shear surface.
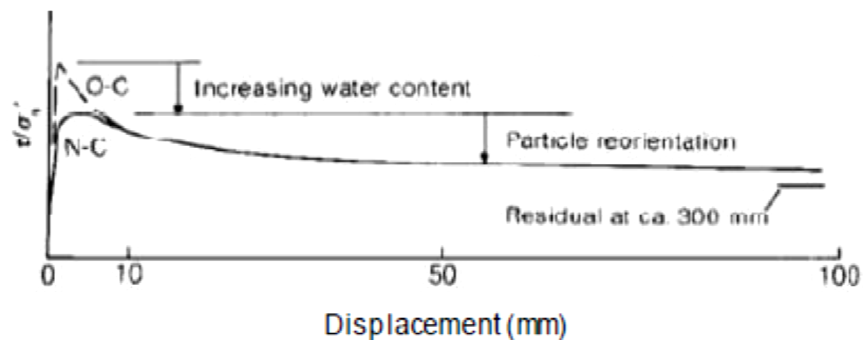
Figure 2.20 Stress-displacement curves at constant σ´ (Skempton, 1985)

Skempton (1985) stated that the reduction in strength of over consolidated clays is due first to an increase in water content due to dilatation and, secondly to orientation of clay particles parallel to the direction of shearing. On the other hand, normally consolidated clays generally have lower peak strengths than over consolidated clays and exhibit a smaller decrease from peak to residual strength. This decrease in strength is accompanied by a reduction in void ratio and is due entirely to the orientation of particles parallel to the direction of shearing.

Over the past two decades, significant efforts have been made to determine the shear strength properties of unsaturated soil by using some simplified test methods or procedures (Fredlund and Rahardjo 1993; Vanapalli et al., 1996; Rassam and Williams 1999; Vilar 2006). It

is generally expected to control suction during the testing of unsaturated soil. The most commonly used technique is axis translation technique (Hilf 1956). Osmotic technique (Zur 1966) and humidity control technique (Esteban and Saez 1988) is also gaining increased attention to determine shear strength properties in high suction range.

The shear strength contribution due to matric suction represented by φ^b, was assumed to be linear based on limited publication (Escario 1980). Gan et al., (1988) performed multi-stage direct shear test on unsaturated glacial till using axis-translation technique. The author observed linear failure envelopes with respect to the net normal stress. However, significant nonlinearity for the failure envelope with respect to matric suction was observed which is presented in Figure 2.21. It is observed that the φ^b angle is close to φ' at matric suction close to zero and decreases significantly at matric suctions in the range of 50-100 kPa and reaches a fairly constant value from $5^\mathbf{o}$ to $10^\mathbf{o}$ when matric suction exceeds 250 kPa.

(a)   (b)
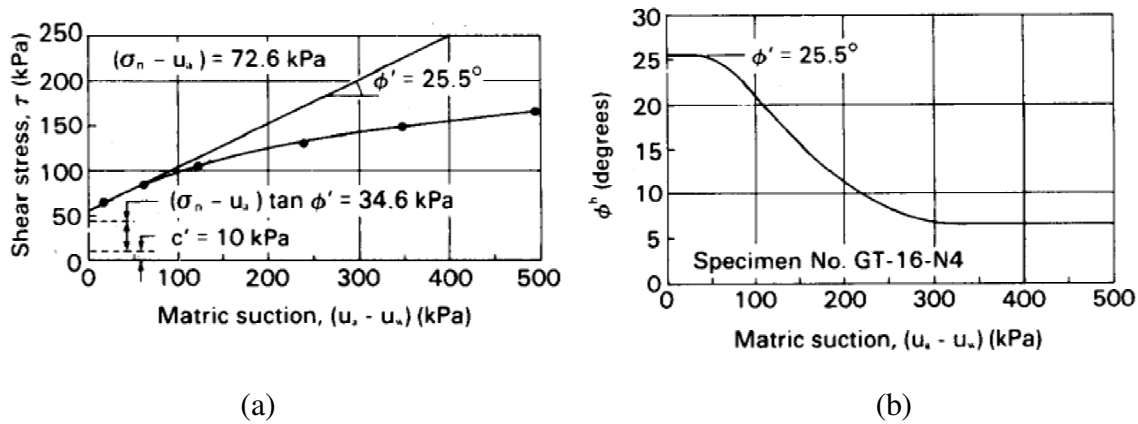
Figure 2.21 (a) Peak failure envelope with respect to suction state and (b) variation of φ^b with suction (Gan et al., 1988)

Zhan et al. (2006) performed suction controlled direct shear test on both compacted and natural expansive clay using axis translation technique. It can be observed non-linearity in the failure envelope for both peak strength and strength at large displacement with respect to the

suction state while the failure envelope with respect to normal stress shows a linear relation (Figure 2.22). The author also reported that dilatancy of the expansive clays increases with the increase in suction which is presented in Figure 2.23. This phenomenon is also reported by
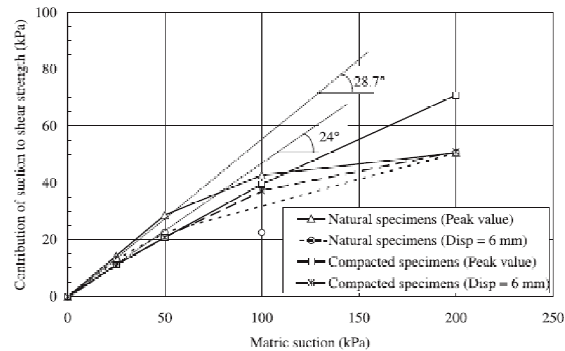
Figure 2.22 Contribution of suction to shear strength for natural and compacted specimens (Zhan et al., 2006)
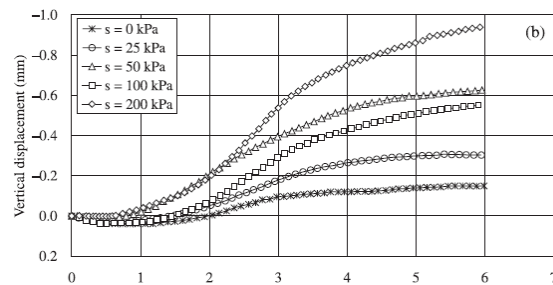
Figure 2.23 Relationship between vertical displacement versus horizontal displacement from direct shear tests on unsaturated natural expansive clay (Zhan et al., 2006)

Hossain and Yin (2010) for suction controlled drained direct shear test performed on completely decomposed granite soil. Due to suction effect on soil dilatancy, Zhan et al. (2006) suggested that, the contribution of suction to peak strength for the expansive clay is more significant than the contribution of suction to post failure shear strength , especially in the high suction range.

Over the last few decades, conventional soil testing equipment such as direct shear and triaxial testing devices have been modified and widely used for the assessment of residual shear

36

strength properties of unsaturated soils (Escario 1980; Escario and Saenz, 1986; Gan et al., 1988; Wheeler, 1988; Zhan et al., 2006). Vaunat et al. (2006, 2007) reported results from a modified Bromhead type ring shear apparatus used for soil testing under controlled high-suction states using vapor transfer technique. The specimen height is 5 mm while its outer and inner diameters are 100 mm and 70 mm, respectively. Low and medium plasticity clayey soils were tested. The authors reported an increase in residual friction angle with an increase in the applied suction. The author also observed that increase in matric suction does not have any influence on the cohesion parameter. This was mainly associated to the partial aggregation of clayey particles, which was believed to have caused the soil to behave more like a granular material.

Most recently Hoyos et al. (2012) reported results from a fully suction controlled ring shear apparatus for soils tested under low suction state using axis translation technique for a large shear deformation. This suction controlled RS device is a modification to the original Bromhead type ring shear, with a sample height of 15 mm and a outer and inner diameter of 152.4 mm and 96.5 mm respectively. SC-SM and SM soils were tested. The authors reported an increase in both cohesion and residual friction angle with an increase in the applied suction for both type of soil tested which is presented in Figure 2.24.
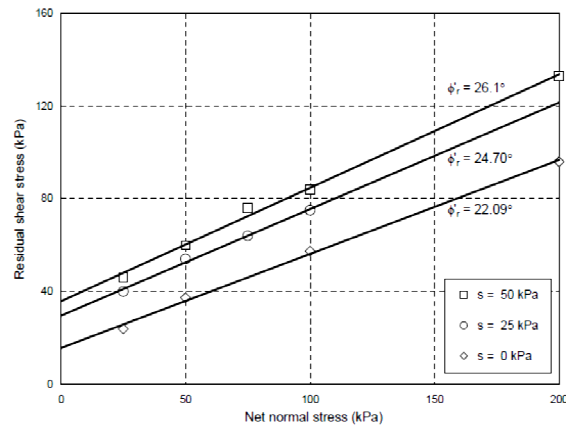
(a)
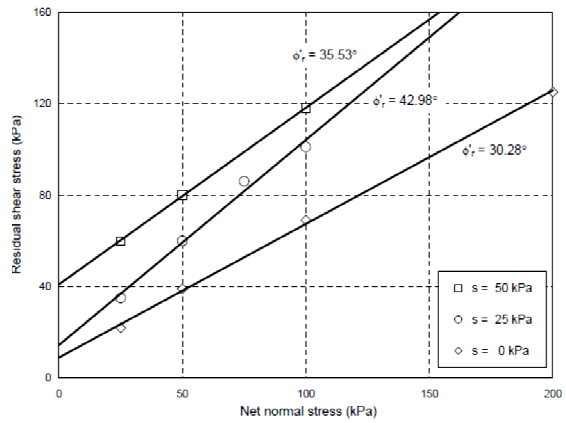
(b)

Figure 2.24 Effect of matric suction on residual failure envelope of (a) SC-SM and (b) SM soil (Hoyos et al., 2012)

The above results, however are focused on low to medium plasticity clay and sand or silts and far from conclusive for high PI expansive clay. Therefore, the current research work introduces a novel suction-controlled ring shear device to determine the shear strength characteristics of high plasticity clay with expansive behavior at a low suction range using axis translation technique.

2.5 Fully Softened Strength

Another important consideration for slopes constructed on high plasticity clay is the softening behavior for top soil due to wet-dry cycle. Skempton (1977) reported that over time the strength of slopes in the highly plastic London Clay lost strength, eventually reaching what Skempton termed as "fully-softened" strength which lies between peak and residual strength as presented in Figure 2.25. Skempton (1977) indicated that the fully-softened strength is comparable to the shear strength of the soil in a normally consolidated state.
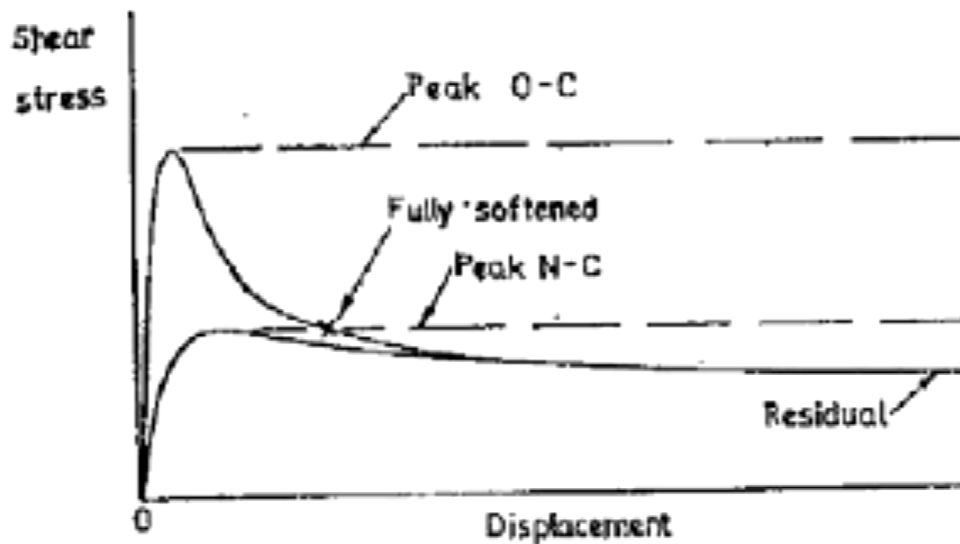
Figure 2.25 Comparisons of peak, residual and fully softened shear strength (Skempton, 1970)

Rogers and Wright (1986) investigated the long term strength of highly plastic clay involved in the failure of a highway embankment in Houston, Texas. Four series of drained direct shear tests were performed on specimens subjected to 1, 3, 9 and 30 cycles of wetting and drying. The author concluded that during failure the strength of the high plasticity clay reached at

fully-softened state due to repeated cycles of wetting and drying. Shear strength parameters obtained from these tests are summarized below in Table 2.1.

Table 2.1 Summary of shear strength parameters from drained direct shear tests on specimens subjected to wetting and drying cycles (Rogers and Wright, 1986)

Number of Wet-Dry Cycles	Cohesion, c'	Friction Angle, ϕ'
1	29 psf	23°
3	77 psf	26°
9	33 psf	25°
30	0	27°

The shear strength parameters summarized in Table 2.1 reveal a significantly lower cohesion value than as compacted specimen (c'=270 psf, φ'=20°). This suggests that cycling wetting and drying of the soil produces a significant shear strength loss, particularly in terms of the effective cohesion intercept, c'. The direct shear test also indicated that the loss in cohesion occurs within a relatively few number of cycles of wetting and drying. In fact most of the strength loss occurred on the first cycle. However, the wetting and drying that specimens were subjected to in the laboratory was much more severe than what would be expected to occur during any cycle of wetting and drying in the field.

Kayyal and Wright (1991) determined the strength of highly plastic Red Beaumont clay and Paris clay after repeated cycles of wetting and drying and observed a significant reduction in strength. Several series of consolidated-undrained triaxial compression tests were performed with pore water pressure measurements. Tests were performed on specimens subjected to repeated wetting and drying and on specimens that were consolidated from a soil-water slurry to

form normally consolidated soil. Results of these tests showed that shear strengths of specimens subjected to repeated cycles of wetting and drying were essentially identical to the shear strength of the normally consolidated specimens. The strength is believed to represent the fully softened shear strength of the soil that is attained after a number of years of exposure in the field.

The shear strength envelopes for specimens of Beaumont clay tested in the as-compacted condition and after wetting and drying are shown in Figure 2.26. Both envelopes are distinctly curved. The strength envelope for the specimens subjected to wetting and drying lies significantly below the envelope for the specimens tested in the as-compacted condition, especially at lower values of normal stress. The envelope for the specimens subjected to wetting and drying shows negligible intercept, which is consistent with the findings from earlier studies that suggested the cohesion value eventually became very small or zero.
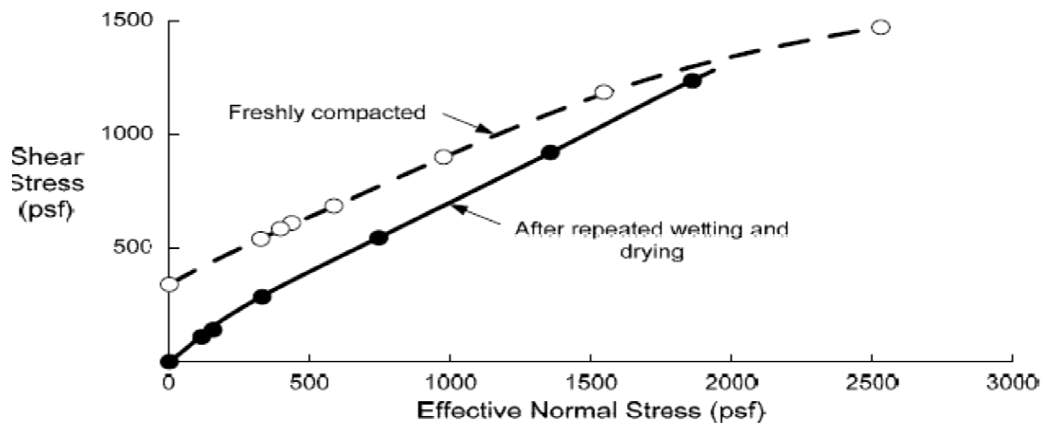
Figure 2.26 Shear strength envelope for specimens of red Beaumont clay in the as-compacted condition and after wetting and drying (Kayyal and Wright, 1991)

The shear strength envelope for specimens of the Paris clay tested in the as-compacted condition and after wetting and drying are shown in Figure 2.27.These envelopes again show a pattern similar to what is shown for the Beaumont clay i.e. both strength envelopes are curved, the

strength of the specimens subjected to wetting and drying is less than the as-compacted strength, especially at low stresses and the intercept of the strength envelope for specimens subjected to wetting and drying is small and could be considered negligible.
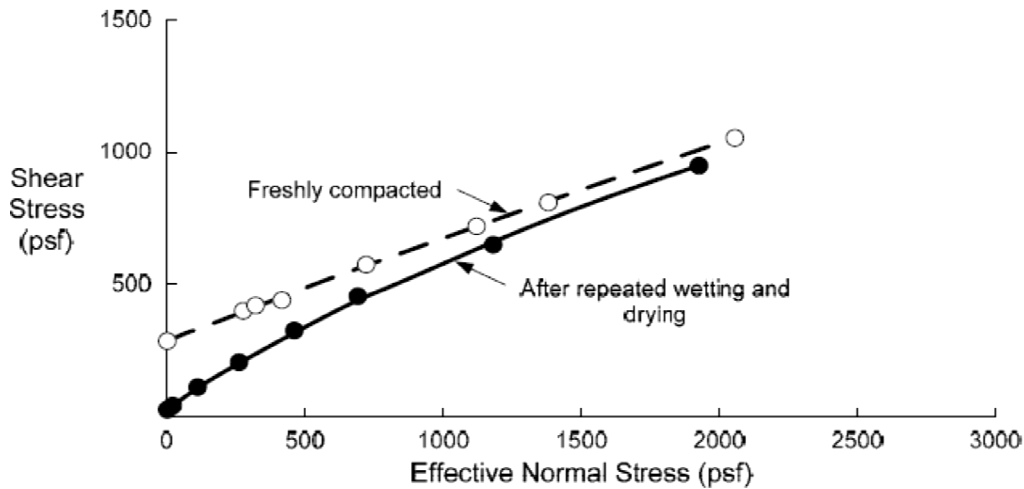
Figure 2.27 Shear strength envelopes for specimens of Paris clay in the as-compacted condition and after wetting and drying (Kayyal and Wright, 1991)

Most recently Stark et al. (2005) proposed a empirical correlation for fully softened friction angle based on the experimental data using Modified Bromhead Ring Shear equipment. The correlation which is presented in Figure 2.28, can be used to estimate the secant friction angle using the liquid limit, clay size fraction and effective normal stress.
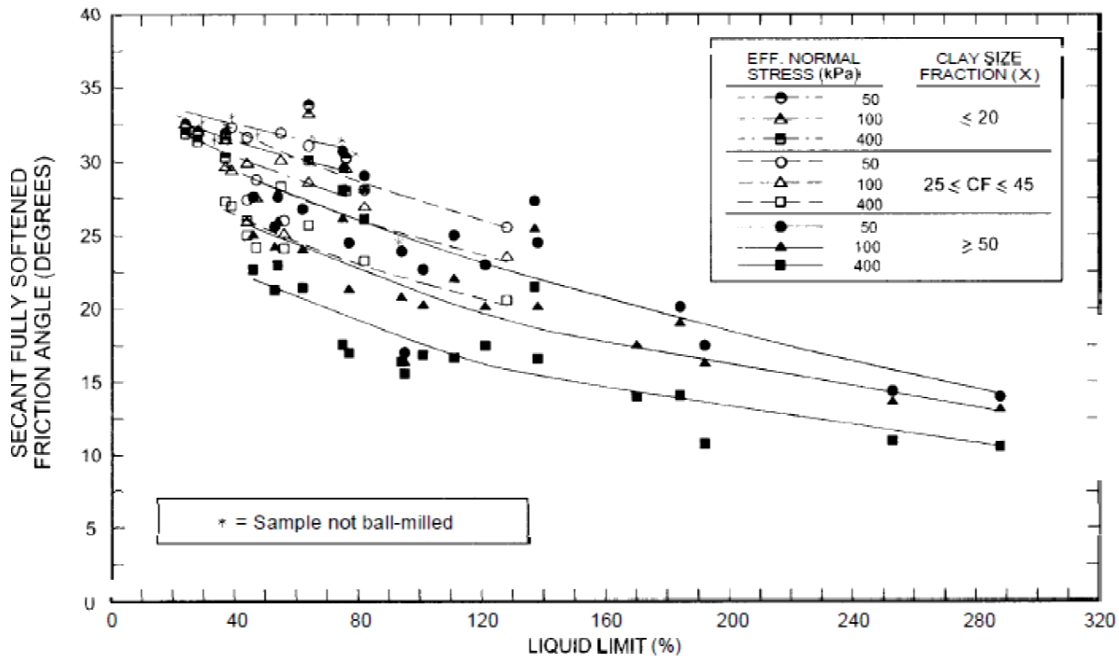
Figure 2.28 Secant fully softened friction angle relationships with liquid limit, clay-size fraction and effective normal stress (Stark et al., 2005)

Zornberg et al. (2007) also reported the shear strength of Eagle Ford clay from triaxial compression test that had experienced seasonal wetting and drying in the field. Figure 2.29 presents the results for as compacted specimens, specimens consolidated from slurry and specimens subjected to cycles of wetting and drying. From Figure it can be seen that, at the fully softened state, the cohesion intercept disappears.
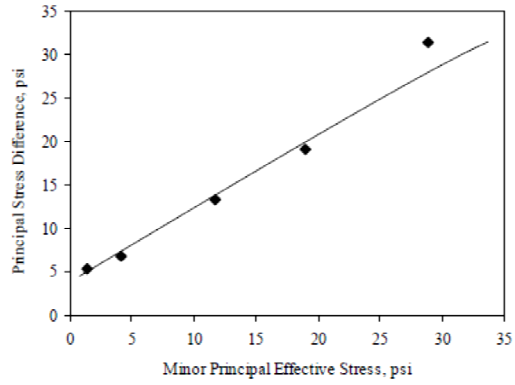
(a)
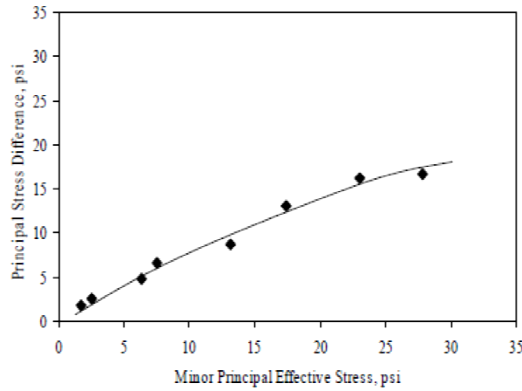
(b)
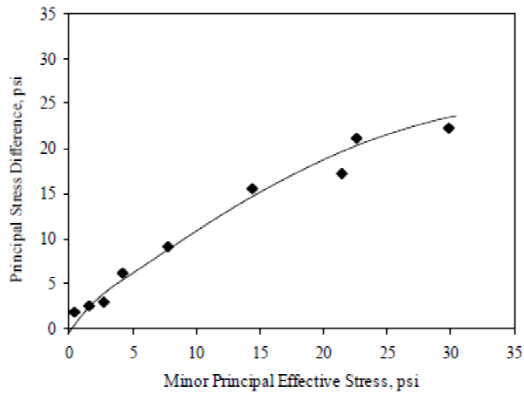
(c)

Figure 2.29 Modified Mohr failure envelope for specimens of Eagle Ford Shale (a) as compacted, (b) normally consolidated from slurry and (c) subjected to cyclic wetting and drying (Zornberg et al., 2007)

CHAPTER 3

METHODOLOGY

3.1 Introduction

In this chapter, sample collection and basic soil characteristics are first presented followed by the detailed field instrumentation program which was carried out to determine active zone and field infiltration characteristic of the slope under study. A description of the modification of Tempe pressure cell used to determine the state dependent soil-water characteristic curve (SDSWCC) along with test procedure and experimental variables are presented then. Finally, test procedure followed to determine the shear strength of unsaturated soil using suction controlled ring shear equipment and also shear strength behavior of saturated soil under cycles of wetting and drying using direct shear equipment are presented.

3.2 Site Description and Investigation

The site selected for the current study is located along Highway US 287 S near St. Paul Overpass in Waxahachie, Texas. The site is overlain by the deposits of Eagle Ford geological formation. The north bound slope has experienced two shallow surficial slides in 2008. The existing embankment is about 9.2 m high with an inclination of 22^0. The surface of the slope was covered with naturally occurring grass. Evidence of tension cracking in the shoulder has been observed before the failure. Similar phenomenon has been observed for the slope under study at the south bound of the highway with cracks at the shoulder as wide as 50 mm which is presented

in Figure 3.1. The low confining pressure at the surface allows clay to crack at relatively low matric suction. These cracks generally become closed with depth as the confining pressure increases (Zhan et al., 2007).

Figure 3.1 Tension cracks along the shoulder

Full scale field investigation was conducted around the monitoring area prior to instrumentation of the slope. Site investigation included geophysical testing and soil test boring. Resistivity Imaging (RI) was conducted to obtain a continuous image of the subsurface. A total of 2 (two) 2D resistivity imaging was conducted at the site. The 2D imaging sections are identified as "Line 1" and "Line 2" as presented in Figure 3.2. The survey sections Line was on the top of the slope. "Line 2" was located at 12 m apart from "Line 1" as presented in Figure 3.2. The RI investigations were conducted using 8-channel Super Sting equipment. The system

consists of 56 electrodes and these electrodes were placed at 1.52 m spacing. Some of the pictures of the field work and survey setup are presented in Figure 3.3.
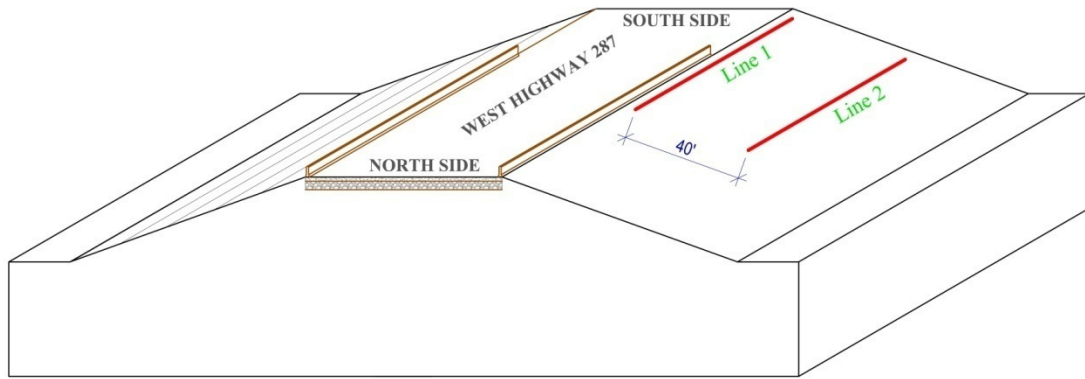
Figure 3.2 Resistivity Imaging layout

<div align="center">

(a)   (b)

</div>
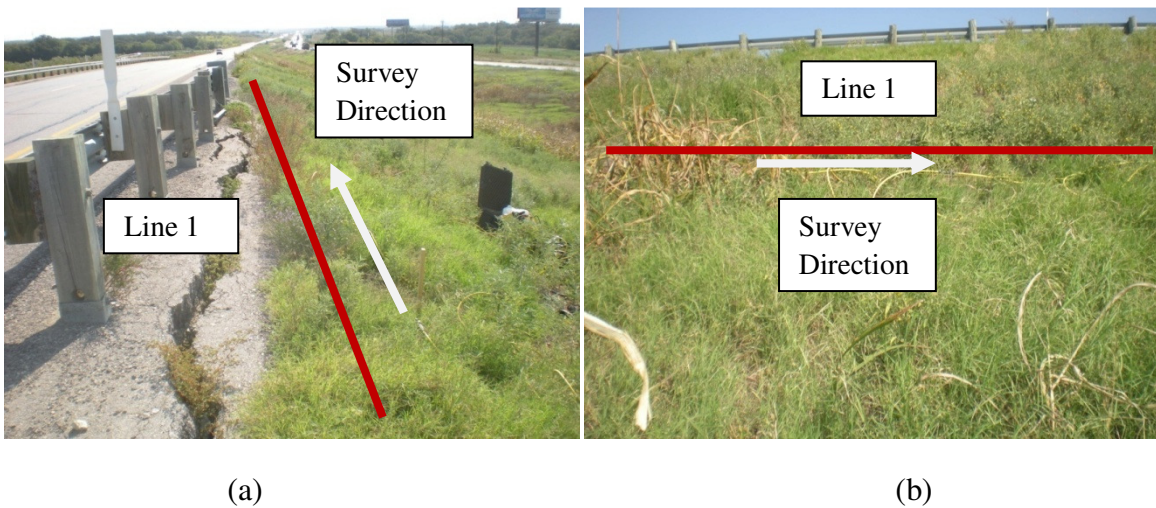
Figure 3.3 Resistivity Imaging field set up (a) line 1 and (b) line 2

RI result conducted along Line 1 is presented in Figure 3.4 (a) which indicates a high resistivity zone for top 2.1 m of soil. A low resistivity zone of less than 5 ohm-m was present in between depth 2.1 to 4.2 m. The low resistivity zone in between 2.1 to 4.2 m might occur due to the presence of high moisture. A similar trend was observed from Line 2 which is presented in

Figure 3.4 (b). A high resistivity zone was observed for top 2.1 m of soil following a low resistivity zone which was observed in between 2.1 to 3.2 m. Resistivity was less than 5 Ohm-m in this zone. However, resistivity was more than 5 Ohm-m from 3.2 m to 8.2 m. A reduction in resistivity was observed in a few locations below 8.2 m depth.
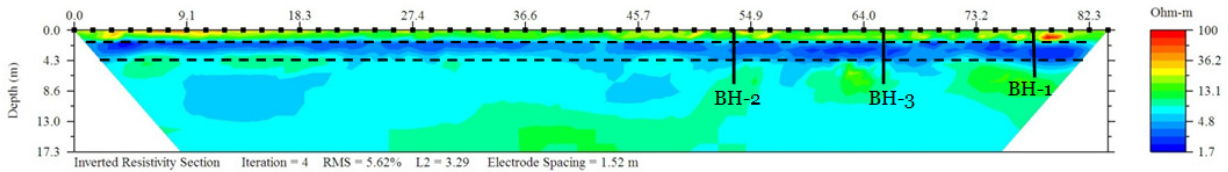
(a)
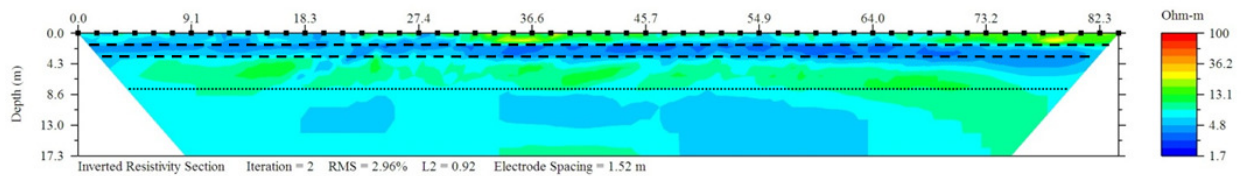
(b)

Figure 3.4 Resistivity Imaging results for (a) line 1 and (b) line 2

A total of 3 (three) boreholes were drilled at the crest of the slope which is presented in Figure 3.5. Soil sampling and Texas Cone Penetrometer (TCP) tests were conducted at borehole locations. The predominant strata below the slope surface were a dark brown high plasticity clay with calcareous nodules. The clay layers are sometimes interlayered with yellow brown clay. A thin layer of crushed limestone was also observed during test boring and hand boring at several location of the slope within top 1-1.5 m of the slope. The upper part of the slope was rich in cracks and fissures. The maximum width of the open cracks measured was about 50 mm at the crest of the slope.
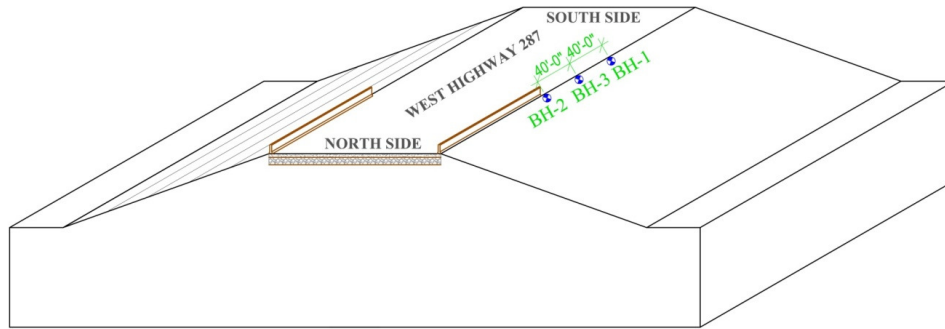
Figure 3.5 Soil test boring location

The moisture content of the collected soil samples from three boreholes is presented in Figure 3.6. It was observed that moisture content of the soil samples collected from BH-1 ranged from 20.2% to 32.6%. Moisture content was in between 18.7% to 36.6% for the samples collected from BH-2. In BH-3, moisture content ranged from 15% to 33.3%.
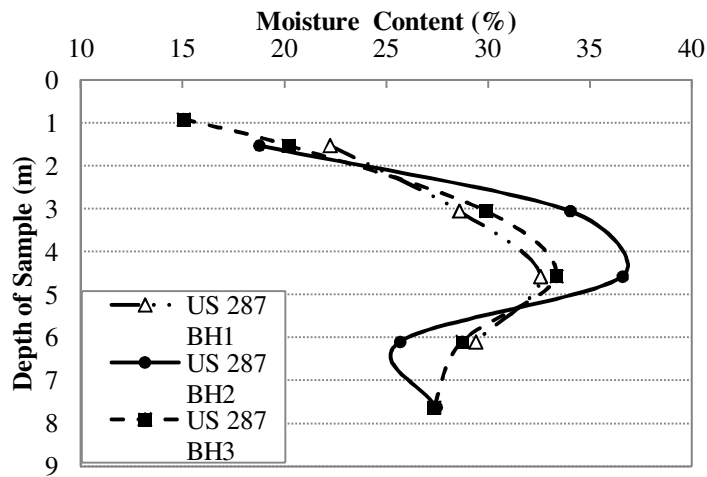
Figure 3.6 Variation of moisture content along boreholes

Figure 3.6 shows that the variation in moisture content followed similar trend for the soil samples collected from different boreholes. Moisture content increased from 1.52 m to 4.5 m.

49

Moreover, moisture content between 1.52 to 4.5 m at BH-2 which falls along the cracked pavement surface is higher than the moisture content along BH-1 and BH-3. RI test results also indicated that resistivity was low in between depth 2.1 m to 4.2 m along the three boreholes which is presented in Figure 3.7. However, moisture content decreased at depths below 4.5 m. This phenomenon was also evident from RI results.
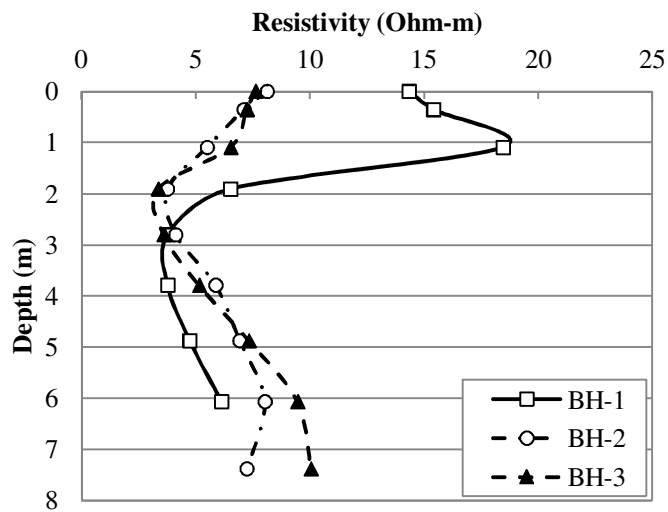
Figure 3.7 Variation of resistivity along boreholes

3.3 Sample Collection and Sample Characteristics

Samples were collected from boreholes at every 1.5 m depth and transported to laboratory where it was stored in humidity controlled room. An experimental program was undertaken to determine the physical characteristics of the collected soil samples which is presented in the following sections.

3.3.1 Grain Size Distribution

The distribution of particle size was determined using wash sieve method according to ASTM D 422-63. The soil was dried at a temperature of approximately 120^0 F, not exceeding 140^0 F according to ASTM D 698-00a so that changes in the soil properties would not occur. Then the bulk soil was crushed and approximately 300 gm of crushed sample was taken for the test. Soil sample was washed with flowing water through No. 200 sieve by allowing water to pass through the soil gently. When clean water came out, the remaining soils were kept in oven for drying. The remaining soils were sieved using #4, #10, #30, #40, #60, #100 and #200 US standard sieve for 10 minutes. The mass of soil retained in each sieve was than measured. Soil passed through No. 200 sieve during wash sieving was then used to conduct hydrometer test according to ASTM D 422-63. Figure 3.3 shows the particle size distribution curve for the collected sample of Eagle Ford Clay.
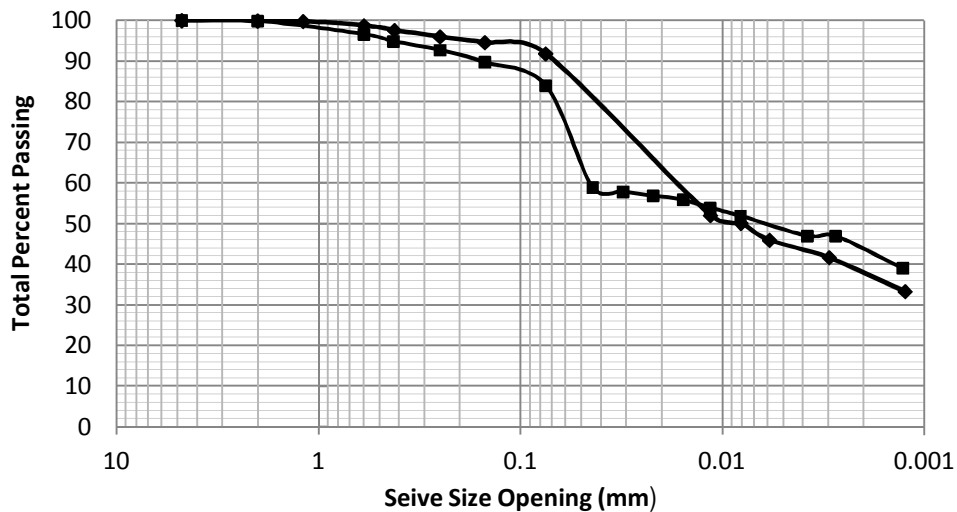
Figure 3.8 Particle size distribution curve for Eagle Ford Clay

3.3.2 Atterberg Limits

Atterberg limits were performed on the on the collected soil samples according to procedures outlined in ASTM D 4318. The Atterberg limits of the samples are presented in Table 3.1. From the sieve analyses and Atterberg limits results soil samples were classified as low to highly plastic clay according to Unified Soil Classification System (USCS). Soil samples collected at depth 1.5 m from BH-1 and BH-2 were classified as low plastic clay (CL). However, soil samples collected from all other depths were highly plastic clay (CH).

Table 3.1 Atterberg Limits of Collected Samples

Bore Hole	Depth (m)	Liquid Limit	Plastic Limit	Plasticity Index
BH-1	1.52	48	23	25
BH-1	3.05	60	27	33
BH-1	4.57	72	24	48
BH-1	6.10	64	26	38
BH-2	1.52	49	23	26
BH-2	3.05	67	29	38
BH-2	4.57	73	28	45
BH-2	6.10	61	26	35
BH-2	7.62	62	25	37
BH-3	1.52	52	25	27
BH-3	3.05	61	27	34
BH-3	4.57	79	28	51
BH-3	6.10	58	26	32
BH-3	7.62	65	25	40

3.3.3 Specific Gravity

Two specific gravity measurements were performed on the fraction of soil passing No. 4 sieve by the water pycnometer method. The specific gravity values from the two measurements were approximately 2.691 and 2.71 for an average of approximately 2.7.

3.3.4 Compaction Curve

Standard Proctor compaction tests were performed according to ASTM D 698-00a to determine the relationship between moisture content and dry unit weight of collected sample (Figure 3.9). The Standard Proctor optimum moisture content is approximately 21.05% with a corresponding dry unit weight of 15.3 kN/m^3. The in situ dry unit weight of the sample is 14.18 kN/m^3. The water content on the dry side and wet side of the compaction curve for in situ unit weight is 18% and 29.5% respectively which is presented in Figure 3.9.
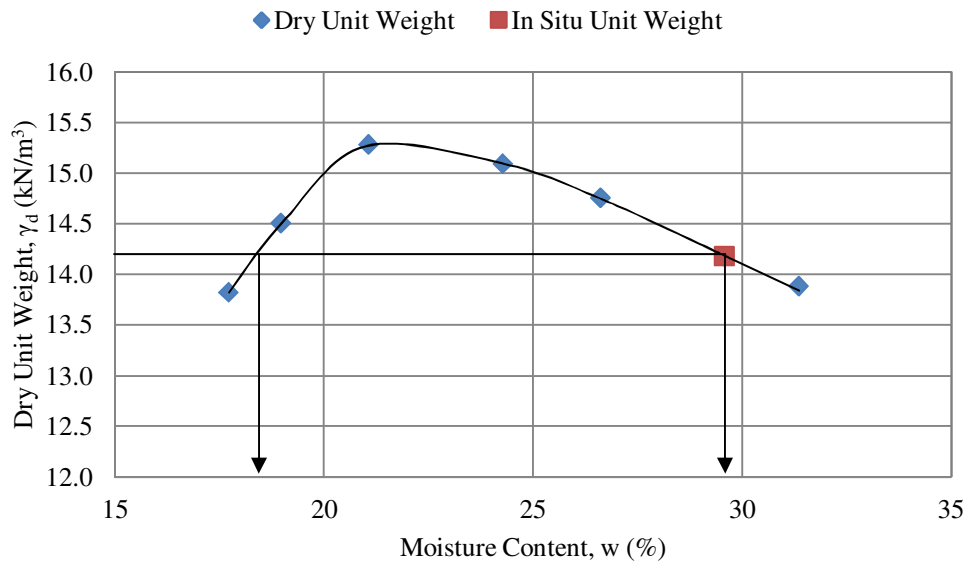
Figure 3.9 Compaction curve for Eagle Ford Clay

3.3.5 Swell Test

One-dimensional swell tests for collected sample were performed in odometer ring for different surcharge condition of 7, 50, 100 and 200 kPa according to ASTM 4546-08. The load was applied on the specimen using dead weight throuhg a loading frame which is presented in Figure 3.10. The specimen was compacted at the in-situ dry density of 14.18 kN/m^3 and a moisture content of 18% (from compaction curve). Results from one-dimensional swell test are presented in Figure 3.11 which shows that the percent expansion of the tested sample at 7 kPa surcharge is approximately 5%. According to Sridharan and Prakash (2000), the soil can be classified as moderate expansive soil. Based on the experimental result, it can be observed that, soil starts to collapse at 70 kPa normal stress upon wetting which is approximately close to 3.8 m depth in the field with total density of 18.5 kN/m^3.
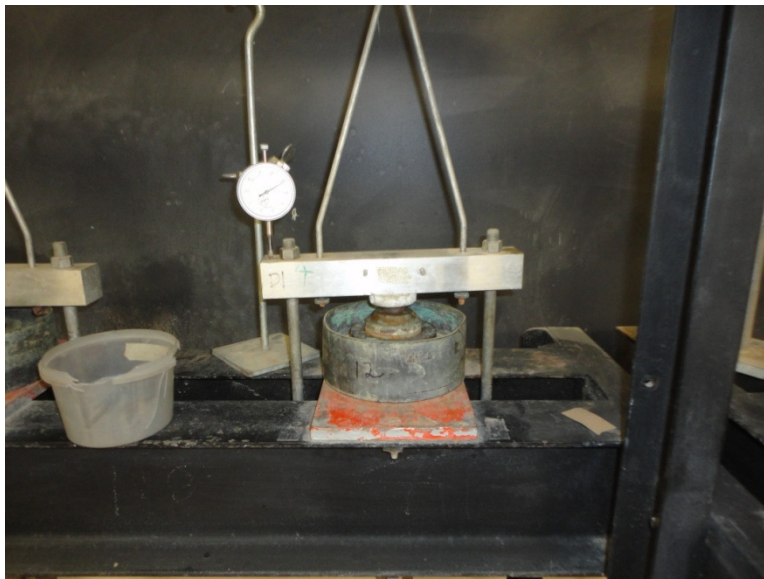
Figure 3.10 Application of surcharge load during swell test
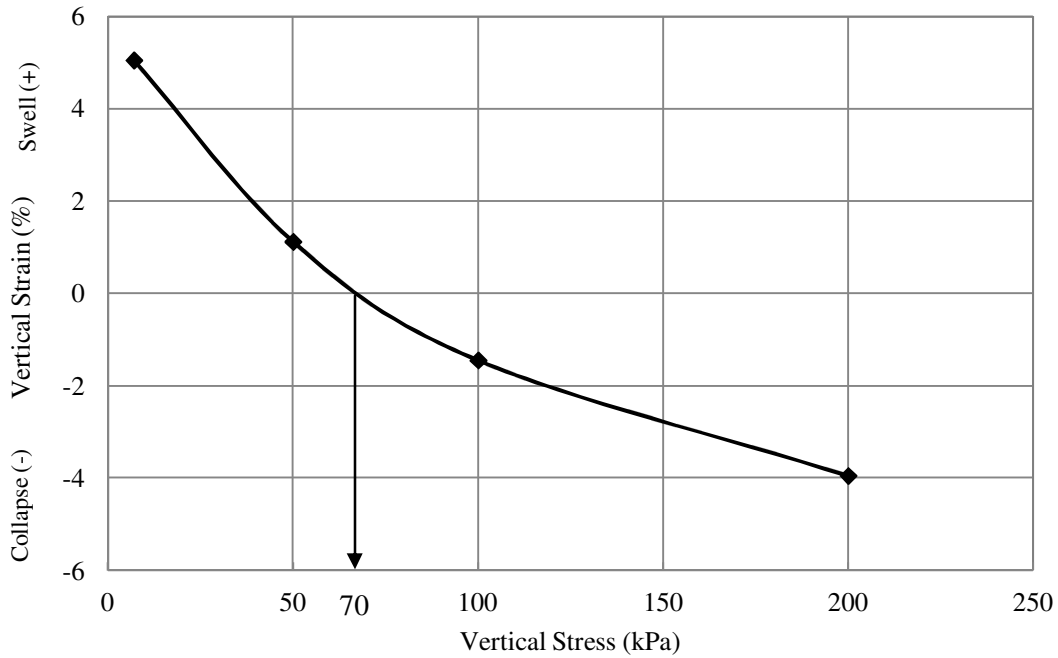
Figure 3.11 Stress versus wetting induced swell/collapse strain

3.3.6 Permeability Test

Two permeability tests were performed using falling head permeameter for the collected samples. The specimens were prepared at the in-situ dry density of 14.18 kN/m^3 and a moisture content of both dry of optimum (18%) and wet of optimum (29.5%). Specimen compacted dry of optimum shows saturated permeability of 1E-7 m/s. On the other hand, specimen compacted wet of optimum yielded a saturated permeability of 3.54E-9 m/s.

3.4 Field Instrumentation

The application of seepage and slope stability analyses requires an understanding of the infiltration amount and its contribution to the moisture content and matric suction changes in the slope which is controlled by soil physical properties and rainfall condition. Moreover, no field

scale investigation was performed to identify the active zone susceptible to strength softening to accurately predict the geohazard potential due to rainfall infiltration. Therefore, it is important to determine the active zone and study the variation of infiltration, moisture content and matric suction due to different rainfall condition through field instrumentation. There have been a few field scale study performed to date to study the effect of rainfall infiltration on the unsaturated expansive soil. Therefore, a detail instrumentation program was undertaken on the slope under this study to determine the active zone and field infiltration behavior of unsaturated expansive clay.

3.4.1 Instrumentation Layout

The instrumentation included soil moisture sensor, water potential probe and a tipping bucket rain gauge. Instrumentation was carried out in the months of November and December of 2010. The layout of the sensors is presented in Figure 3.12. The location and depth of sensors are also presented in Table 3.2. There were two rows of instrumentation for monitoring water content and soil suction (i.e. I1 at the crest and I2 at the middle of the slope). A total of 6 moisture sensors and 6 water potential probes were installed at different depths and locations of the slope. The sensors were then connected to data loggers to obtain continuous reading of the insitu measurement.
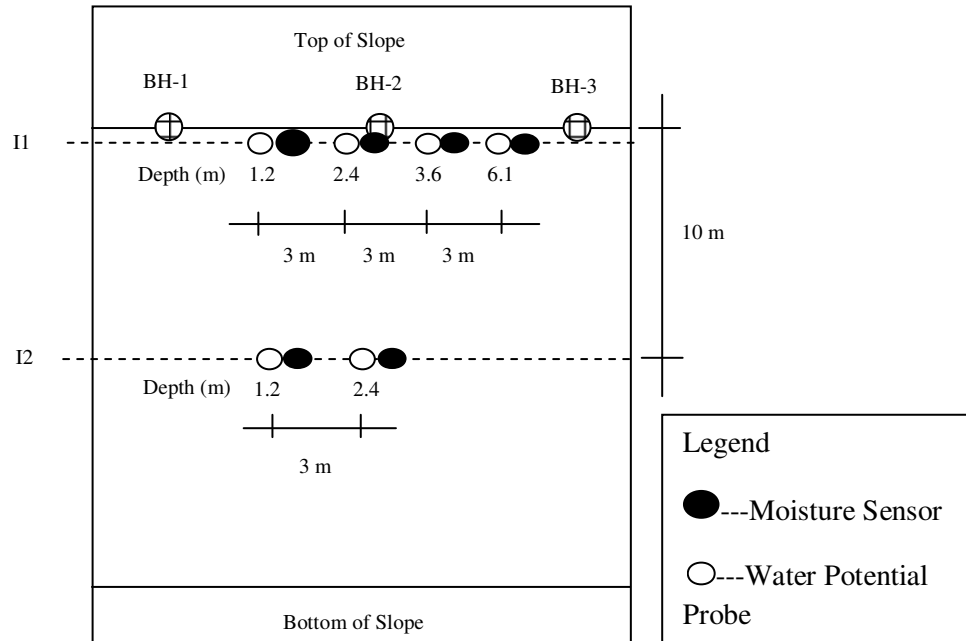
Figure 3.12 Instrumentation Layout

Table 3.2 Instrumentation Detail

Designation	Location	Depth (m)	Sensor Type	No. of Sensors
I1M1.2	Crest	1.2	Moisture Sensor	4
I1M2.4	Crest	2.4	Moisture Sensor	
I1M3.6	Crest	3.6	Moisture Sensor	
I1M6.1	Crest	6.1	Moisture Sensor	
I1P1.2	Crest	1.2	Water Potential Probe	4
I1P2.4	Crest	2.4	Water Potential Probe	
I1P3.6	Crest	3.6	Water Potential Probe	
I1P6.1	Crest	6.1	Water Potential Probe	
I2M1.2	Middle	1.2	Moisture Sensor	2
I2M2.4	Middle	2.4	Moisture Sensor	
I2P1.2	Middle	1.2	Water Potential Probe	2
I2P2.4	Middle	2.4	Water Potential Probe	

3.4.2 Soil Moisture Sensors

Model EC-5 soil moisture sensors were used to measure the volumetric water content of the soil. The sensor has two probes separated from each other which can be directly pushed into the soil. The overall dimension of the probes is 8.9 cm x 1.8 cm x 0.7 cm. The sensor measures the dielectric constant of the surrounding medium in order to find its volumetric water content. It can measure volumetric water content from 0-100% within accuracy of ±2%. A picture of the EC-5 soil moisture used for this study is presented in Figure 3.13.

Figure 3.13 EC-5 soil moisture sensors

Four moisture sensors were installed at depths of 1.2, 2.4, 3.6 and 6.1 m at the crest of the slope near the edge of the shoulder. Two more moisture sensors were installed at depths of 1.2 and 2.4 m at the middle of the slope. To install the moisture sensors, six separate boreholes of 100 mm diameter were drilled using a hand auger. Each of the boreholes was installed with one moisture sensor and one water potential probe. All the boreholes were spaced 3 m apart at each location (Figure 3.12). The depth of the boreholes was limited to the depth of sensor installation. After installing the sensors at the bottom of the borehole, it was backfilled with the in situ cut

soil. Some pictures of the field work during installation of the sensors in presented in Figure 3.14.

(a)

(b)

Figure 3.14 (a) Performing hand boring prior to installation of sensors, (b) Installation of moisture sensor into the borehole

3.4.3 Water Potential Probes

Model MPS-1 water potential probes were used to measure the matric suction of the soil. The water potential probe consists of a porous ceramic disc with overall dimension of the probe is 7.5 cm x 3.2 cm x 1.5 cm. The sensor uses the technique which introduces a known material with static matrix of pores into the soil and allows it to come into hydraulic equilibrium according to the second law of thermodynamics. As the two materials are in equilibrium, measuring the suction of the material gives the suction of the surrounding soil. The water potential probe uses the same principle, but instead measures the dielectric permittivity of the porous ceramic disc to determine its suction. The sensor MPS-1 can measure only the matric suction of the surrounding soil and is limited to suction measurements of -10 to -500 kPa. A picture of the MPS-1 water potential probe is presented in Figure 3.15.

Figure 3.15 MPS-1 Water Potential Probe

Four probes were installed at depths of 1.2, 2.4, 3.6 and 6.1 m at the crest of the slope near the edge of the shoulder. Two more probes were installed at a depth of 1.2 and 2.4 m at the

middle of the slope (Figure 3.11). To install all the water potential probe, six separate boreholes of 100 mm diameter were drilled using a hand auger. Each of the boreholes was installed with one moisture sensor and one water potential probe. All the boreholes were spaced 3 m apart at each location. The depth of the boreholes was limited to the depth of sensor installation. After installing the sensors at the bottom of the borehole, it was backfilled with the in situ cut soil.

3.4.4 Data Acquisition System

After the installation of all sensors, the lead wires from the sensors were connected to an automatic data acquisition system to monitor the moisture content, matric suction and rainfall intensity on a continuous basis. A total of 3 (three) Em-50 data logger (Figure 3.16) were set up in the field to accommodate all the sensors. The Em-50 is a 5 port, self contained data logger which can measure the data in a continuous interval. The measurement interval for the current study was set to 60 minutes which allowed storing 24 data per day. The finished instrumented site is presented in Figure 3.17.

Figure 3.16 Em-50 Data logger
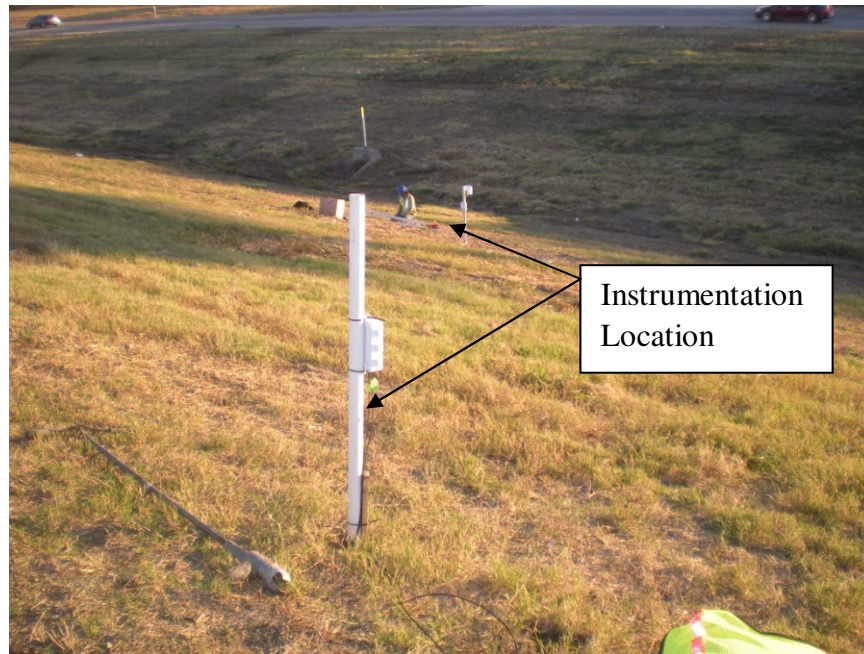
Figure 3.17 Instrumentation locations after installation

3.5 Experimental Program

An experimental program was developed to determine the soil water retention characteristics of expansive clay at field dry density which will be used to model the infiltration behavior due to different rainfall condition. To determine the shear strength of unsaturated expansive clay ring shear tests were performed at different suction level based on the field instrumentation results obtained. Finally, the softening behavior due to wetting and drying was evaluated based on the direct shear test on the saturated specimen. The results from laboratory testing and field instrumentation was combined with numerical modeling to study the effect of rainfall infiltration and associated geohazard potential of slope constructed on expansive clay.

3.5.1 Soil-Water Characteristic Curve (SWCC)

The SWCC defines the relation between matric suction and water content of the soil (Fredlund 2006). The parameters obtained from the SWCC can give a significant measure to understand the behavior of unsaturated soil. SWCC is usually determined in the laboratory without applying any vertical stresses to the specimen. But the phenomenon is different in the field where soil usually has a complex stress history. Therefore, to correctly predict pore-water pressure distributions and its effect on slope stability, it is essential to investigate the influence of stress state on SWCC. In this section, the experimental design to identify the influence of stress state on SWCC of Eagle Ford Clay is presented by using a newly modified Tempe cell in which the total net normal stress can be controlled one-dimensionally and axial deformation is measured.

3.5.1.1 Equipment Design

An apparatus for measuring state dependent soil-water characteristic curve of Eagle Ford clay under K_o stress condition was developed by modifying a conventional Tempe cell (TC) which is presented in Figure 3.18. The equipment uses axis translation technique to measure the matric suction of the soil specimen. A schematic diagram of the apparatus is also illustrated in Figure 3.19.
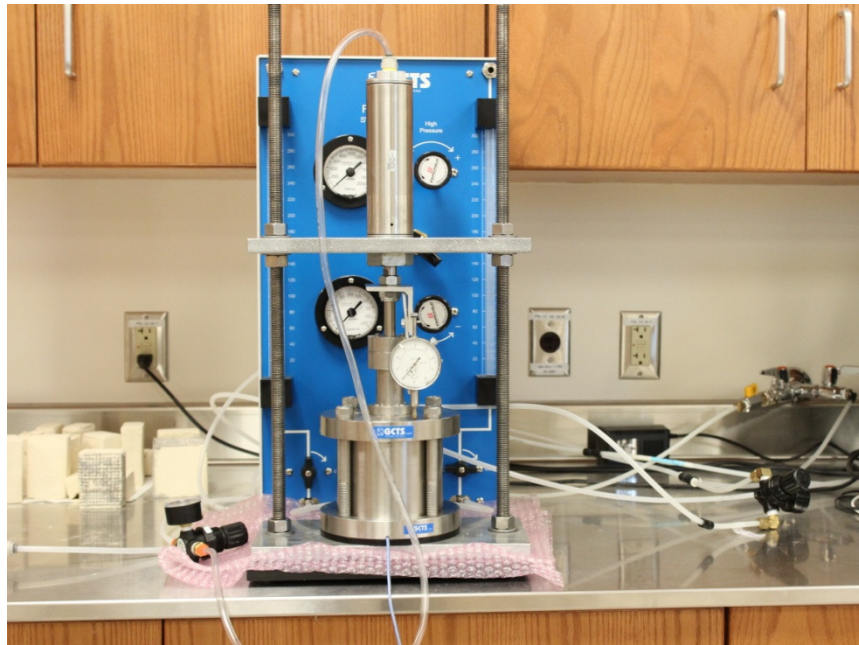
Figure 3.18 Modified Tempe Pressure Cell
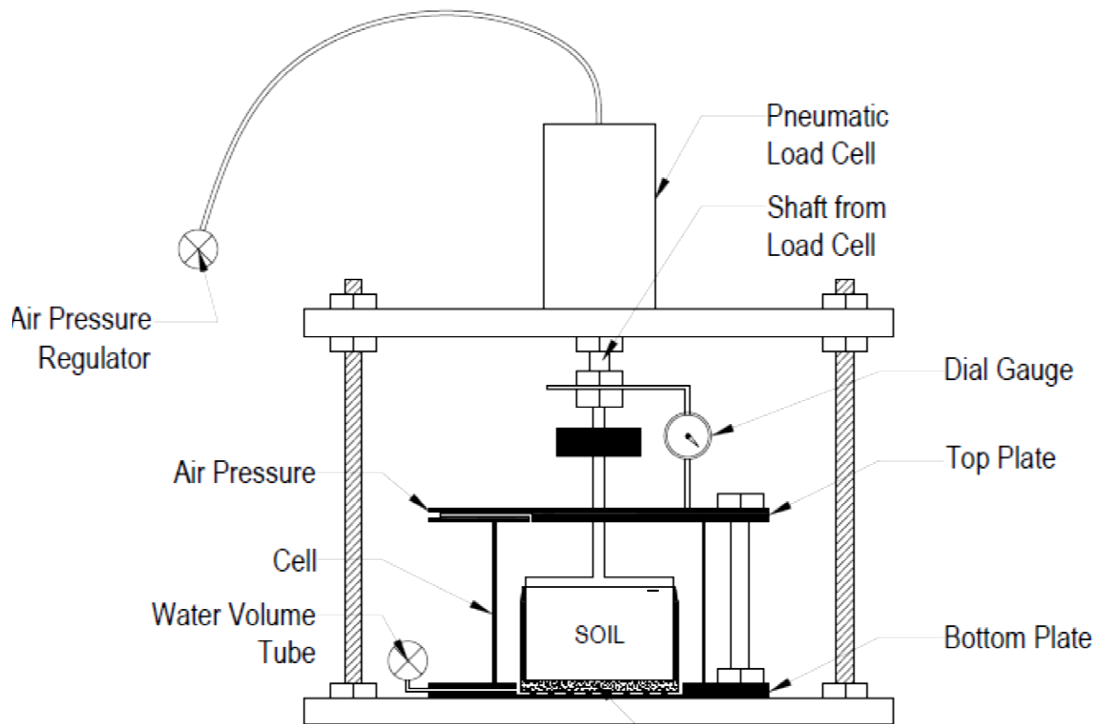
Figure 3.19 Schematic diagram of modified Tempe cell

A stainless steel loading frame was manufactured at UTA machine shop to accommodate the Tempe cell inside the frame and for application of the vertical load. A pneumatic loading piston was attached at the top plate of the loading frame to apply the vertical load through the load shaft of the Tempe cell to the specimen. The top of the pneumatic cell was attached through a pressure regulator with the air supply system. A dial gauge was attached with the load shaft of the piston using an L-shape steel angle to register volume change of the specimen during the test.

A retaining ring with three legs was manufactured from stainless steel at UTA machine shop to accommodate a soil specimen of 62 mm inside diameter and 23 mm height. The picture of the ring is presented in Figure 3.20. The legs with same dimension were attached with the ring to ensure avoiding any eccentricity during load application. Its rigid wall is used to maintain K_o stress conditions. Vertical stress (σ) was applied through the loading frame to a soil specimen inside the ring.

Figure 3.20 Retaining ring for SWCC measurement

The pneumatic loading piston (Model-Speedaire WP595048 M) used for this study was supplied by Grainger with a maximum capacity of applying 250 psi vertical pressure. The piston was calibrated before initiation of any test using a load cell (LM 317) supplied by OMEGA. The calibration procedure of the piston is illustrated in Figure 3.21. During calibration, the load cell was attached at the bottom plate of the loading frame and the piston was mounted at the top of the load cell. The top of the piston was connected with the main air supply system of the building through a pressure regulator. Successive increment of air pressure was supplied using the pressure regulator to the piston and the applied load on the load cell was measured for each increment. Data acquisition was carried out using Advantech Adams 4018 and 4017 cards (Cruz et al., 2011). Finally, the input pressure (kPa) was plotted against the output load (N) to complete the calibration of the piston which is presented in Figure 3.22.
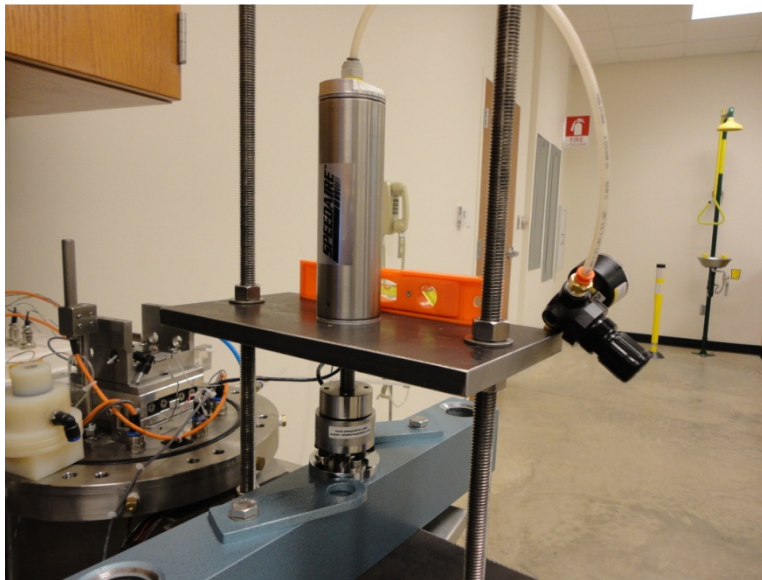
Figure 3.21 Illustration of calibration procedure
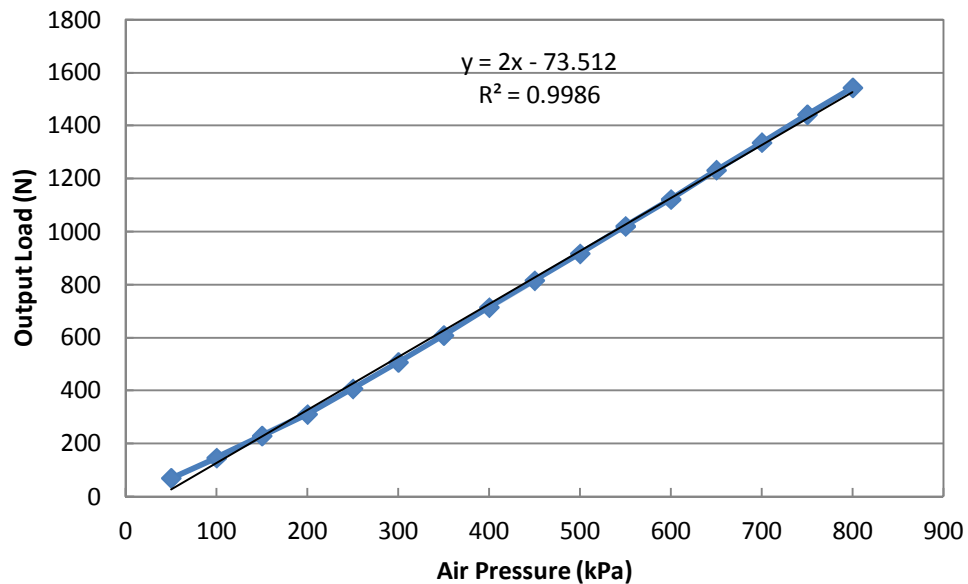
Figure 3.22 Calibration of Pneumatic Loading Piston

3.5.1.2 Test Program

The testing program undertaken for this study was to evaluate the influence of different stress state and initial water content on the SWCC which is presented in Table 3.3. The SWCCs were measured only following the desorption path and sorption was not taken into account in this study. To identify the influence of stress state, four different net normal stresses ($\sigma - u_a$) of 0, 25, 50 and 100 kPa were considered. Two initial water contents, one is on the dry side (18%) and the second one is on the wet side (29.5%) of the optimum water content, were selected. The dry density of all the samples was kept constant to 14.18 KN/m^3 to achieve the field dry density that was observed during site investigation.

Table 3.3 Testing Program for soil-water characteristics

Initial Water Content (w%)	Dry Density, γ_d (kN/m^3)	Net Normal Stress, (kN/m^2)	Number of Test
18	14.18	25	3
		50	
		100	
29.5	14.18	25	3
		50	
		100	

3.5.1.3 Sample Preparation

The soil was air-dried for several days, pulverized and passed through a US # 10 sieves. A prescribed amount of distilled water was sprayed on the air-dried sample in several layers to achieve the desired initial water content. The soil was then thoroughly hand mixed and placed in humidity controlled room in a plastic bag for at least 48 hours to allow uniform moisture distribution.

All samples for the testing program were statically compacted to 72 mm in diameter and 40 mm in height using a conventional triaxial loading frame (Figure 3.23). The samples were prepared in a single layer in a constant volume mould to achieve the required initial condition of water content and dry density. A compaction displacement rate of 1.25mm/min was adopted in order to minimize the potential for fabric variations throughout the sample (Venkatarama, 1993). A specimen of 62 mm in diameter and 23 mm in height was cut from the compacted sample to accommodate in the retaining ring (Figure 3.24).
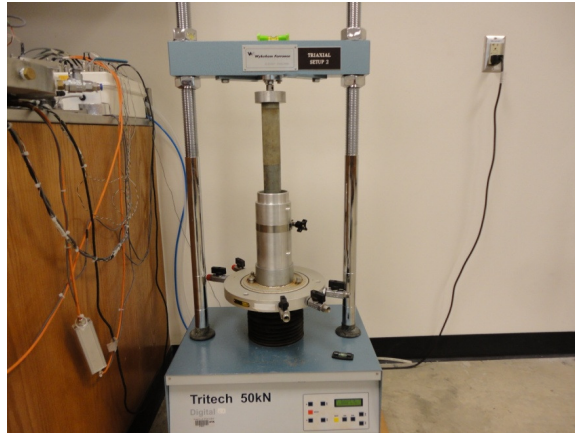
Figure 3.23 Preparation of specimen using static compaction process
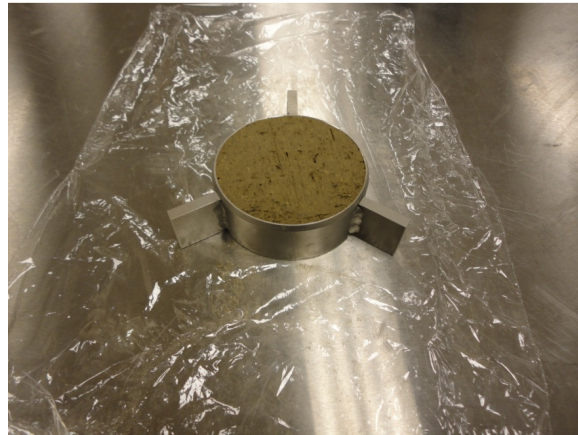
Figure 3.24 Prepared specimen for SWCC measurement

The specimens prepared from the compaction, were than inundated in distilled water for saturation. Before inundation, one filter paper and one porous stone were placed at both side of the specimen (Figure 3.25, a). The porous stones were fixed to the sample with two perforated plates in order to allow drainage at top and bottom and attached by four screws, in order to prevent any volume change (Figure 3.25, b). The specimens were left submerged in distilled water for 72 hours to allow full saturation (Figure 3.25, c). The degree of saturation was close to

99 % which was verified at the end of the process. It can be reasonably assumed that the initial condition is essentially corresponds to zero matric suction.

<center>(a)   (b)   (c)</center>
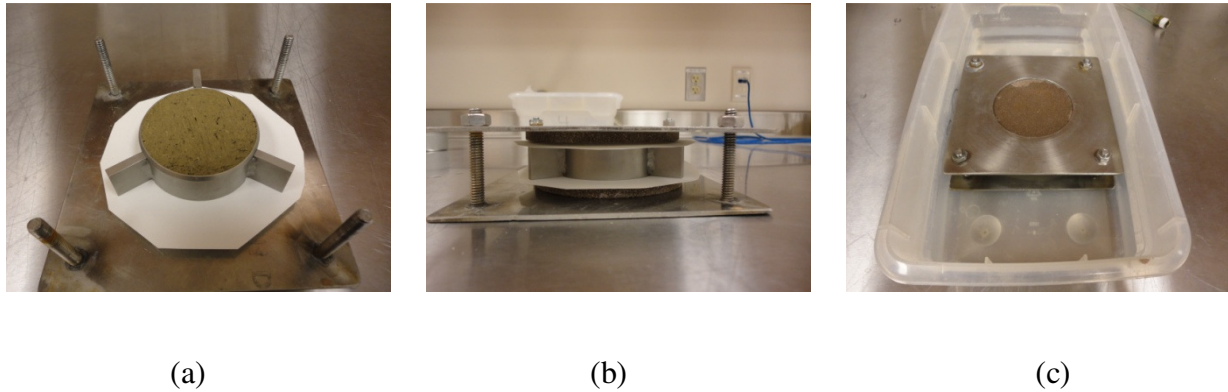
Figure 3.25 Saturation of the specimen, (a) placement of filter paper and porous stone, (b) attaching perforated steel frame and (c) inundating in distilled water.

3.5.1.4 Saturation of Ceramic Disc

During the specimen preparation, the ceramic discs (15 bar) in the Tempe cell were saturated in order to achieve continuity between the pore water and water in the compartment beneath the ceramic discs which will also prevent any air passage through the ceramic discs. The ceramic discs attached at the bottom plate of the cell were inundated with deaired water and the top plate was attached with the screw. Then, an air pressure of 200 kPa was applied to the system and left for 24 hours in order to remove any air bubbles inside the voids of the ceramic discs. During the air pressure application, the connection to the water volume tube at the bottom plate was kept open to allow full drainage.

3.5.1.5 Test Procedure

Once the saturation of both specimen and ceramic discs were completed, the specimen with the retaining ring was placed on top of the ceramic disc at the bottom plate of the cell. A

loading cap was placed at the top of the specimen to apply vertical load from the loading piston (Figure 3.26a). Then the top plate was attached with screws to make the cell air tight and the load shaft of the piston with the attached dial gauge was brought into the position to apply vertical load (Figure 3.26b). Before the test, any possible leakage of the system was examined thoroughly.
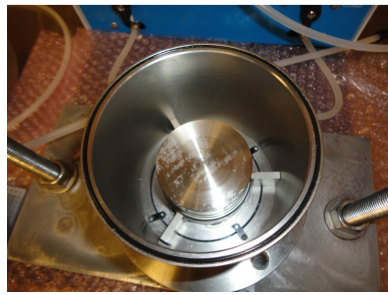
(a)
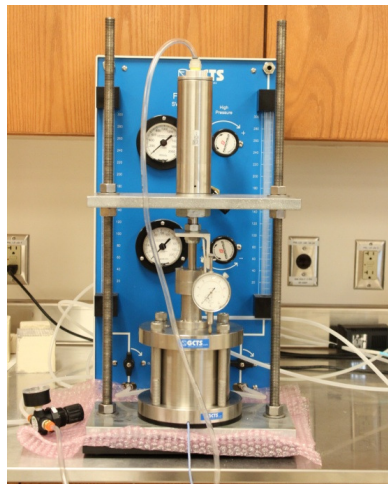
(b)

Figure 3.26 Illustration of test assembly

After the full assembly of the testing system, the outflow collection system connected to the two water volume tube was flushed to remove any air bubbles. Only one water volume tube was monitored for water level change and the other one was kept closed during testing except to flush the system. The desired net normal stress (ex. 25 kPa) was then applied to the specimen through the piston and left for consolidation for approximately 12 hours or when the volume change stopped. After consolidation was done, the initial air pressure (ex. $u_a - u_w = 50$ kPa) was applied into the cell and outflow readings were recorded in the water volume tube until no outflow was observed which indicates that the specimen is in equilibrium with the applied pressure. However, once the air pressure was applied, the normal stress was also increased to obtain the desired net normal stress. For an example, if the desired net normal stress is 25 kPa and the applied air pressure is 50 kPa than to maintain the net normal stress, the total normal stress is increased to 75 kPa. This generally required 2-3 days for each range of pressure. Once the equilibrium is established a higher pressure was applied and outflow readings were monitored. This method only allowed obtaining the SWCC for suctions below 450 kPa because of the limited of air pressure supply (800 kPa) in UTA civil engineering laboratory building. As a result, filter paper technique was used to complete the SWCC curve for the specimens.

During the test, the system was flushed twice a day to avoid accumulation of any air bubble which can affect the volume change readings. The change in water content of the sample at each stage of pressure application was calculated by measuring the water volume that passes through the ceramic disk. After long testing periods the diffused air accumulates underneath the ceramics and introduces an error in either the pore water pressure measurements in constant water content tests or in the pore water volume change in drained tests. Padilla et al. (2006) also

stated that the accumulation of diffused air can lead to the possible dry out of the ceramic, retarding flow of water through ceramic disks and causing impedance of the hydraulic conductivity of ceramics. The author concluded that, air diffusion through 15 bar ceramic disks is considerable as compared to the 5 bar or 3 bar ceramics, even at 50% of the rated bubbling pressure. Therefore, the author suggested flushing the system twice or more a day to avoid any accumulation of air bubbles.

3.5.1.6 SWCC using Filter Paper Technique

Matric suction was measured by filter paper technique (FP) following the procedure recommended by Ridley et al. (2003). According to the authors this procedure has been used with great success for many years and the results present high repeatability. The procedure involved placing an initially dry filter paper (Whatman N. 42) on each side of the sample and covering the system with a disk of Plexiglas in order to guarantee a perfect contact between the sample and the filter paper. After that, the sample and the disks were covered and sealed by several layers of cling film and tape. The covered sample was then placed in a sealed glass jar and stored for 7 days in a temperature controlled room. After the equilibrium time is reached, the filter papers were removed with a pair of tweezers and placed in a small can with closed lid instead of plastic bag that has been originally proposed by Ridley et al. (2003). The water contents of the filter papers were determined using a balance sensitive up to 0.0001 g. The filter papers were than dried in the oven for at least 10 hours at 110 $^\circ$ C with the lid half open (Bulut et al., 2001). The samples were air-dried for a couple of hours until the next desirable water content state was reached and the process was repeated. During the all stages of the suction measurement the filter paper was always handled with a pair of tweezers and the filter paper was placed in can

73

as quickly as possible. The complete assembly of the filter paper technique is shown in Figure 3.27.

Figure 3.27 Filter paper testing assembly

The procedure described above for measuring suction was repeated every week until the sample reached an air-dry condition. This occurred when the water content of the filter paper reached equilibrium with surrounding atmosphere at suction of approximately 30 Mpa.

Several relationships between the filter paper, water content and suction have been developed for different filter paper brands by different researchers. In the present work, the calibration curve for Whatman N. 42 recommended by ASTM D5298-03 was used. This calibration curve is presented as follows:

$$\log(\psi) = 5.327 - 0.0779\, w\,, for\ w < 45.3\% \qquad (3.1)$$

$$\log(\psi) = 2.412 - 0.0135w, for\ w \geq 45.3\% \qquad (3.2)$$

Where,

ψ = matric suction

w = filter paper water content (%)

3.5.1.7 Equations to Best Fit SWCC Laboratory Data

There are several empirical, closed-form equation has been proposed to best-fit the soil-water characteristic curve. All these equations can be divided into two parameter equations and three parameter equations (Fredlund, 2006). Each of the proposed equations has one variable which is related to the air entry value of the soil and the second variable is related to the rate at which soil desaturates. The third variable allows the low suction range near the air entry value to have a shape that is independent of the high suction range near residual condition. In this research, two models were used to fit the SWCC data which are discussed below.

<u>Van Genuchten Model, VG (1980)</u>

The *Van* Genuchten equation (Eq. 3.3) has three fitting parameters denoted by α, n and m

$$\Theta = \frac{\theta - \theta_r}{\theta_s - \theta_r} = \left\{ \frac{1}{[1 + (\alpha\psi)^n]} \right\}^m \qquad (3.3)$$

where the parameter α is related to the inverse of air entry value, the parameter n is related to the pore size distribution of the soil and the parameter m is related to the symmetry of the curve. The parameter m is frequently set equal to (*1-1/n*) which reduces the flexibility of the equation but

results in greater stability during fitting. Soils with steeper SWCC are characterized by smaller n and soils with higher air entry suction values are characterized by smaller α values.

3.5.1.8 Model to Predict Permeability Function

There are several empirical and statistical, closed-form equations have been proposed to derive the hydraulic conductivity function based on the soil water characteristic curve and conductivity at saturation. All these equations can be divided into two or three parameter equation. First two parameters are related to the air-entry value and desaturation rate from the SWCC and the third parameter is related to the results near the residual content. In this research, model proposed by Maulem (1976 a) has been used to determine the hydraulic conductivity function which is presented below:

$$k_r(\psi) = \frac{\{1 - (\alpha\psi)^{n-1}[1 + (\alpha\psi)^n]^{-m}\}^2}{[1 + (\alpha\psi)^n]^{0.5*m}} \qquad (3.4)$$

3.5.2 Suction Controlled Ring Shear Testing

The purpose of this experimental program is to determine the shear strength characteristics of unsaturated high plasticity clay (CH) with expansive behavior at both peak and residual condition. The novel suction controlled ring shear (RS) device was used in this work for testing unsaturated soils using the axis-translation technique. The novel ring shear device features two independent servo-controlled actuators: a pneumatic actuator for applications of normal loads and an electromechanical rotary actuator for application of torque loads and rotary motion. It allows the application of vertical loads up to 8000 N, monotonic torque up to 113 N-

m, constant suction states up to 500 kPa, and more than 360-degree range of continuous angular deformation.

3.5.2.1 Components of RS Device

The general design of the RS device is based upon the original design concept introduced by Bromhead (Gamboa, 2011), in which the soil specimen seats inside the annular space formed between two concentric rings of a lower rotational cell. The RS device is composed of three main modules as shown in Figure 3.28.
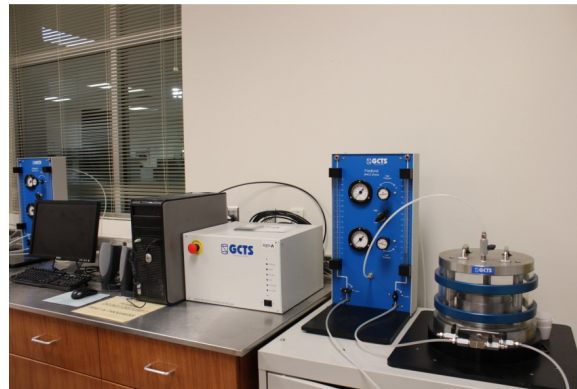
Figure 3.28 Complete Suction Controlled Ring Shear Test Layout

The main cell houses the rotational shear system including normal load and torque actuators. An isometric view of the main cell is presented in Figure 3.29, featuring all of the following: (1) Top cover plate; (2) Core confining cell with a 1500-kPa air pressure capacity; (3) Bottom base plate; (4) Adjustable stainless steel upper annular platen; (5) Stainless steel lower annular platen; (6) Vertical load shaft; (7) Self-contained electrical sensors for real time calculations of vertical load and shear torque; (8) Rotary servo-controlled actuator for application of torsional loads up to 820 N-m; (9) Pneumatic servo-controlled actuator for application of

vertical loads up to 8000 N; and (10) Linear variable differential transducer (LVDT) for monitoring of vertical deformations.
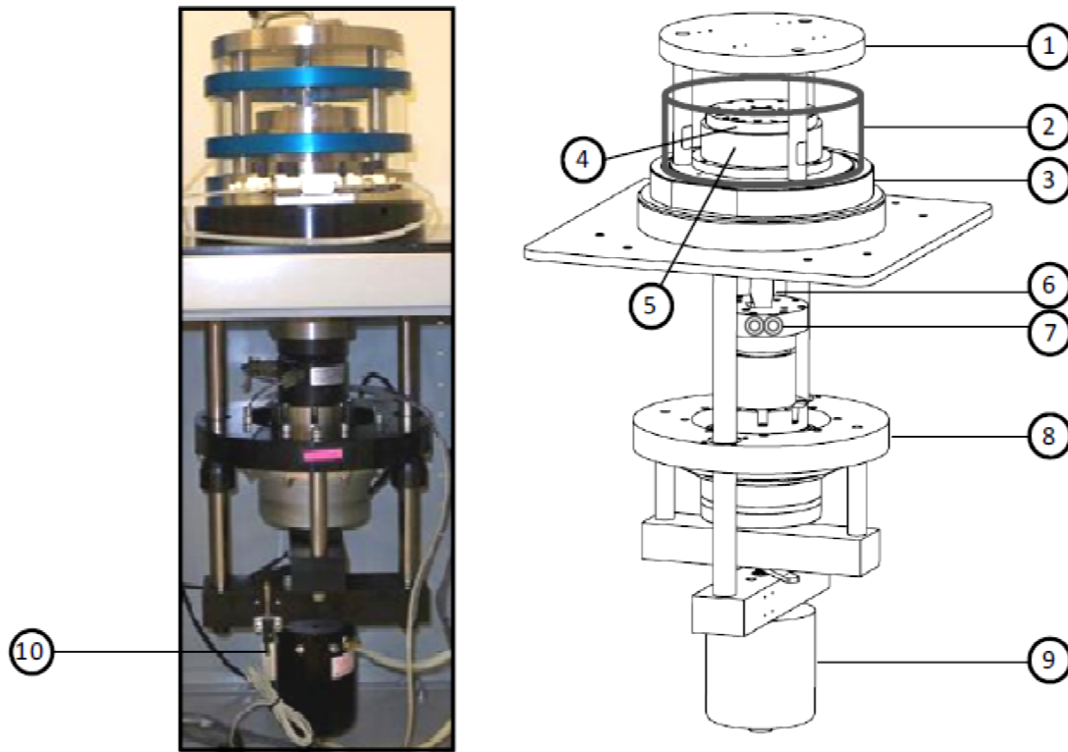
Figure 3.29 Isometric view of main cell and servo-controlled normal load and torque application system (Velosa, 2011)

Data acquisition and process control (DA/PC) system allows the real time calculation of normal and shear stresses and average linear and angular displacements. The data acquisition and process control system, as shown in Figure 3-30, consists of all of the following: (1) One SCON-1500 digital servo controller and acquisition system; (2) GCTS CATS software for real time measurement/control of normal stress, shear stress, and angular deformations; and (3) IBM-PC unit.

Figure 3.30 Data acquisition and process control system

A Model PCP-15U pressure control system (from Geotechnical Consulting and Testing Systems) is used for direct control of pore-air pressure at the top of the soil specimen, featuring dual pressure regulators and gauges for precise measurement and control of matric suction using axis-translation technique. Air pressure is directly supplied to the main cell from the PCP-15U panel, as shown in Figure 3.31. A flushing line is also connected to the bottom base plate of the main cell for removal of diffused air during constant-suction RS testing.
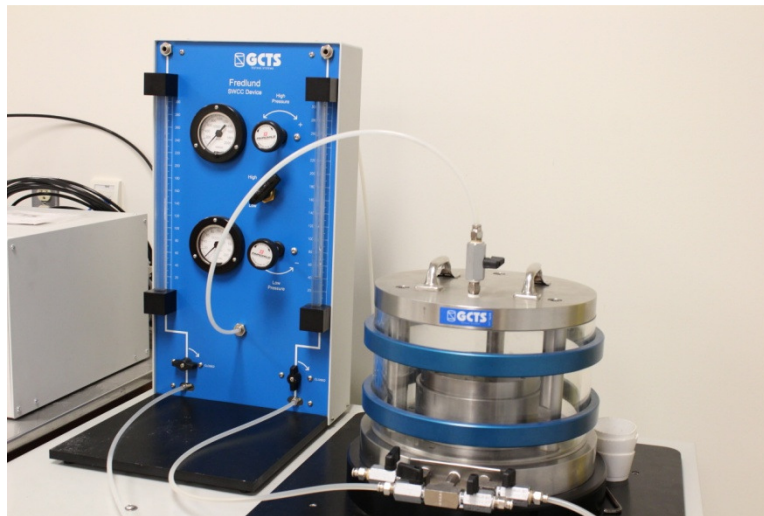
Figure 3.31 PCP-15U suction control panel and RS chamber

3.5.2.2 Test Program

The testing program undertaken for this study was to evaluate the influence of different suction state on the shear strength of unsaturated Eagle Ford clay which is presented in Table 3.4. Tests were performed on the collected samples of Eagle Ford clay from the failed slope along US Hwy 287 S. From field instrumentation results, it was found that typical field suction values ranges between 10 – 400 kPa in shallow depth. The purpose of the RS test program was to simulate the field condition. However, due to limitation of the high air-entry ceramic disks (5 bar), limited air pressure supply (800 kPa) and limited capacity of the Torque (113 N-m) generated by this RS system, unsaturated shear strength parameters were determined for matric suction up to 100 kPa.

Table 3.4 Suction Controlled RS Test Program

Soil	Test No.	$(\sigma - u_a)$, kPa	$(u_a - u_w)$, kPa	No. of Stages
CH	1	25	uncontrolled suction, at 32 % m/c	2
		50		
	2	25	25	3
		50		
		100		
	3	25	50	3
		50		
		100		
	4	25	100	3
		50		
		100		

3.5.2.3 Test Procedure

The main steps involved in the set up process to the completion of the test are described in this section.

<u>Saturation of Ceramic Discs</u>

The ceramic discs (5 bar) at the bottom annular platen were saturated in order to achieve continuity between the pore water and water in the compartment beneath the ceramic discs which will also prevent any air passage through the ceramic discs. The bottom annular platen was filled with deaired distilled water and fixed to the bottom plate as is shown in Figure 3.32(a). The confining cell was installed and a pressure of 200 kPa was applied which is presented in Figure 3.32 (b). The assembly was left 24 hours under the cell pressure to allow full saturation of the ceramic discs. The ceramic discs were kept under distilled water in between the tests to avoid drying out.
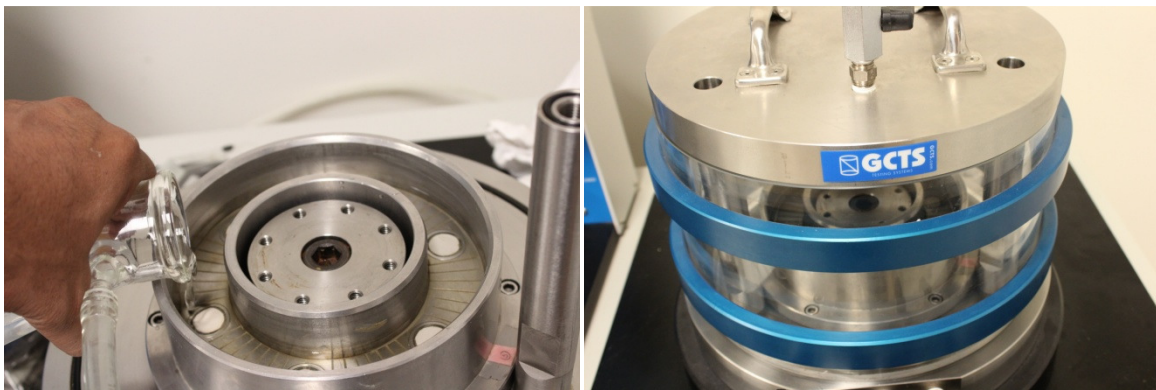
(a)   (b)

Figure 3.32 (a) Application of deaired water in the bottom platen and (b) application of air pressure for saturation of ceramic discs in the confining cell

<u>Sample Preparation</u>

The soil was air-dried for several days, pulverized and passed through a US # 40 sieve to eliminate the calcareous nodules observed in the soil samples. A prescribed amount of distilled water was sprayed on the air-dried sample in several layer to achieve the desired initial water content. The soil was then thoroughly hand mixed and placed in a humidity controlled room in a plastic bag for at least 48 hours to allow uniform moisture distribution.

Soil samples were compacted directly into the lower annular platen using static compaction method to achieve a dry density of 14.15 kN/m^3, the same density which was observed in the field. In this method, compaction was achieved by the monotonic movement of a piston that presses the soil which was confined within the concentric rings of the lower annular platen having a outer diameter of 152.4 mm and inner diameter of 96.5 mm. According to the standard test method for ring shear testing (ASTM D6467-06a), the inside to outside diameter ratio of the tested sample is 0.63. The ring-shaped top platen was used to press the soil down against the lower annular platen. A conventional triaxial loading frame was used to apply the monotonic force as shown in Figure 3.33. The samples were prepared in a single lift at a compaction displacement rate of 1.25 mm/min. The effective surface area of the sample is 10924 mm^2 and the average specimen height is 15 mm.
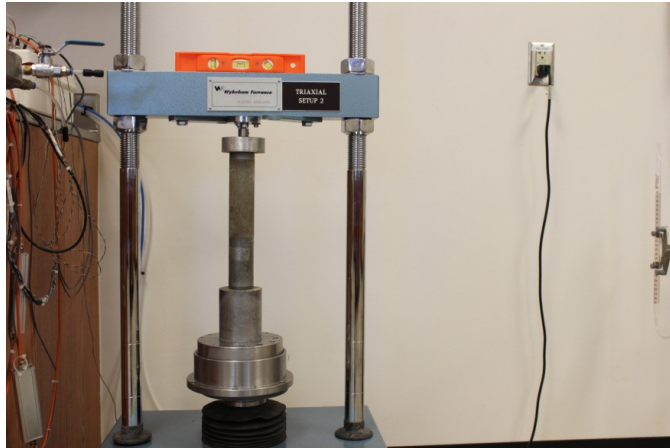
Figure 3.33 Static compaction of ring shaped samples using conventional triaxial frame

RS Assembling Process

After being compacted into the bottom annular platen, the sample was quickly transferred to the ring shear frame in order to minimize evaporation or water loss from the sample. The bottom annular platen was then fixed with the bottom base plate of the ring shear frame. The load shaft was then brought up through the controller and the upper platen was fixed to the top of the piston shaft with six screws. The whole system was flushed to avoid any trapped air in the system. The flushing and volume water indicator of the PCP-15U suction control panel were set in the appropriate positions before the test starts. The confining cell was then installed and the top cover plate was attached with three screws. Finally, the air pressure line from the PCP-15U panel was connected at the top cover plate to apply suction.

Equalization Stage

Once the total RS device is completely assembled, the equipment is ready to perform the programmed test. The first stage of the test prior to shearing is to bring the sample to an initial

net normal stress ($\sigma - u_a$) and a corresponding matric suction ($u_a - u_w$). A vertical load was applied using the upper annular platen to induce a net normal stress. The soil was then allowed to consolidate under this load for at least 24 hours. The desired suction state was then achieved by increasing the pore air pressure (u_a) in the main cell. However, the external normal stress also needed to be adjusted to maintain the constant net normal stress condition. For the current study, the equalization stage was considered to be accomplished when no water volume change was observed.

Shearing Stage

Multi-stage testing scheme was adopted for the current study to perform the suction controlled RS testing. In order to validate the suction controlled multistage testing over single stage, Velosa (2011) performed suction controlled RS test on specimens of SM soil. According to the author, no significant variation was observed between the two testing scheme. After initial consolidation and equalization of the pore fluids to achieve the desired net normal stress ($\sigma - u_a$), the first shearing stage was initiated at a constant angular displacement rate of 0.023°/min equivalent to 0.025 mm/min linear displacement rate which was also reported to be adequate for testing unsaturated clayey soils by Velosa (2011). The adopted displacement rate is also close to the recommended displacement rate for conventional ring shear testing on saturated clays which is 0.024°/min (Meehan et al., 2007). Merchán et al., (2008) also reported that, shearing at a controlled displacement rate equal to 0.32 mm/min is low enough to keep drained conditions based on the test performed on Boom clay. The shearing was continued until a clear residual state had been reached. At this point, shearing was stopped and the net normal stress was further increased to the next corresponding level. The sample was then allowed to consolidate under this

new load until no more vertical soil deformation was registered, while the initial suction state was kept constant. Shearing was then initiated and continued till a new residual state had been reached. The same procedure was followed for the remaining net normal stresses.

3.5.3 Direct Shear Testing on Saturated Soil

In this section, the experimental set up undertaken to determine the fully softened strength of high plasticity clay with expansive behavior is presented and discussed. Based on the previous study on Texas high PI clay, significant strength loss at top few meters of slope (moisture variation zone) has been observed which led to subsequent shallow slope failure (Rogers and Wright (1986), Kayyal and Wright (1991) and Zornberg et al. (2007)). The authors stated that, the fully softened strength is lower than peak strength and greater than residual strength. Therefore, to accurately predict the geohazard potential of a slope failure due to rainfall infiltration, the phenomenon of strength reduction should be considered which led to the current experimental investigation.

3.5.3.1 Test Program

In order to determine the effect of cyclic wetting and drying, three tests were performed on the saturated samples under drained condition at three different normal stress (25, 50 and 100 kPa) using direct shear machine as presented in Table 3.5. Most of the shallow slope failure on high PI expansive clay is limited to top 2-3 meters. Therefore, the range of vertical stress selected for testing was assumed to be sufficient for current study. Rogers and Wright (1986) reported that most of the strength of high PI clay is lost after one cycles of wetting and drying. Therefore, only one cycles of wetting and drying was considered for the current study. However,

85

three different testing procedure was adopted for the current research which will be explained later.

Table 3.5 Direct Shear Test Program

Soil	Test No.	σ, kPa	Wet-Dry Cycle	No. of Stages	Condition
CH	1	25	No	3	Conventional
		50			
		100			
	2	25	1	3	No volume change
		50			
		100			
	3	25	1	3	Volume change
		50			
		100			

3.5.3.2 Sample Preparation

The soil was air-dried for several days, pulverized and passed through a US # 40 sieve to eliminate the calcareous nodules observed in the soil samples. A prescribed amount of distilled water was sprayed on the air-dried sample in several layer to achieve the desired initial water content. The soil was then thoroughly hand mixed and placed in a humidity controlled room in a plastic bag for at least 48 hours to allow uniform moisture distribution.

All samples for the testing program were statically compacted to 72 mm in diameter and 40 mm in height using a conventional triaxial loading frame (Figure 3.34). The samples were prepared in a single layer in a constant volume mould to achieve the required initial condition of water content and dry density. Dry density of all the samples was kept constant (14.15 kN/m^3) to achieve similar initial condition. A compaction displacement rate of 1.25mm/min was adopted

86

in order to minimize the potential for fabric variations throughout the sample (Venkatarama, 1993).
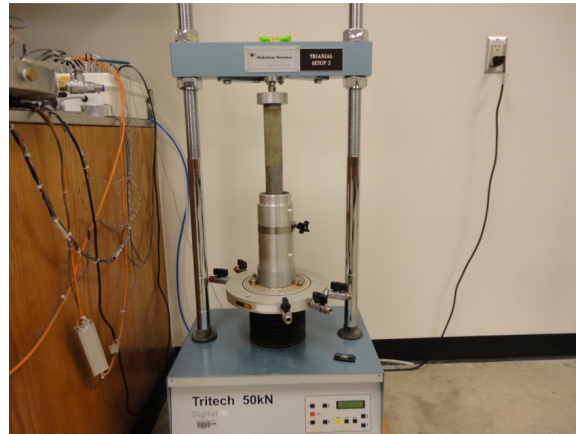
Figure 3.34 Preparation of sample for direct shear test using static compaction process

3.5.3.3 Wetting and Drying Procedure

After the compaction, a specimen of 63.5 mm in diameter and 25.4 mm in height was cut from the compacted sample to accommodate in a stainless steel retaining ring. During Test 2, the specimen was inundated in distilled water for saturation. Before inundation, one filter paper and one porous stone were placed at both side of the specimen. The porous stones were fixed to the sample with two perforated plates in order to allow drainage at top and bottom and attached by four screws, in order to prevent any volume change. The specimens were left submerged in distilled water for 24 hours to allow full saturation. An schematic diagram of the test set up is presented in Figure 3.35.

After the initial wetting phase, the specimen was air-dried for 24 hours and then placed in an oven for 24 hours. The sample was again rewetted for 24 hours to complete one cycles of wetting and drying. Finally, the sample was taken out of the ring and placed in the direct shear

box for testing. During the wet-dry cycle, subsequent weight measurement was taken before and after each cycles to determine the changes in water content. Specimens remained in the frame throughout the each phase of wetting and drying until prior to shearing.
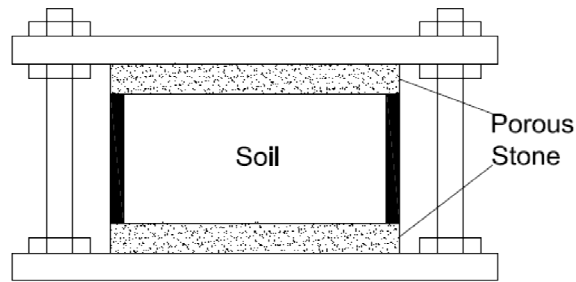
Figure 3.35 Schematic diagram of the test set up for specimens subjected to
wetting and drying (Test 2)

However, test 3 was also conducted following wet-dry cycle, but without restricting the volume change. One filter paper and one porous stone were placed at both side of the specimen. The specimen was then placed on a perforated plate to allow drainage only from the bottom. After the final wetting phase, the sample was trimmed to 1 inch size to accommodate in the direct shear box for testing. An schematic diagram of the set up for test 3 is presented in Figure 3.36.
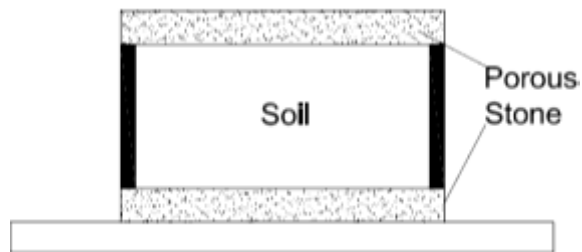
Figure 3.36 Schematic diagram of the test set up for specimens subjected to
wetting and drying (Test 3)

3.5.3.4 Test Procedure

Test specimen was placed in a direct shear box after the final phase of wetting. Multistage testing scheme was adopted for the current study where the samples were consolidated at the initial normal stress for approximately 24 hour. The shearing was then initiated at a constant displacement rate of .025 mm/min which was also adopted in suction controlled ring shear testing and standard displacement rate for testing saturated clay in drained condition according to ASTM D3080. The shearing was continued until a clear residual state had been reached. At this point, shearing was stopped and the normal stress was further increased to the next corresponding level. The sample was then allowed to consolidate under this new load for 24 hours. Shearing was then initiated and continued till a new residual state had been reached. The same procedure was followed for the remaining normal stresses.

CHAPTER 4

RESULTS AND DISCUSSIONS

<u>4.1 Introduction</u>

In this chapter, all the results are presented, discussed and compared with the existing literature. The results from the field instrumentations which include rain gauge, moisture sensors and water potential probes data for a period of 18 months are presented first. The results of the experimental program are then discussed in details. The experimental program undertaken for this study can be divided into the field of both unsaturated and saturated soil. The experimental results from unsaturated soil testing explain the effect of stress state and volume change behavior on soil water characteristic curve and also the effect of matric suction on the shear strength properties of expansive clay. Finally, the effect of wetting and drying on the saturated strength of expansive clay under this study is presented.

<u>4.2 Field Instrumentation Results</u>

4.2.1 Variation of Moisture Content and Matric Suction

Based on the field instrumentation results, the variation of moisture content and matric suction in the slope is presented in Figure 4.1 to 4.6. The study was conducted for a period of 18 months between November 2010 and May 2012 which is discussed in the following sections.

4.2.1.1 Crest of Slope

Variation of in situ moisture content and matric suction profile at 1.2 m depth is presented in Figure 4.1 (a) and (b). The initial moisture content was relatively low (4%) and matric suction was high (-600 kPa). However, a total precipitation of 181.9 mm was observed

(a)

(b)
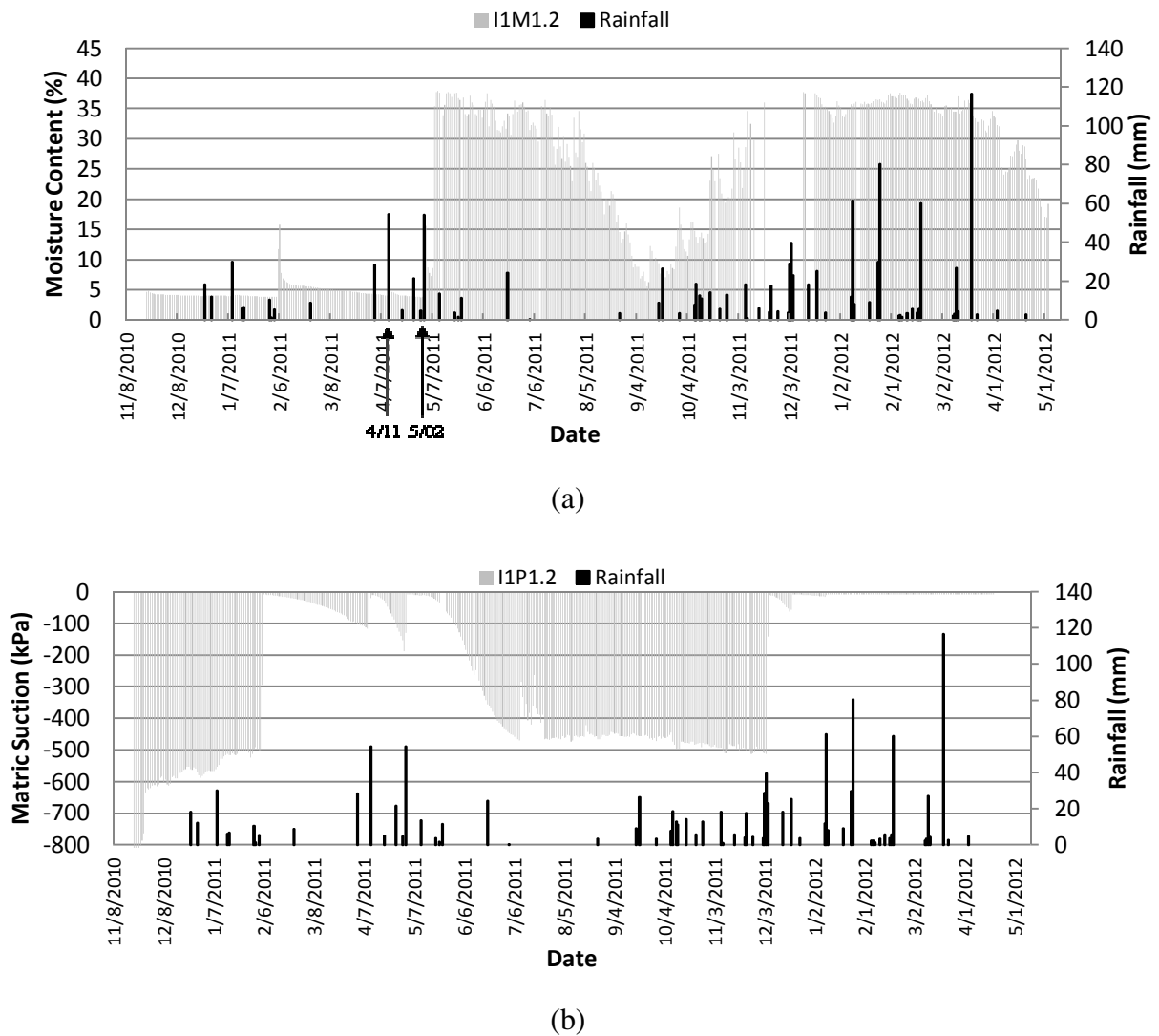
Figure 4.1 In situ variation of (a) moisture content and (b) matric suction at 1.2 m depth
at top of slope

in a period of one month between April and May 2011 with the highest precipitation of 54.2 mm during two rainfall event in April and May. As a result, the moisture content increased to a maximum of 37% and matric suction decreased to -10 kPa. Based on the back calculation of several slope failure constructed on Paris and Beaumont clay, Aubeny and Lytton (2004) suggested that the wet limit of suction at the surface during a slope failure is 2 pF (i.e. approximately -10 kPa).

During the relatively dry summer of 2011, the moisture content decreased gradually from 37% to 10% and accordingly, matric suction increased from -100 kPa to -450 kPa. Therefore, it is clear that, at 1.2 m, variation of moisture content due to rainfall is evident. Moisture content in the soil started to increase with the rainfall observed between September and December 2011 but the suction in the soil remain unchanged. This may be due to change in soil moisture retention characteristic at the upper part because of cracking during dry period. Zornberg et al. (2007) also reported significant change in soil moisture retention characteristics due to formation of cracks in high plasticity clays. The total rainfall observed between this periods was 176 mm with the highest daily observed rainfall of 29 mm. Moisture content at the crest of slope at 1.2 m depth remained closed to 37% between period of January to March 2012 as there was high volume of rainfall observed in this period. The matric suction also remained unchanged to a value of -10 kPa due to large volume of infiltration of rain water during this period. Infiltration of rainwater was also observed to be dependent on the initial matric suction of the soil. During the rainfall event on September 11, 2011, a total of 26.4 mm rainfall was observed but both moisture content and matric suction remains unchanged. The in situ matric suction prior to the rainfall was approximately -450 kPa. On the hand, same of amount of rainfall was registered on December

19, 2011 and a drop in suction was observed from -50 kPa to approximately -10 kPa. The different behavior for the same amount of rainfall may be due to low initial permeability as a result of high initial suction on September 11, 2011. During the rainfall event on December, the initial suction was low which led to higher coefficient of permeability and more infiltration of rainwater into the soil.

The in situ moisture content and matric suction profile at 2.4 m depth is presented in Figure 4.2 (a) and (b). It was observed that the soil was initially wet with a moisture content of 27 % and matric suction of -25 kPa. There was no significant change observed at this sensor location due to different rainfall events throughout the investigating period. During installation of sensors at this location, a limestone layer was observed at 1 m depth which possibly hindered the flow of water into the sensor location. However, the moisture content started to decrease during the dry period which was also reflected through the increase in matric suction. The changes in both moisture content and suction is more gradual compared to the changes observed at 1.2 m depth. The maximum suction observed at 2.4 m depth during the dry period was approximately -230 kPa.
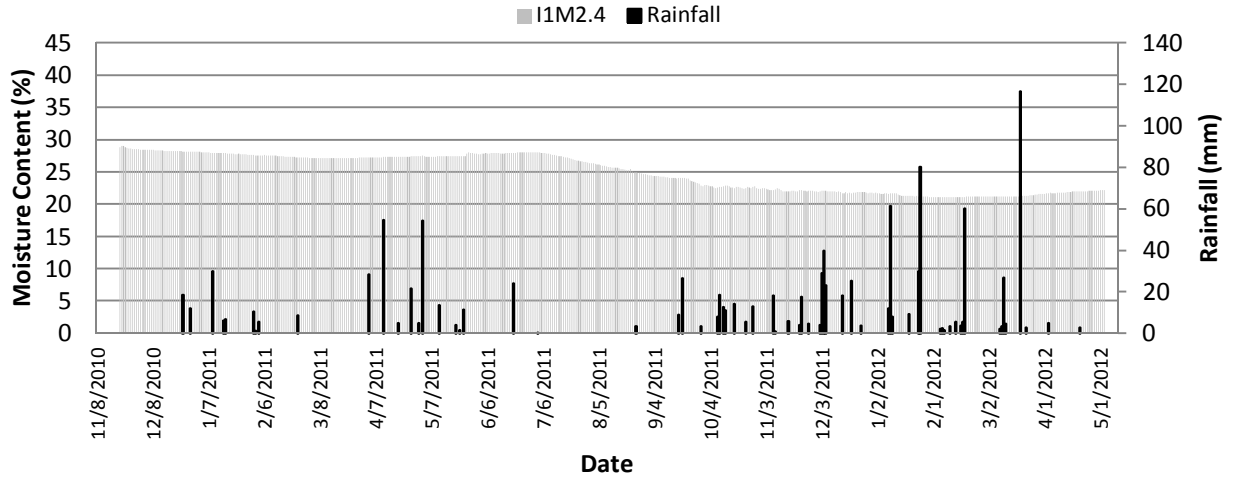
(a)
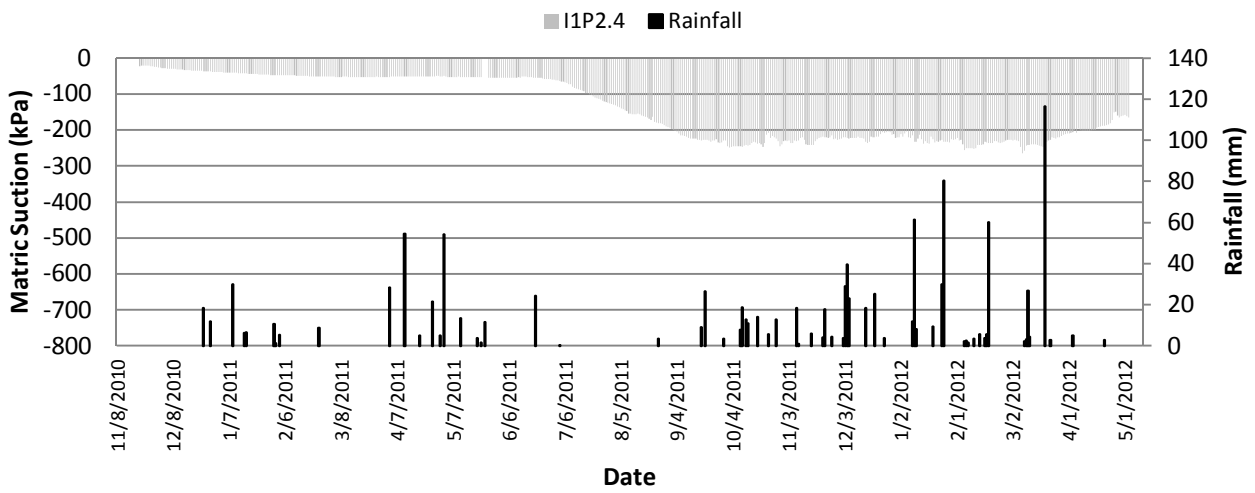
(b)

Figure 4.2 In situ variation of (a) moisture content and (b) matric suction at 2.4 m depth at top of slope

Both moisture content and suction profile for sensors installed at 3.6 m depth are presented in Figure 4.3 (a) and (b). Field data shows both the moisture sensor and water potential
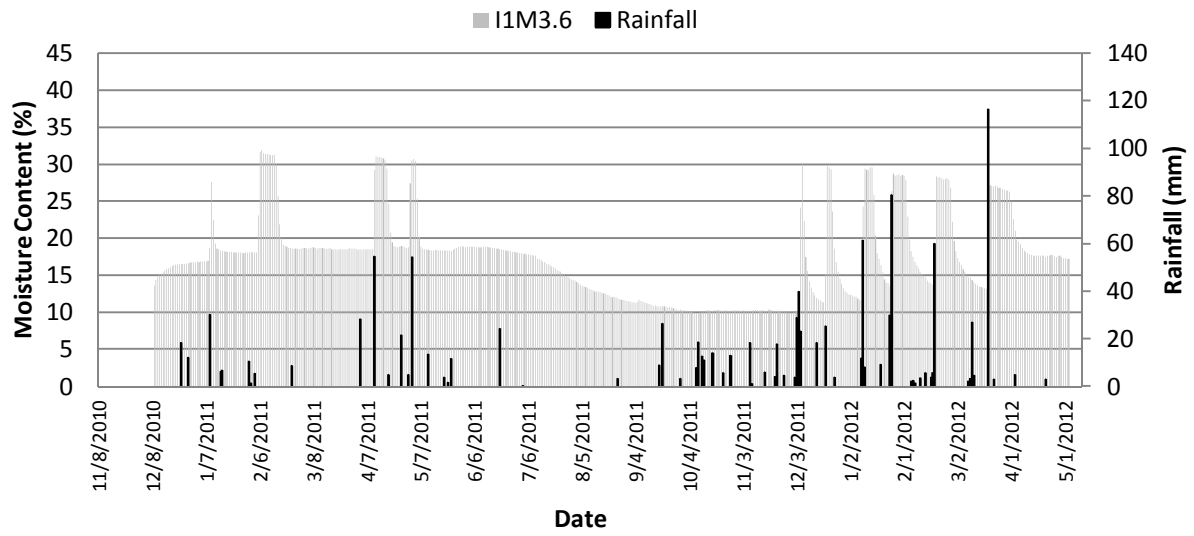
(a)
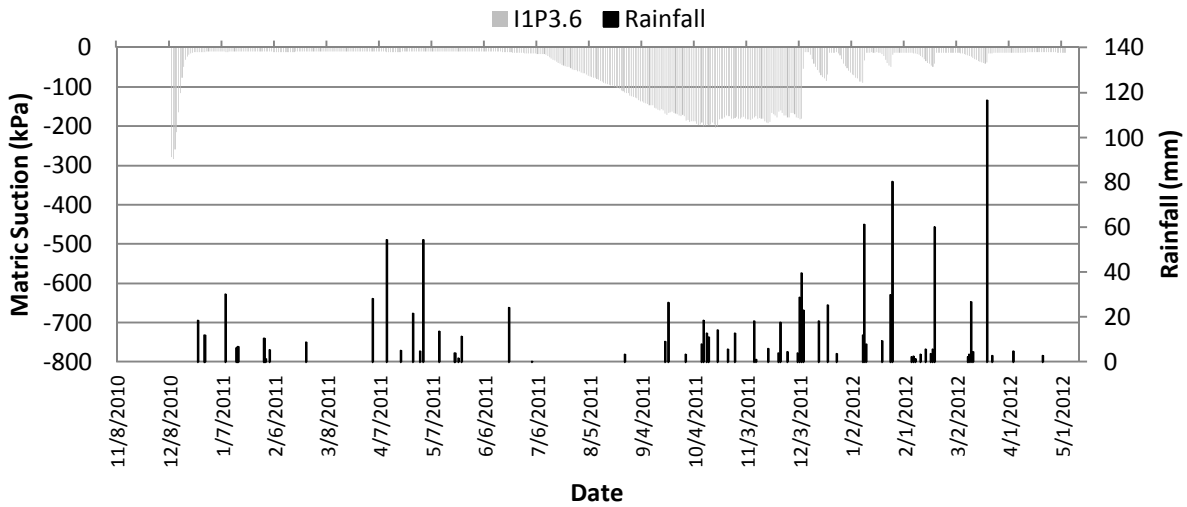
(b)

Figure 4.3 In situ variation of (a) moisture content and (b) matric suction at 3.6 m depth at top of slope

probe at this location responded to the large volume of precipitation. Infiltration of rain water can

increase the moisture content up to 30% at 3.6 m depth. During the dry period, gradual increase

in suction was observed with a maximum value of -200 kPa.

The moisture content and suction distribution presented in Figure 4.4 (a) and (b) at 6.1 m depth, remain unchanged due to change in weather condition. The moisture content remained approximately 30% with a suction of -10 kPa throughout the investigating period.
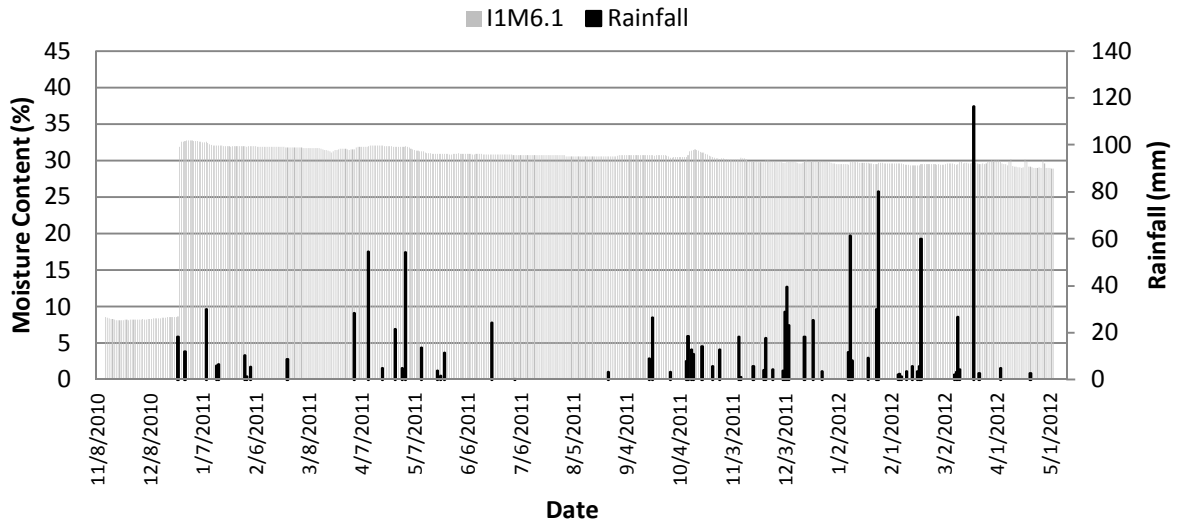
(a)
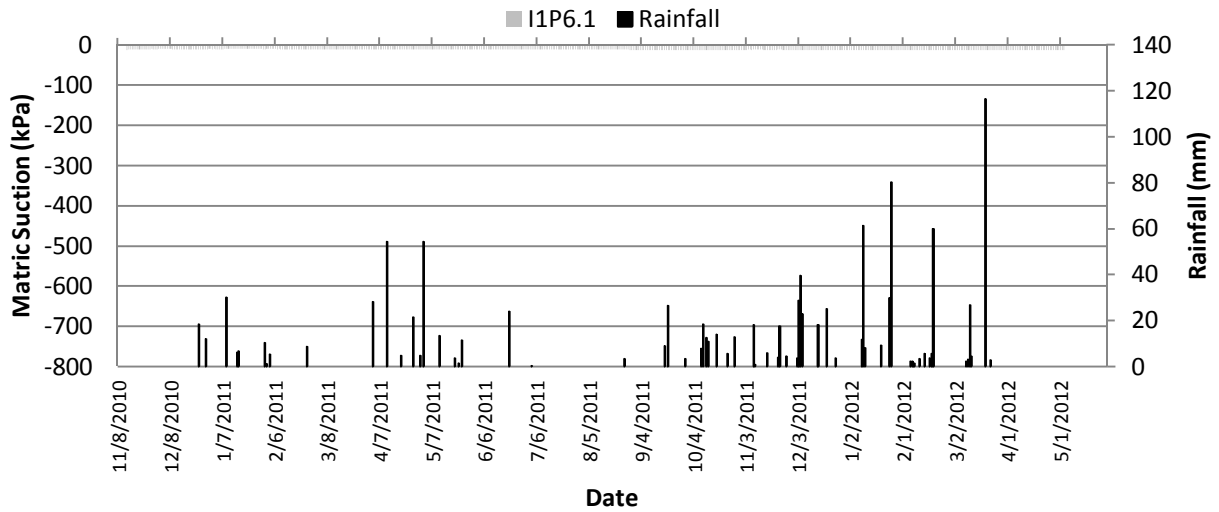
(b)

Figure 4.4 In situ variation of (a) moisture content and (b) matric suction at 6.1 m depth at top of slope

Results obtained from the instrumentation installed at the crest of the slope indicates that the variation in the moisture content and matric suction were different at different depth. The maximum variation often occurred near the ground surface (i.e. at 1.2 m depth) and the magnitude of variation often decreased with increase in depth. On the basis of both moisture content and suction profile, it can be estimated that the depth of influence of the wet-dry cycle was up to 3.6 m at I1 section. Therefore, reduction in soil shear strength due to cyclic variation of weather condition is limited to a depth of 3.6 m which also matches close to the observed failure depth (3.04 m) on slopes constructed on high PI clay. Based on the swell test (Figure 3.10) under different normal stress for expansive clay under this study, it was observed that, swelling can occur up to a depth of 3.8 m upon wetting which also indicates the depth to which strength reduction can occur due to cyclic swell shrink phenomenon of expansive clay.

4.2.1.2 Middle of Slope

Variation of moisture content and matric suction distribution at 1.2 m depth is presented in Figure 4.5 (a) and (b). It can be observed that, the initial moisture content was relatively low (4%) and the matric suction was approximately -100 kPa. The maximum moisture content observed at this location was 27% due to infiltration of rain water. However, the moisture content decreased rapidly with the ceasation of the rainfall. The matric suction distribution presented in Figure 4.5 (b) did not show rapid recovery as was observed for moisture sensor. The minimum suction observed was -10 kPa due to loss of suction during rainfall. During the relatively dry summer of 2011, the matric suction increased from -150 kPa to -400 kPa.
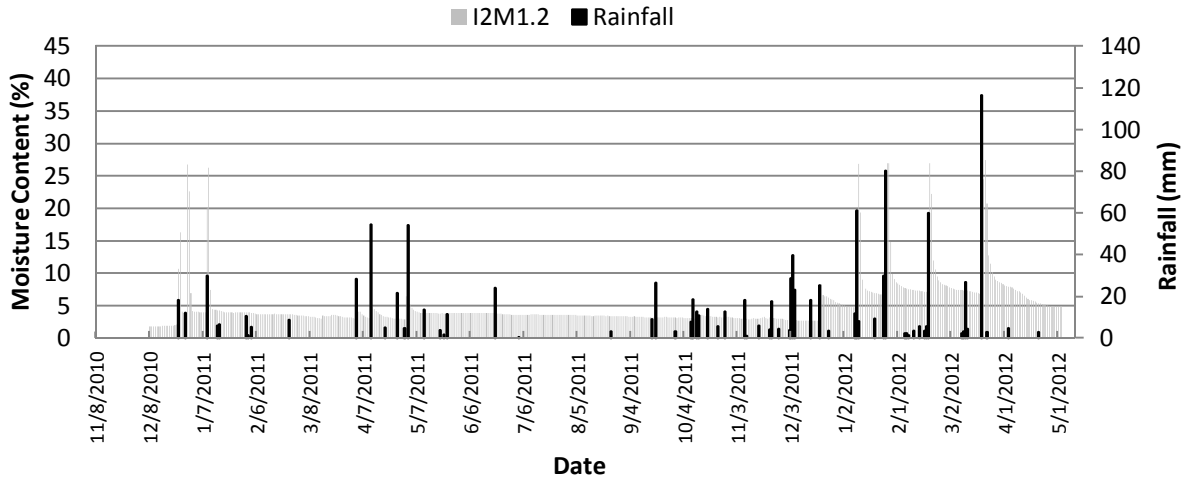
(a)
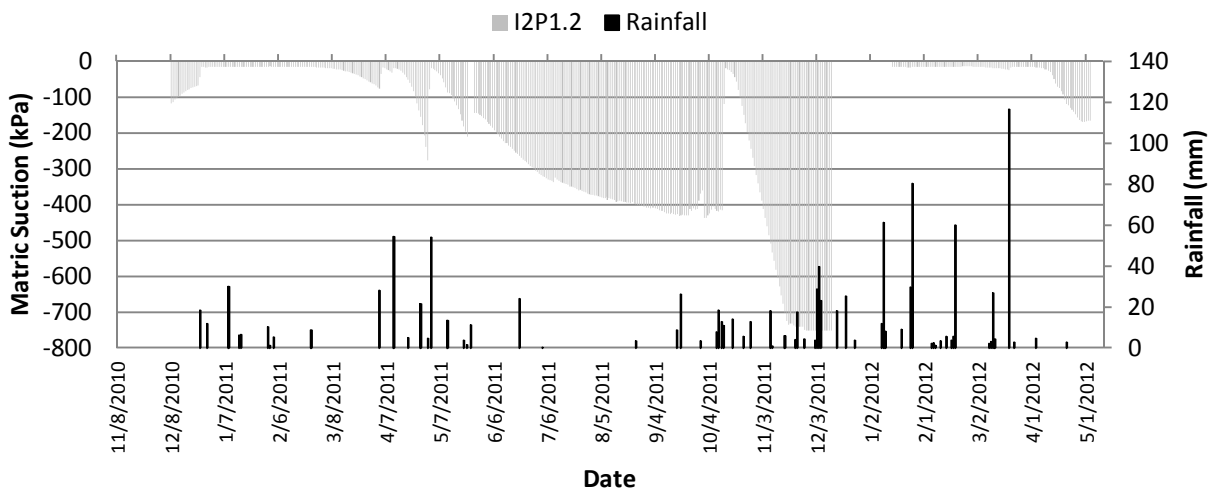
(b)

Figure 4.5 In situ variation of (a) moisture content and (b) matric suction at 1.2 m depth at middle of slope

The in situ moisture content and matric suction profile at the 2.4 m depth is presented in Figure 4.6 (a) and (b). It was observed that the soil was initially wet with a moisture content of 25 % and corresponding suction value of -15 kPa. During the dry period of summer 2011, moisture content decreased gradually from 25% to 13% and accordingly, matric suction increased from -10 kPa to -700 kPa.
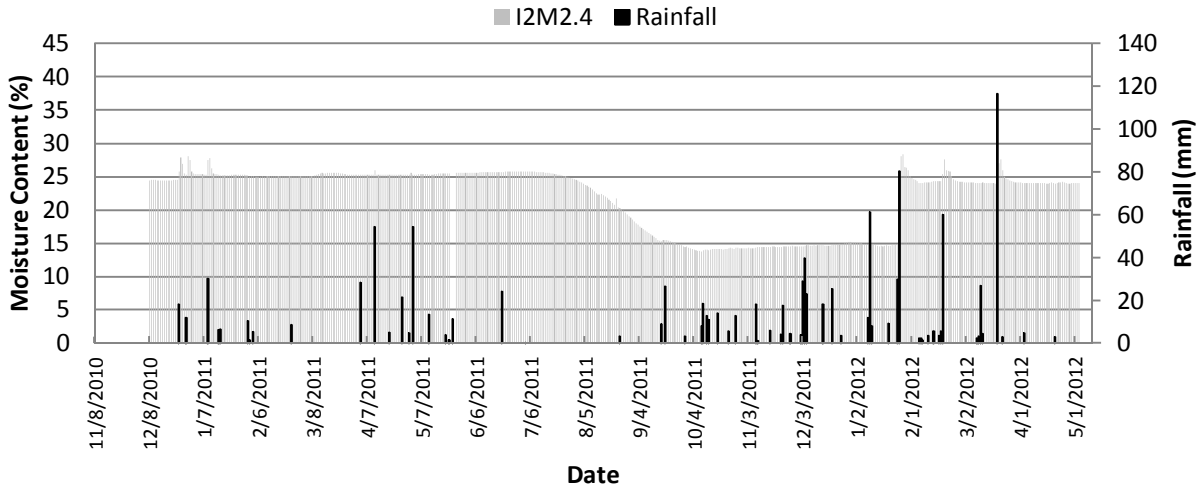
(a)
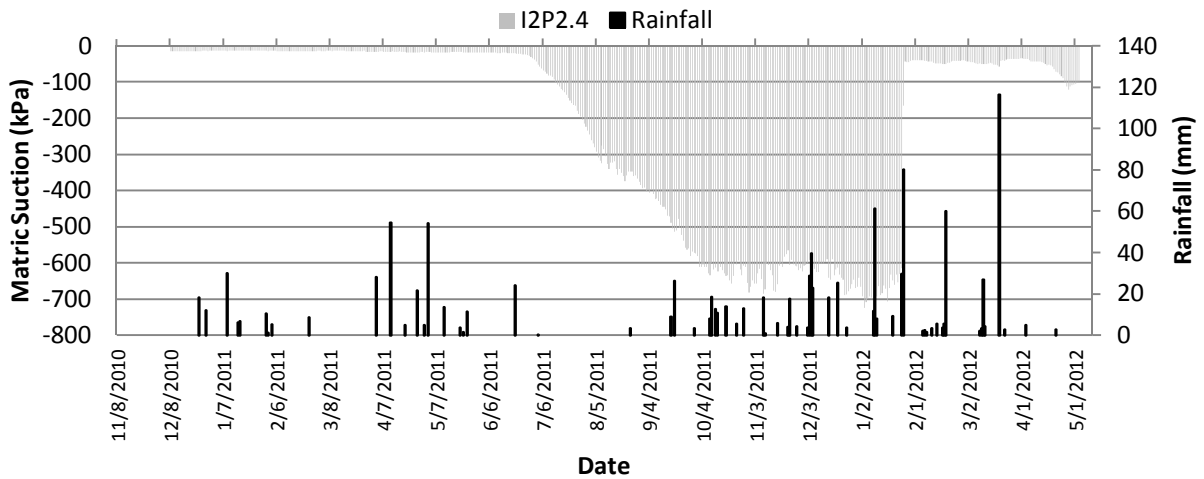
(b)

Figure 4.6 In situ variation of (a) moisture content and (b) matric suction at 2.4 m depth at middle of slope

Field data shows that, high volume of precipitation was observed between January and March 2012. As a result, the moisture content during this wet period increased to 25% and the suction decreased to approximately -40 kPa from -700 kPa. Data obtained from the sensors at the middle of slope indicated that the maximum variation often occurred near the ground surface which was also observed at the crest and the variation was more gradual at deeper depth. From

99

the instrumentation data it can be observed that the depth of moisture variation extends to a depth of 2.4 m at the middle of slope

However, the variation in both moisture content and matric suction were found to be different at the same depth but at different location of slope. From Figure 4.1 (a) and 4.5 (a) it can be seen that, moisture content at 1.2 m depth was higher at the crest compared to the middle of the slope. The smaller change in the water content at the middle of slope may be due to the decreased amount of crack formation at the lower part of the slope. Due to the formation of cracks, more water from infiltration can be stored at the crest compared to the middle of the slope. Moreover, the infiltration rate is higher at the crest of the slope compared to the middle of slope due to formation of cracks at the crest (Figure 3.1). Zhan et al. (2007) also observed high infiltration rate in the cracked region of a slope constructed on expansive clay from double-ring infiltration test. The authors found that the measured value of infiltration rate varied by three orders of magnitude from 10^{-4} to 10^{-7} m/s in the cracked and non-cracked region.

4.2.1.3 Effect of Rainfall Intensity and Duration on Moisture Content and
Matric Suction Profile

Variations in moisture content profile and associated matric suction profile during different rainfall events are presented here. Observations made during the rainfall event on April 11, 2011 and May 2, 2011 was selected for discussion. It was observed that the rainfall amount was same (54.2 mm) for both rainfall event but the intensity and duration of the rainfall is different. A short duration high intensity rainfall was observed on April 11 with a maximum rainfall amount of 45.4 mm/hr. On the other hand, a low intensity long duration rainfall was observed on May 2 with a maximum rainfall amount of 11 mm/hr. Variation of moisture content

and matric suction measurement with time and depth during the two rainfall period are presented in Figure 4.7 through Figure 4.10.

Figure 4.7 (a) and (b) shows the changes in moisture content and matric suction with time in response to the rainfall event on April 11, 2011. It can be observed that, during the heavy rainfall event on April 11, all the sensors installed up to 3.6 m depth started to respond on the very first hour of the initiation of the rainfall. The rainfall was continued for 4 hours with 45.4 mm of rain at the first hour and with an average of 3 mm/hr of rain for the following hours. The moisture content at 1.2 m depth increased to 23% from 4% at the second hour of rainfall and then started to decrease rapidly as the intensity of the rainfall decreased. Matric suction at 1.2 m depth at the crest decreased from -125 kPa to -10 kPa and -35 kPa to -15 kPa at the middle of the slope. The moisture content at 3.6 m depth also shows a rapid increase on second hour of rainfall from 18% to 32% but there was no change in suction observed. This phenomenon may be due to the initial low suction value (-10 kPa) prior to rainfall. An increase in moisture content from 25% to 27% at 2.4 m depth at the middle of the slope was also observed. Therefore, rainfall caused changes in both moisture content and matric suction up to 3.6 m depth.
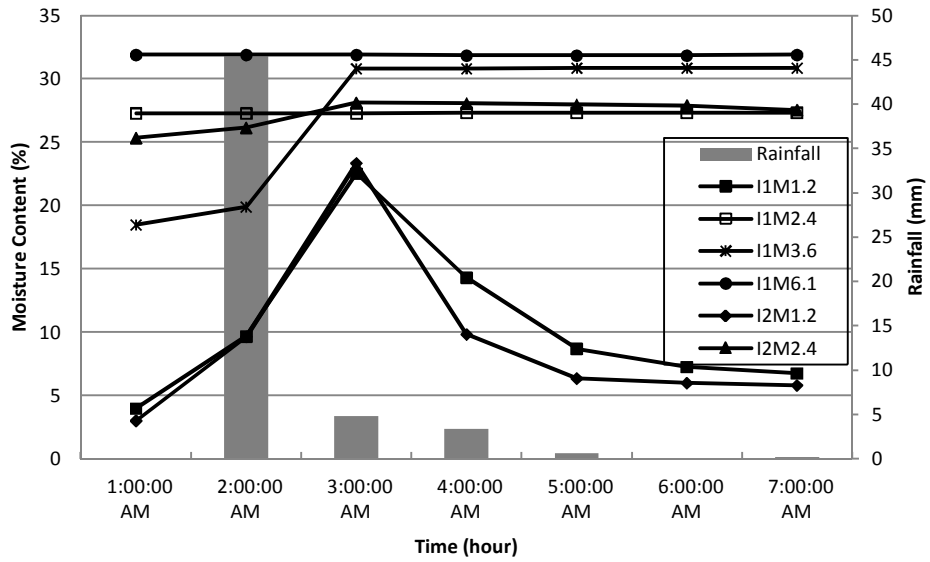
(a)
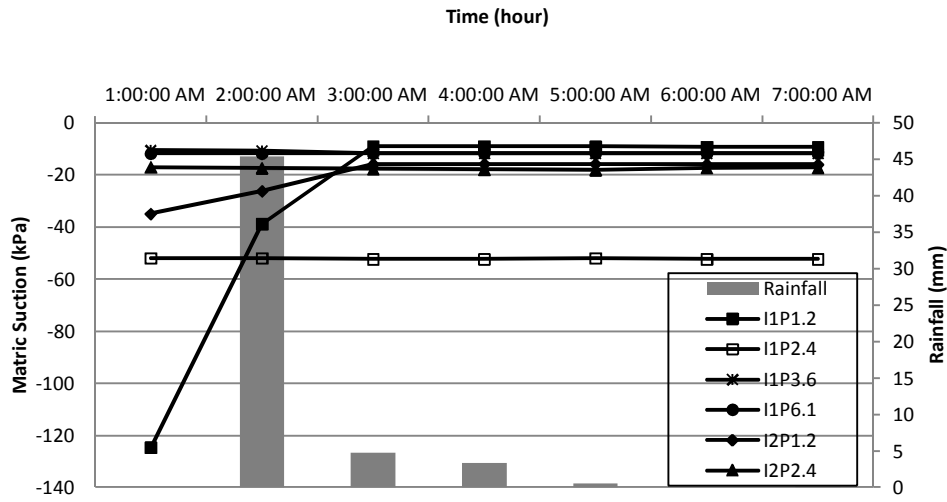
(b)

Figure 4.7 Variation of in situ (a) moisture content and (b) matric suction during rainfall event April 11
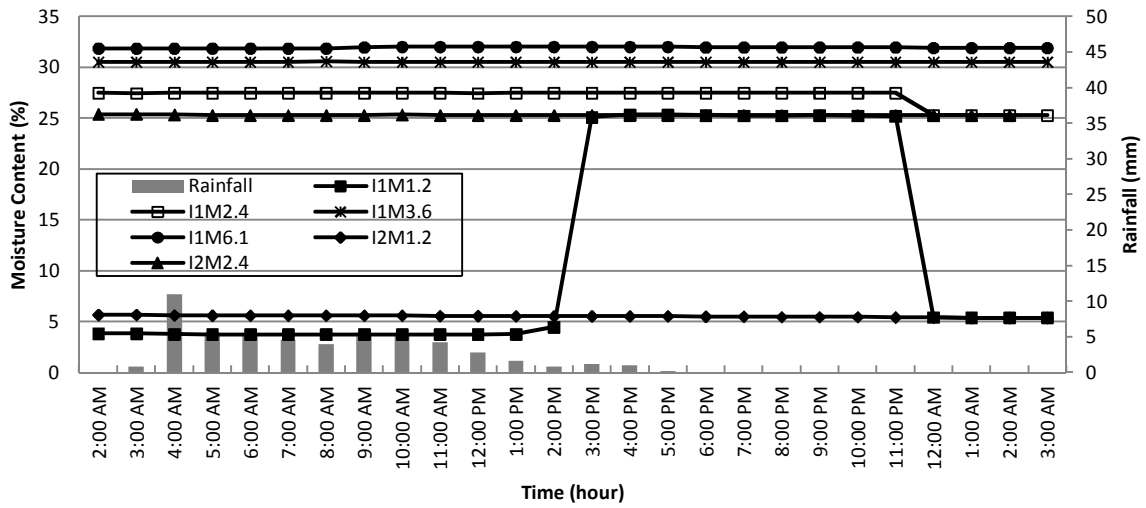
(a)
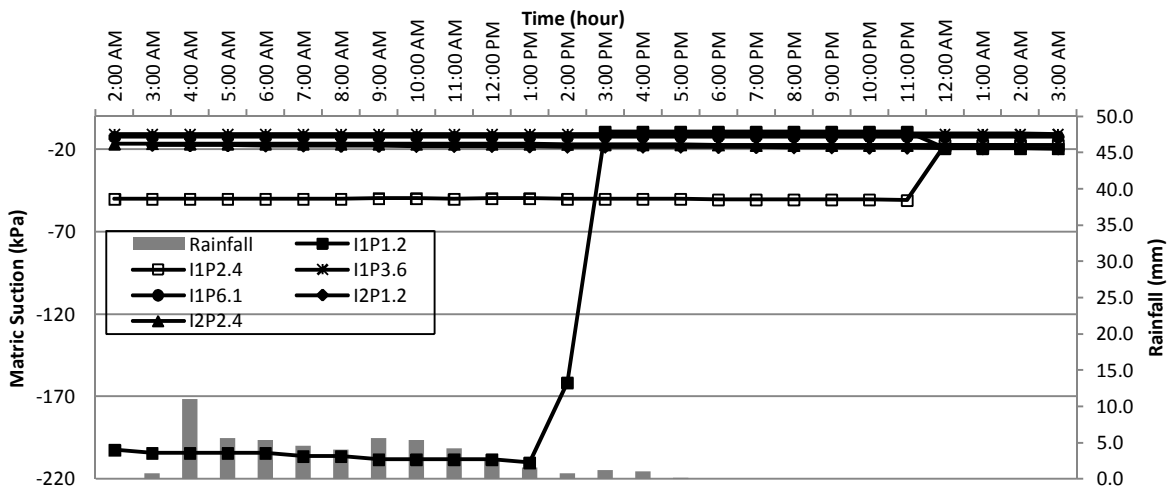
(b)

Figure 4.8 Variation of in situ (a) moisture content and (b) matric suction during rainfall event May 2

A delayed response of 12 hours was observed during the rainfall event on May 2 which is presented in Figure 4.8 (a) and (b). The rainfall continued for 14 hours with the highest rainfall intensity of 11 mm. Both the moisture sensor and water potential probe installed at 1.2 m depth at the crest of the slope started to respond after 12 hour of rainfall and the moisture content increased from 4% to 25%. The matric suction also decreased to a value of -10 kPa from the

initial suction of -200 kPa. The change in matric suction at 2.4 m depth at the crest showed a further delay 9 hours and reduced from -55 kPa to -20 kPa. The moisture content observed at 3.6 m depth prior to rainfall was approximately 32% and the suction was -10 kPa and did not show any changes due to the rainfall event. There was no increase in moisture content and subsequent decrease in matric suction was observed at the same depth (1.2 m) but at the middle of the slope. This phenomenon may be due to the presence of open cracks at the crest of the slope which accelerated the flow of water into the soil. Aubeny and Lytton (2003) suggested that the rate of moisture change increases 10 times when cracks are present in high PI clay slopes. In comparison to the rainfall event on April 11, there was no rapid recovery of water content was observed which may be due to the continuous infiltration of rain water into the slope for a longer period of time.

Both the moisture content and matric suction profiles at the crest of the slope for the two rainfall event considered are presented in Figure 4.9 and 4.10. The moisture content and matric suction profiles were presented from 1:00 am to 7:00 am for the rainfall event on April 11 and the rainfall started at 2:00 am and ceased at 5:00 am. In case of rainfall event on May 2, the moisture content and matric suction profiles were presented from 1:00 pm to 12:00 am on May 3. In later case, the rainfall started at 3:00 am and ceased at 4:00 pm on May 2 but the sensors started to respond at 2:00 pm with a delay of 12 hours.

Moisture Content (%)

(a)
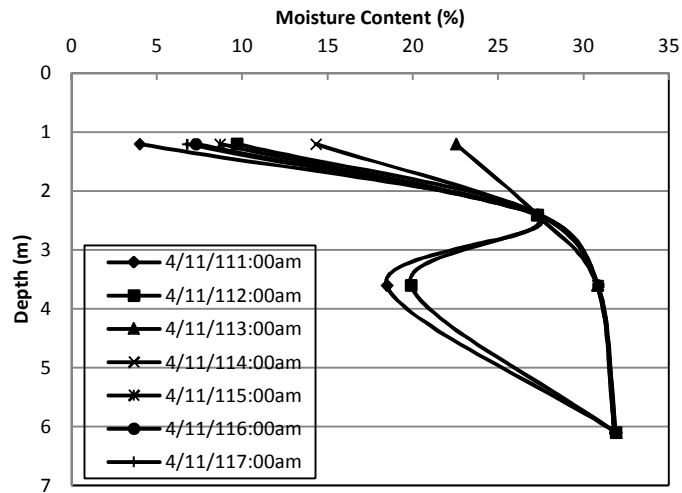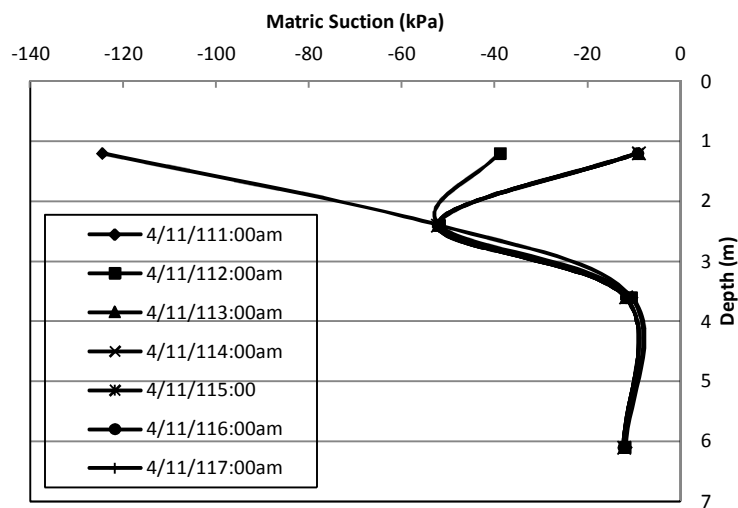
Matric Suction (kPa)

(b)

Figure 4.9 Variation of in situ (a) moisture content and (b) matric suction profile during rainfall event April 11 at the crest of slope
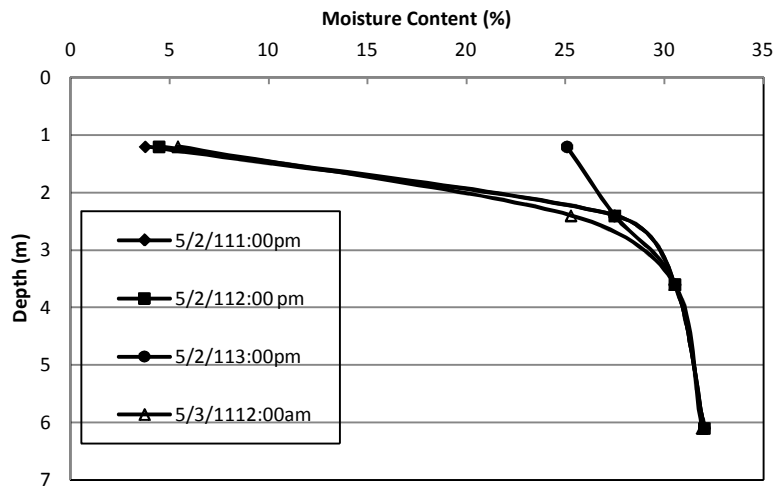
(a)
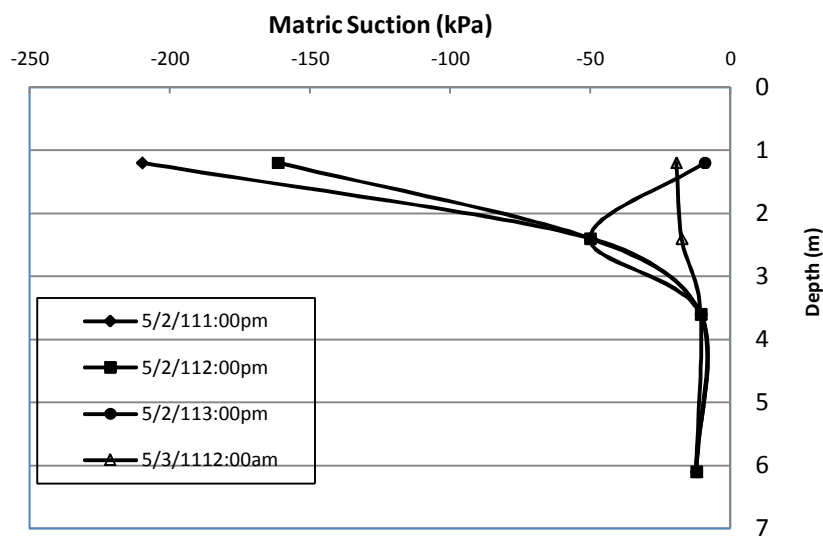
(b)

Figure 4.10 Variation of in situ (a) moisture content and (b) matric suction profile during May 2 at the crest of slope

Prior to the commencement of the rainfall, the moisture content profile generally showed an increase in in situ moisture content and decrease in matric suction with depth. Field results shows that the changes in moisture content and matric suction is rapid for rainfall with high intensity and shorter duration. On the other hand, delayed response of moisture content and

matric suction was observed for low intensity rainfall. For both the rainfall events, the in situ moisture content measurement showed a recovery towards the initial moisture content profile prior to the commencement of rainfall (Figure 4.9 and 4.10 a). But the in situ matric suction profile did not show any recovery towards the initial value even after the ceasation of the rainfall event. However, a direct conclusion cannot be made about the response time because of different initial condition of the rainfall events. The matric suction at 1.2 m depth before the rainfall event on April 11, 2011 was approximately -125 kPa and the matric suction was -220 kPa at the same depth prior to rainfall event on May 2, 2011. Zhan and Ng (2004) suggested that variations in rainfall infiltration rate are often restricted by the hydraulic properties of the soil and initial pore pressure conditions. The author also postulated that, the sensitivity of an infiltration system to rainfall intensity is not as great as its sensitivity to the initial negative pore water pressure distribution and hydraulic properties of soil.

However, in order to investigate the validity of observed phenomenon, observations made during the rainfall event on February 18, 2012 were selected for discussion. It was observed that the rainfall amount was (60 mm) for the selected rainfall event. A low intensity long duration rainfall was observed with a maximum rainfall amount of 8.2 mm/hr. Figure 4.11 shows the variation of moisture content and matric suction measurement with time during the rainfall period.
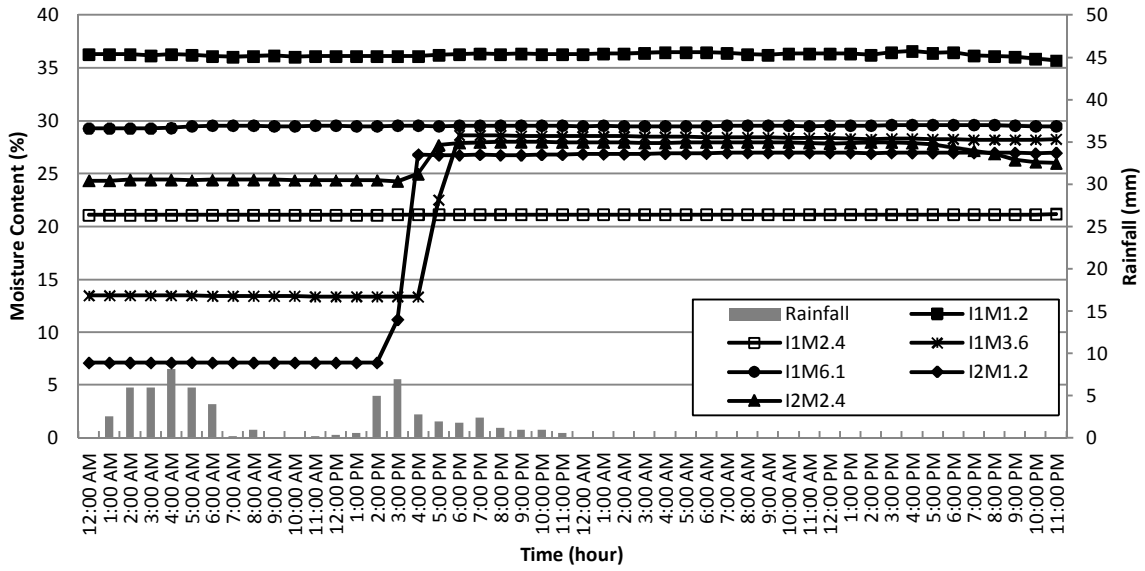
(a)
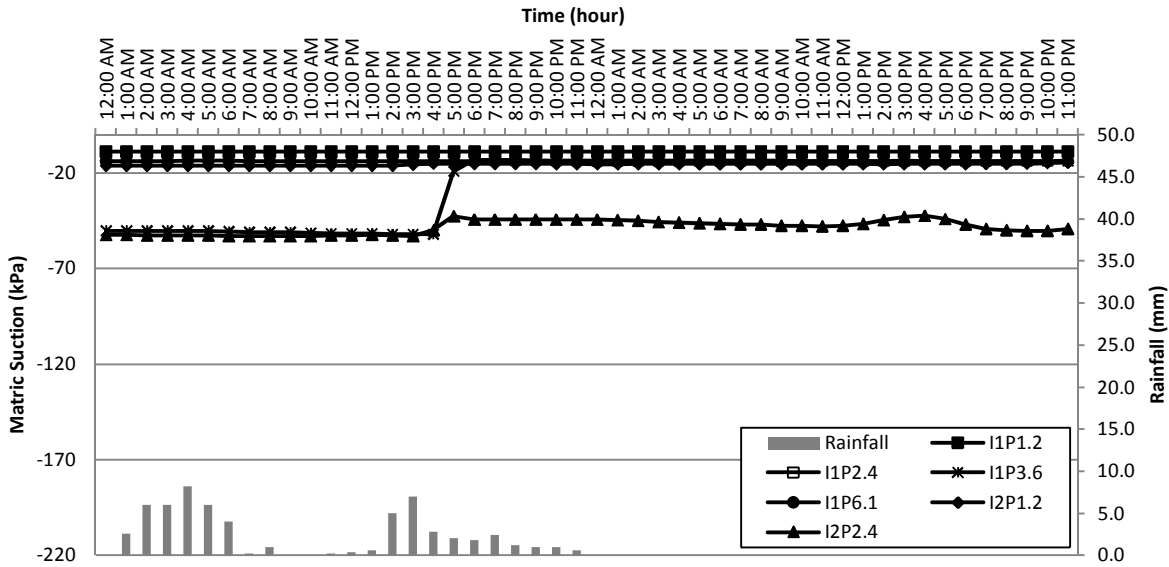
(b)

Figure 4.11 Variation of insitu (a) moisture content and (b) matric suction profile during rainfall event on February 18, 2012

Field observation shows a delayed response of 14 hours during the rainfall event on February 18, 2012. The rainfall continued for 23 hours with the highest rainfall intensity of 8.2 mm. The rainfall started at 1:00 am and stopped at 11:00 pm with 2 hours of no rainfall between

9:00 and 10:00 am. An increase in moisture content was observed at 1.2 m and 2.4 m depth at the middle of slope after 14 hours from initiation of rainfall. The moisture content also increased at 3.6 m depth at the crest of the slope but there was no change in moisture content observed at 1.2 m and 2.4 m depth at the crest of slope which may be due to initial high moisture content prior to rainfall event. The initial suction at 1.2 m depth was approximately -15 kPa and did not show further reduction due to rainfall. However, the matric suction dropped from -55 kPa to -43 kPa at 2.4 m depth at the middle and -52 kPa to -13 kPa at 3.6 m at the crest of slope. Matric suction at other sensor location was close to -15 kPa prior to rainfall event and did not show any further reduction. Though the matric suction prior to rainfall event on February 18, 2012 was low compared to the rainfall event on May 2, 2011, a delayed response in increase of moisture content was observed. Therefore, it can be seen that rainfall intensity can significantly affect the infiltration rate with high intensity rainfall producing higher infiltration rate.

4.3 Soil Water Characteristic Curve

The soil water characteristic curve (SWCC) of expansive Eagle Ford clay collected from the slope along US Hwy 287, was determined for different net normal stresses, initial water content and density in the laboratory using modified Tempe pressure cell. The following sections discuss all the experimental results showing the effect of net normal stress, initial water content, volume change behavior and density on the SWCC of expansive clay.

4.3.1 Effect of Volume Change

Volume change behavior is commonly ignored during construction of SWCC due to limitations of measuring change in volume during testing. Ng. et al. (2000) observed no effect on

SWCC with and without considering volume change for sandy silt/clay using volumetric pressure plate tests. However, the above conclusion may not be appropriate when considering soil that has high swelling and shrinkage behavior. Therefore, volume change was measured from the dial gauge readings during the tests. SWCC of the compacted specimens considering both volume change and no volume change was constructed. The SWCC of the specimen compacted wet of optimum at 25 kPa net normal stress considering both volume change and no volume change (NVC) is presented in Figure 4.12. The experimental results were fitted with Van Genuchten (1980) equation for both the cases.
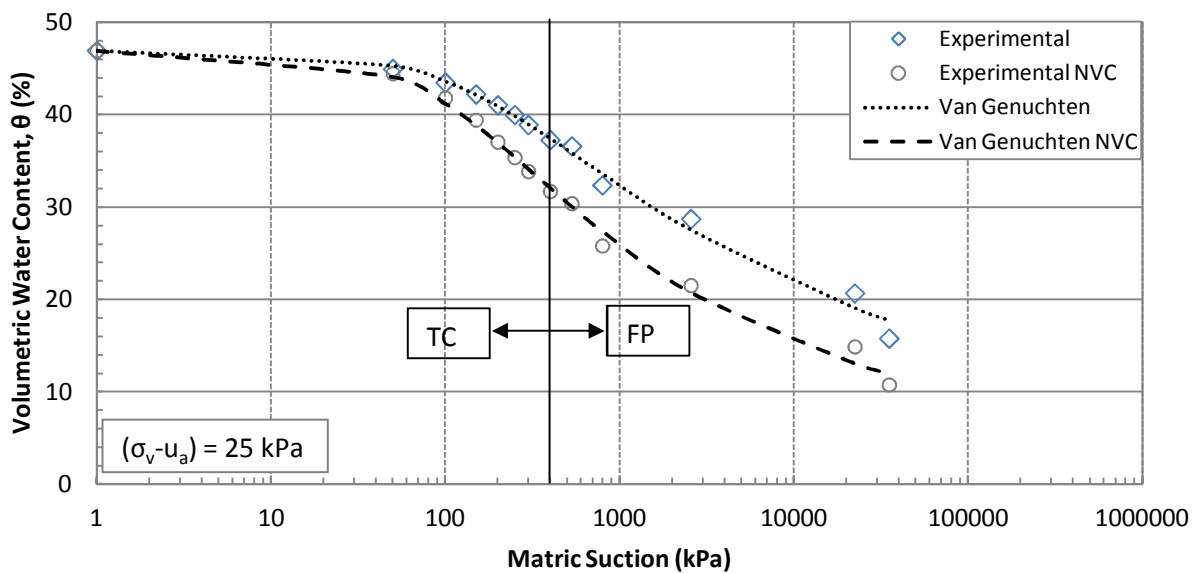
Figure 4.12 Comparison of SWCC with and without volume change considered at 25 kPa net normal stress (wet of optimum)

Based on the experimental results, SWCC considering volume change shows high air entry value (100 kPa) as compared to the one with no volume change (60 kPa) considered. Moreover, slope of curve is steeper in latter case compared to volume change curve which will over predict the desaturation rate of the soil.

Similar results were also obtained for other specimens compacted both at wet and dry of optimum and tested at different net normal stresses which are presented from Figure 4.13 through Figure 4.16.
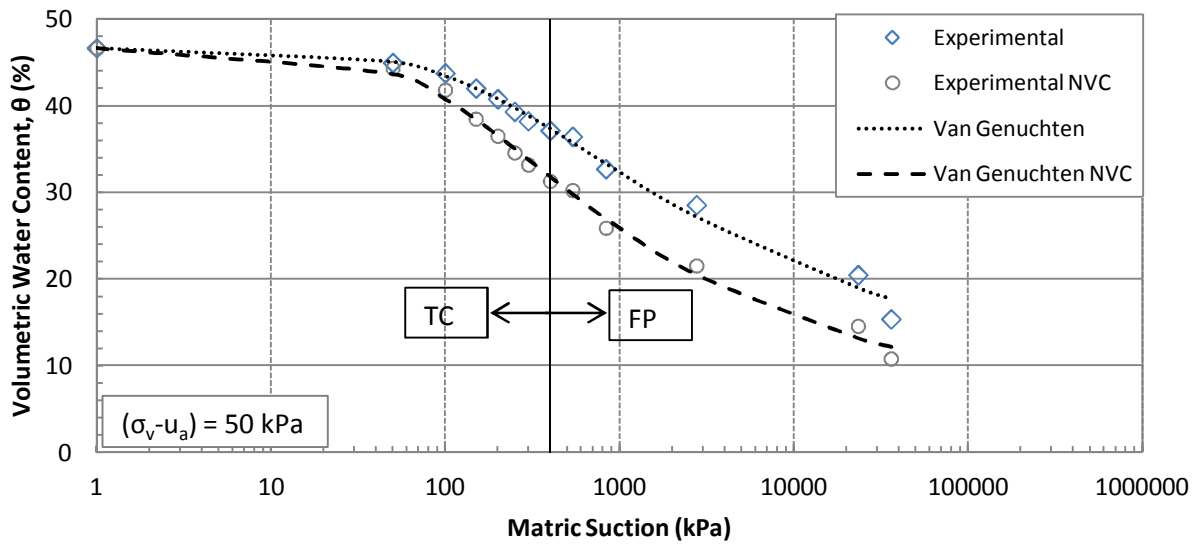
Figure 4.13 Comparison of SWCC with and without volume change considered at 50 kPa net normal stress (wet of optimum)
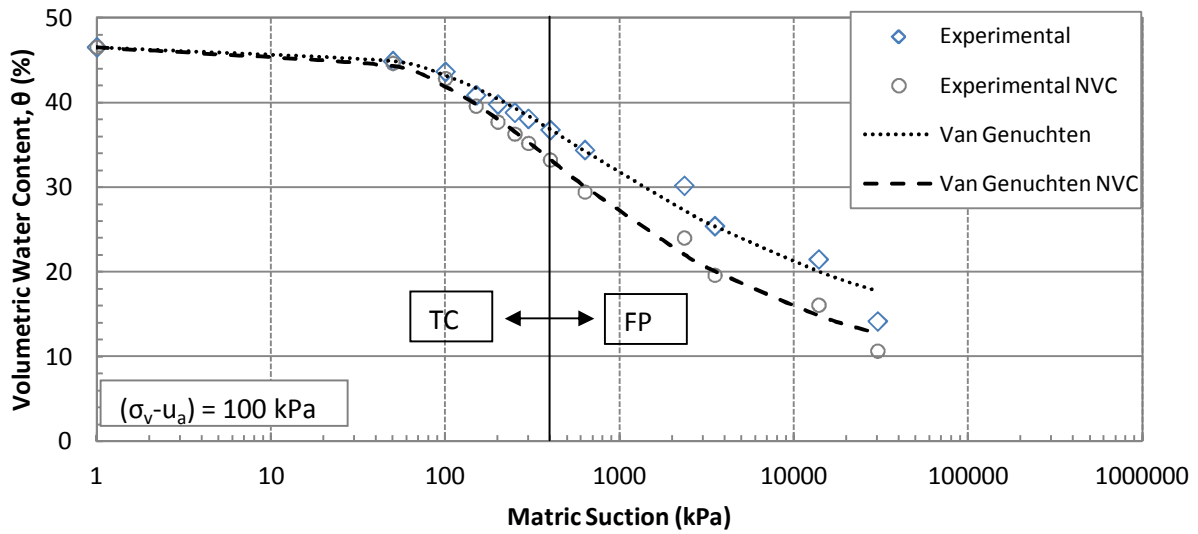
Figure 4.14 Comparison of SWCC with and without volume change considered at 100 kPa net normal stress (wet of optimum)
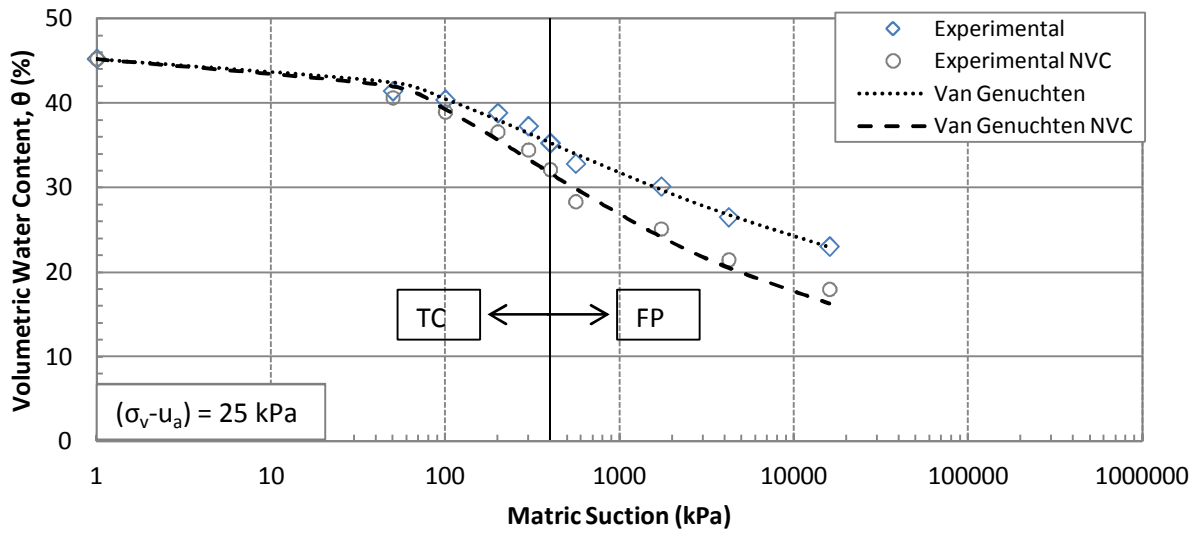
Figure 4.15 Comparison of SWCC with and without volume change considered at 25 kPa net normal stress (dry of optimum)
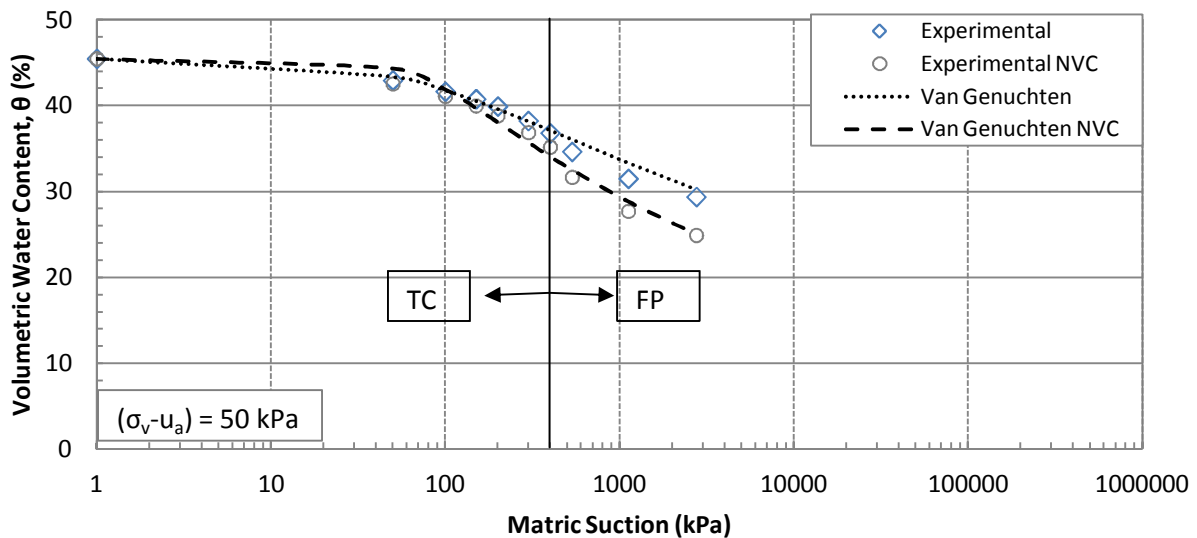
Figure 4.16 Comparison of SWCC with and without volume change considered at 50 kPa net normal stress (dry of optimum)

The fitting parameters obtained using Van Genuchten equation considering with and without volume change for specimens compacted wet of optimum and dry of optimum water content is presented in Table 4.1 and 4.2. It can be noted that, the α values increase if no volume change is considered which is associated with the decrease in air entry value. Moreover, the predicted n value also increases which is also reflected from the steeper slope of the SWCC without considering volume change.

By using measured saturated water permeability (k_s = 3.54E-9 m/s), the best fit parameters were input to the equation proposed by Maulem (1976) for obtaining the permeability functions. The permeability functions obtained for 25 and 50 kPa net normal stresses for the specimens compacter wet of optimum are presented in Figure 4.17 and 4.18.

Table 4.1 Best Fitting Van Genuchten Parameters with and without Volume (wet of optimum)

	25 kPa		50 kPa		100 kPa	
Parameters	VC	NVC	VC	NVC	VC	NVC
α (1/kPa)	0.0064	0.0089	0.0063	0.0096	0.0064	0.0072
n	1.2190	1.3116	1.2184	1.3009	1.2357	1.3122
m	0.1797	0.2376	0.1792	0.2313	0.1908	0.2379

Table 4.2 Best Fitting Van Genuchten Parameters with and without Volume Change (Dry of Optimum)

	25 kPa		50 kPa	
Parameters	VC	NVC	VC	NVC
α (1/kPa)	0.0159	0.0123	0.0123	0.0134
n	1.1454	1.2407	1.1335	2.335
m	0.1269	0.1940	0.1178	0.0833
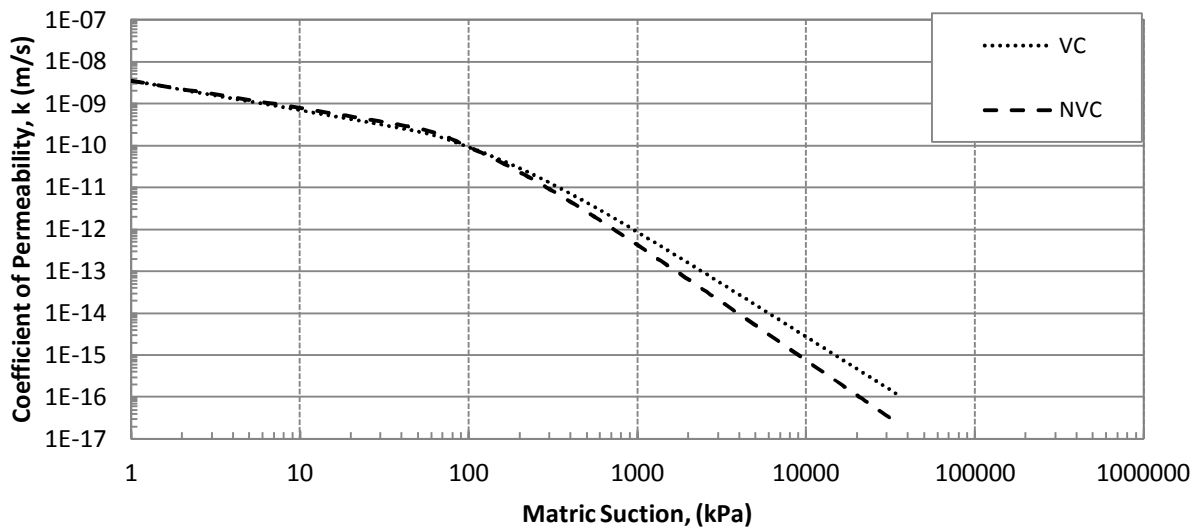
Figure 4.17 Permeability function computed from measured SWCC under 25 kPa net normal stress with and without volume change considered
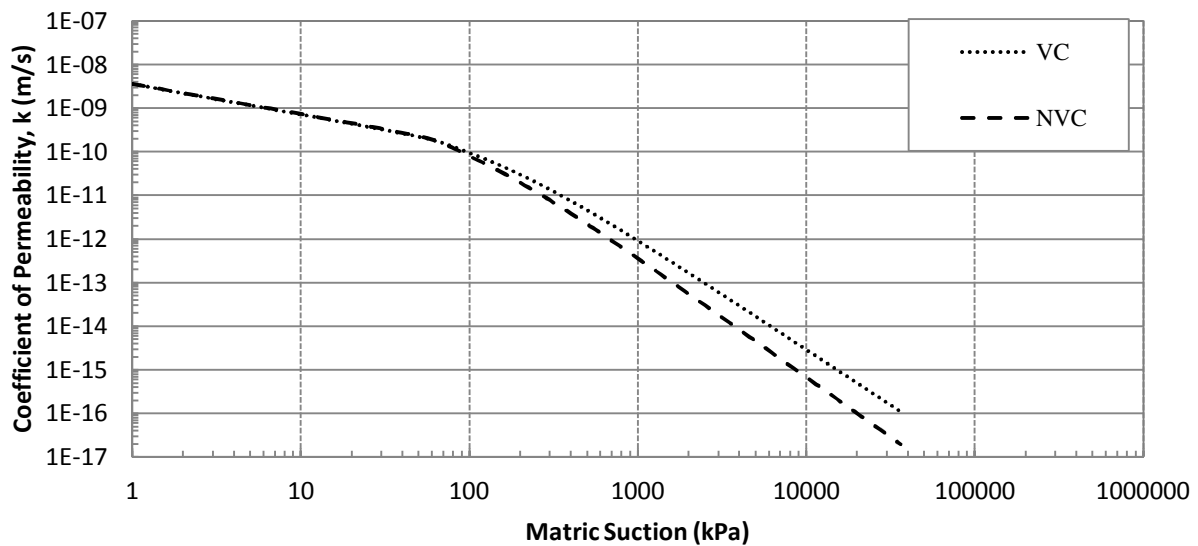
Figure 4.18 Permeability function computed from measured SWCC under 50 kPa net normal stress with and without volume change considered (wet of optimum)

Based on the experimental results, it can be observed that, for a certain value of matric suction, permeability of soil without considering volume change has lower value as compared to the volume change consideration. According to this behavior, permeability function predicted from no volume change assumption will under predict the infiltration rate and subsequently produce higher factor of safety.

4.3.2 Effect of Stress State

SWCC of soil shows the moisture retention characteristics of soil. According to Ng et al. (2000), with higher net normal stresses, the presence of smaller pore size distribution increases which reduces the rate of reduction in water content. Soils with larger pore size distribution, desaturates at faster rate as compared to soils with smaller pore sizes because it takes less pressure to desaturate the larger pores filled with water.

115

SWCC of expansive clay, compacted wet of optimum water content did not show any variation due to different net normal stresses. Figure 4.19 shows best fit curve using Van Genuchten equation for samples compacted wet of optimum water content (29.5%) with a dry density of 14.18 kN/m^3 at 25, 50 and 100 kPa net normal stresses. The air entry value for all the three tests shows a consistent value of 100 kPa though tested at different net normal stress conditions. The fitting parameters obtained for three samples are presented in Table 4.3 which shows a similar value. The parameter α which is inversely related to the air entry value shows a fairly constant value which supports the conclusion that the air entry value is similar for all the three specimens. Once, the air entry value is exceeded, the 'n' parameter which is the desaturation rate, controls the slope of the curve. From Figure 4.19, it can be seen that the slope of the SWCC for all the three specimens is constant which is also reflected through the similar value of n in Table 4.3. Therefore, it can be noted that specimens compacted wet of optimum do not appear to be strongly dependent on the applied stress history due to identical micro-structure formation appearance of no interclod pores.
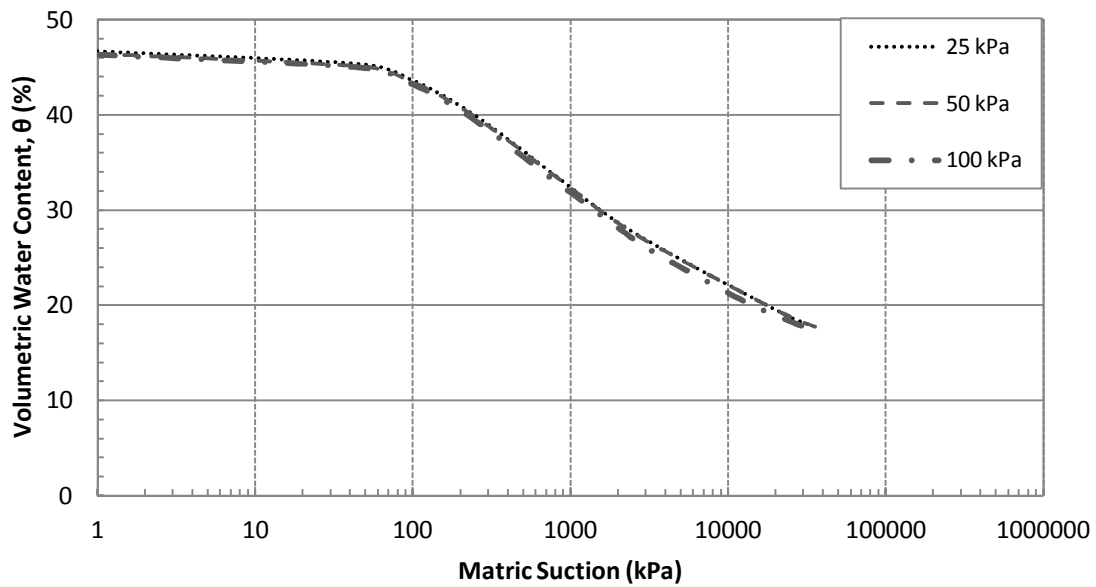
Figure 4.19 SWCC for specimens compacted wet of optimum at different net normal stress

Table 4.3 Fitting Parameters for Specimens Compacted Wet of Optimum

Parameters	Net Normal Stress (σ-u_a), kPa		
	25	50	100
α (1/kPa)	0.0064	0.0063	0.0064
n	1.2190	1.2184	1.2357
m	0.1797	0.1792	0.1908

By using measured saturated water permeability (k_s = 3.54E-9 m/s), the best fit parameters were input to the equation proposed by Maulem (1976) for obtaining the permeability functions. The permeability functions obtained for 25, 50 and 100 kPa net normal stresses for the specimens compacter wet of optimum are presented in Figure 4.20.
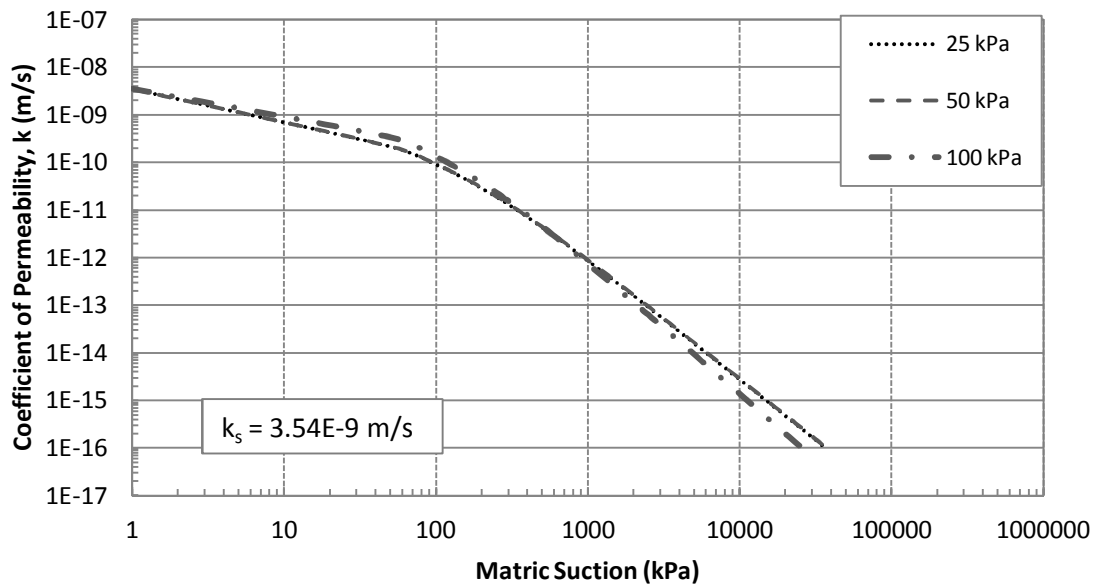
Figure 4.20 Permeability function computed from measured SWCC under 25,50 and 100 kPa net normal stresses (wet of optimum)

From Figure 4.18, it can be observed that, the permeability functions obtained for three different net normal stresses for specimens compacted wet of optimum are identical as was observed from the SWCC.

On the other hand, SWCC of expansive clay, compacted dry of optimum water content shows a shift to the right with high net normal stresses. Figure 4.21 shows best fit curve using Van Genuchten equation for samples compacted dry of optimum water content (18%) with a dry density of 14.18 kN/m^3 at 25 and 50 kPa net normal stresses. The air entry value of the specimen
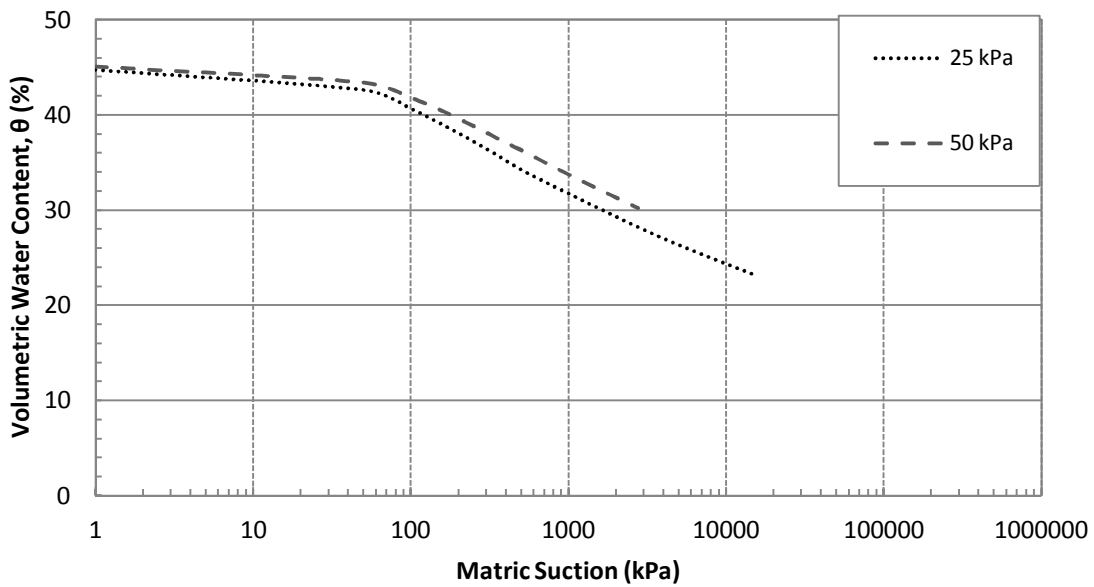
Figure 4.21 SWCC for specimens compacted dry of optimum at different net normal stress

at 25 kPa shows a value of 62 kPa while for 50 kPa net normal stress, the value increases to 80 kPa. The increase in air entry value indicates, higher suction is required to desaturate the specimen due to smaller pore size distribution. Therefore, with the increase in normal stress the rate of reduction in water content decreases. The fitting parameters describing the SWCC using Van genuchten equation is presented in Table 4.4. From Table it can be seen that, the α parameter slightly decreases with the increase in net normal stress thereby increasing the air entry value which was observed from Figure 4.21. Moreover, a slight decrease in the estimated value of n was observed for 50 kPa net normal stress indicating a flatter slope of the SWCC and lower desaturation rate. Therefore, it can be observed that, SWCC of specimens compacted dry of optimum is dependent on the applied stress history. Similar results were also observed by

Vanapalli et al. (1999) for sandy clay till. The above phenomenon is attributed due to the reduction in interclod pore spaces with increasing normal stresses.

Table 4.4 Fitting Parameters for Specimens Compacted Dry of Optimum

	Net Normal Stress (σ-u_a), kPa	
Parameters	25	50
α (1/kPa)	0.0159	0.0123
n	1.1454	1.1335
m	0.1269	0.1178

By using measured saturated water permeability (k_s = 1E-7 m/s), the best fit parameters were input to the equation proposed by Maulem (1976) for obtaining the permeability functions. The permeability functions obtained for 25 and 50 kPa net normal stresses for the specimens compacter dry of optimum are presented in Figure 4.22. It can be observed that, the change in permeability functions for different net normal stresses are not significant which may be due to small change in SWCC parameters for the net normal stresses considered for this study.
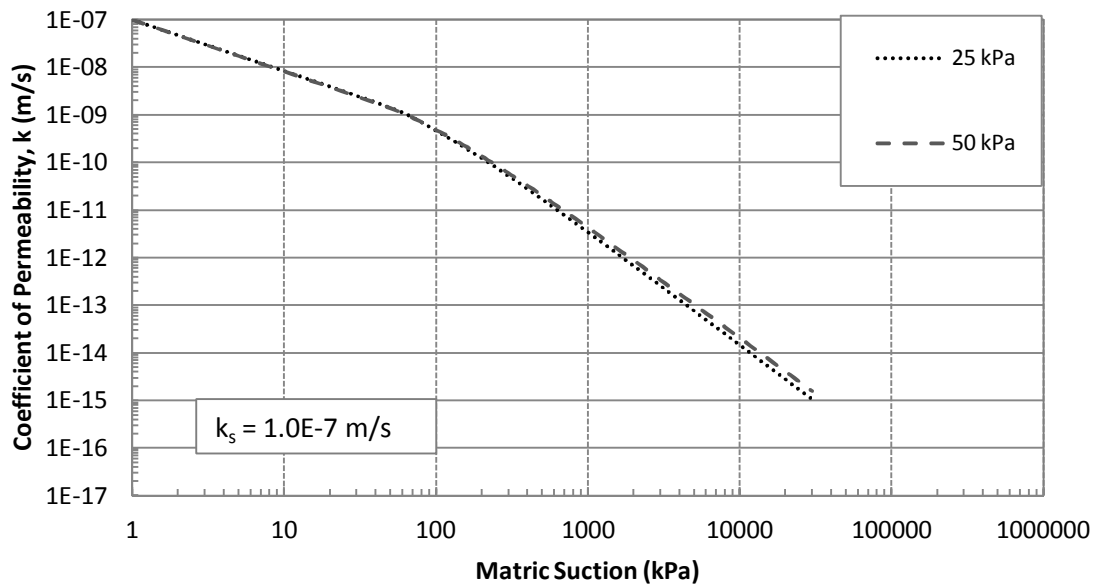
Figure 4.22 Permeability function computed from measured SWCC under 25 and 50 kPa net normal stresses (dry of optimum)

4.3.3 Effect of Initial Water Content

Soil water characteristic curves with different initial water content but at same density are presented in Figure 4.23 for net normal stress of 25 kPa. The drying characteristic with respect to suction is different for specimens with different initial water contents. Specimens compacted wet of optimum (29.5%) shows a higher air entry value compared to the specimens compacted dry of optimum (18%) which indicates that the resistance to desaturation is low for specimens in dry of optimum as compared to the wet of optimum. Similar result was also observed for net normal stress of 50 kPa which is presented in Figure 4.24.
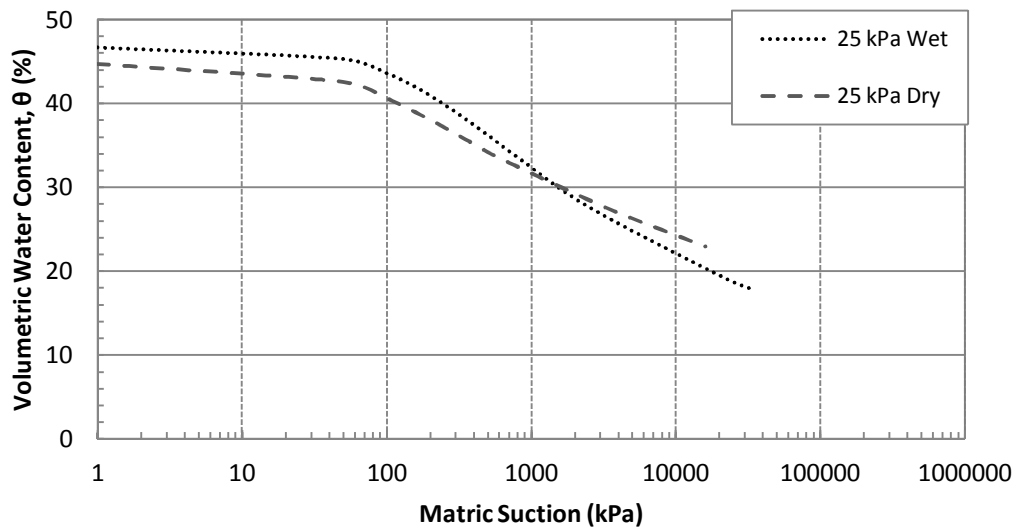
Figure 4.23 SWCC for specimens at 25 kPa net normal stress with different initial water content
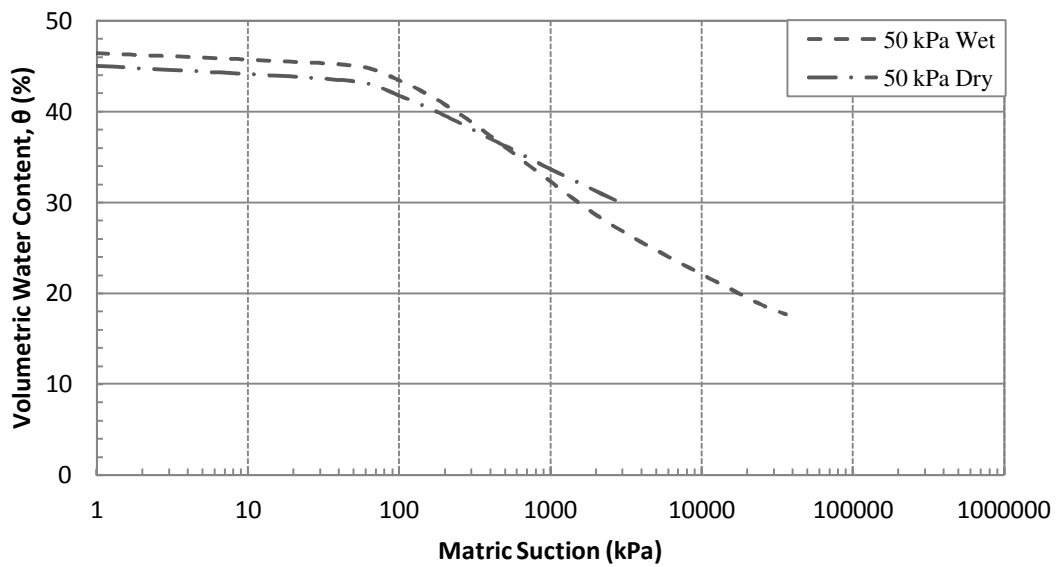
Figure 4.24 SWCC for specimens at 50 kPa net normal stress with different initial water content

The fitting parameters describing the SWCC using Van genuchten equation (1980) for 25 and 50 kPa net normal stresses with different initial water contents are presented in Table 4.5. From Table it can be seen that, the α parameter decreases for specimens compacted wet of optimum as compared to dry of optimum. This decrease in α parameter indicates an increase in air entry value as these are inversely related.

Table 4.5 Fitting Parameters for Specimens at Different Net Normal Stress and Initial Water Content

| | Net Normal Stress, $(\sigma-u_a)$, kPa | | | |
	Dry of Optimum (18%)		Wet of Optimum (29.5%)	
Parameters	25	50	25	50
α (1/kPa)	0.0159	0.0123	0.0064	0.0063
n	1.1454	1.1335	1.2190	1.2184
m	.1269	0.1178	0.1797	0.1792

The difference in the observed behavior for specimens on the wet and dry side of optimum water content, may be due to formation of different macro-structure. The specimens compacted dry of optimum contain large pore spaces between the clods of soil as compared to the pore spaces within the clods (Benson et al., 1990; Vanapalli, 1999). Suction required to remove water from larger pore spaces is relatively low as compared to the microscopic pore spaces between soil particles within the clods of clay. Therefore, the macrostructure of the specimens compacted dry of optimum controls the initial desaturation.

On the other hand, specimens compacted wet of optimum do not contain inter connected pore spaces and offer more resistance to desaturation as compared to the specimens compacted dry of optimum. For specimens compacted on the wet side, the micro-structure controls the

desaturation resulting in a higher resistance and flatter slope of the SWCC as compared to the specimens compacted dry of optimum.

4.4 Unsaturated Shear Strength

Multi-stage shearing test have been performed using suction controlled ring shear device in order to study the influence of suction on the shear strength of unsaturated Eagle Ford clay under this study. Three tests have been carried out at suction states, $(u_a - u_w)$ = 25, 50 and 100 kPa under three different net normal stresses, $(\sigma - u_a)$ = 25, 50 and 100 kPa. The effect of net normal stresses on the shear strength for a suction of 25 kPa is presented in Figure 4.25. It can be readily observed that both the peak and residual strength increases with the increase in net
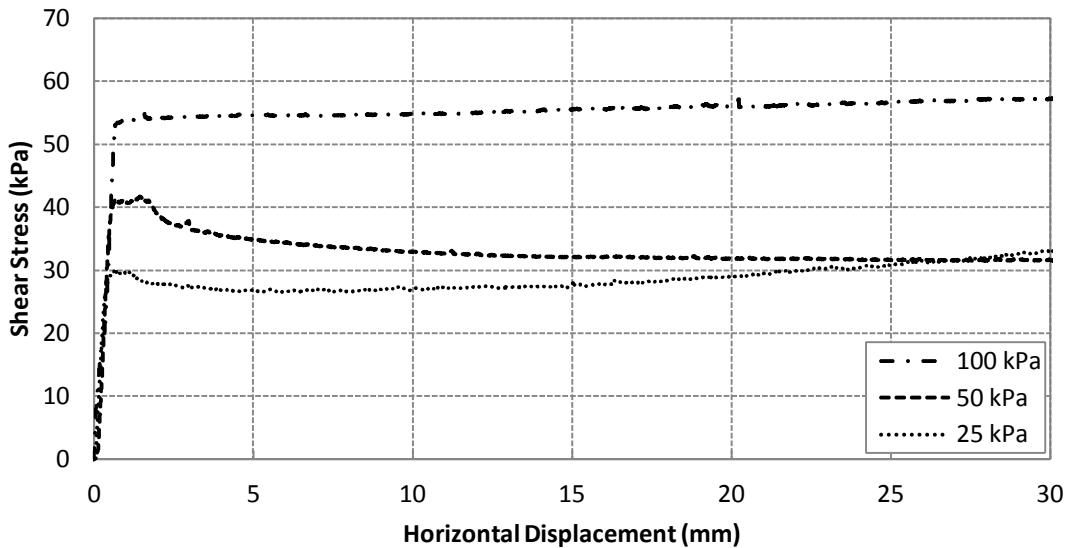
Figure 4.25 Results from multi-stage RS test under matric suction, $(u_a - u_w)$ = 25 kPa and net normal stress, $(\sigma_n\text{-}u_a)$ = 25, 50 and 100 kPa

normal stresses. However, no clear peak was observed for net normal stress of 100 kPa rather it showed a hardening behavior. Similar increase in shear strength with increasing net normal stresses was also observed for suction states of 50 and 100 kPa which are presented in Figure

4.26 and 4.27. In both cases, a clear peak was observed which subsequently reached to a residual state condition indicating a hardening-softening behavior.
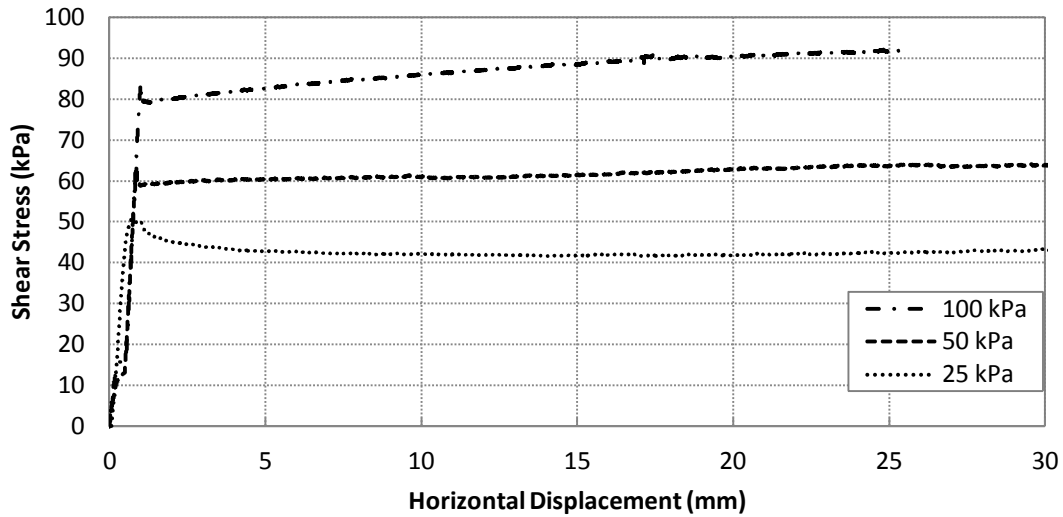
Figure 4.26 Results from multi-stage RS test under matric suction, $(u_a - u_w) = 50$ kPa and net normal stress, $(\sigma_n\text{-}u_a) = 25$, 50 and 100 kPa
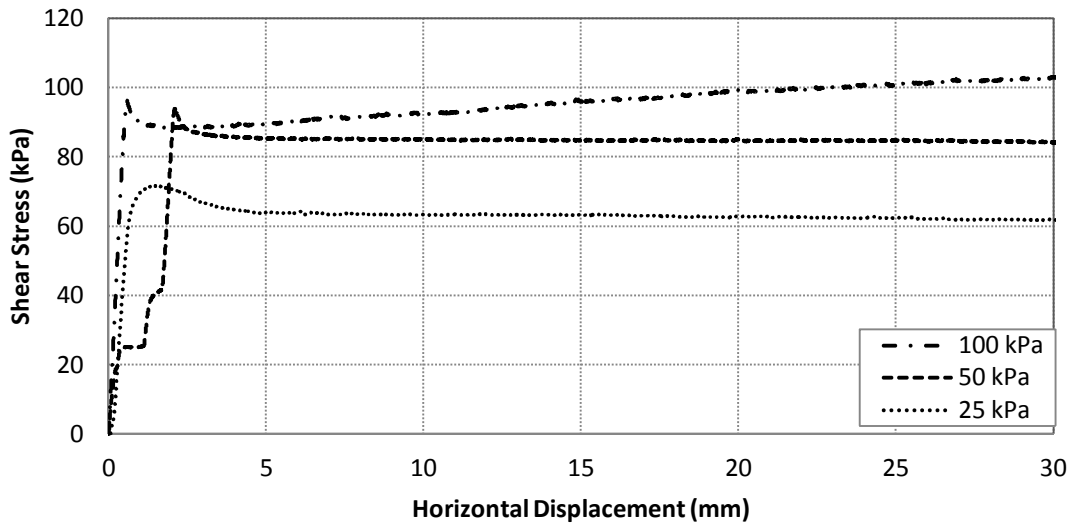
Figure 4.27 Results from multi-stage RS test under matric suction, $(u_a - u_w) = 100$ kPa and net normal stress, $(\sigma_n\text{-}u_a) = 25$, 50 and 100 kPa

The shear stress versus horizontal displacement curves at three suction states and 25 kPa net normal stress are presented in Figure 4.28. It can be noted that sample shows an increase in shear strength reaching a peak value and then shows a gradual decrease with increasing

125

horizontal displacement until a residual state is reached. It can be readily observed that both the peak and residual strength increases with increase in suction. Such an increase can be interpreted due to the process of particle aggregation during drying which makes the material more granular at high suctions. Similar behavior was also observed by Merchán et al., (2008); Hossain and Yin (2010) and Velosa, (2011). Merchán et al., (2008) suggested that the increase in suction increases the dilatancy of the material for low to medium plasticity clay which in turn increases the strength with increasing suction. Similar results were also observed for net normal stresses at 50 and 100 kPa which are presented in Figure 4.29 and 4.30.
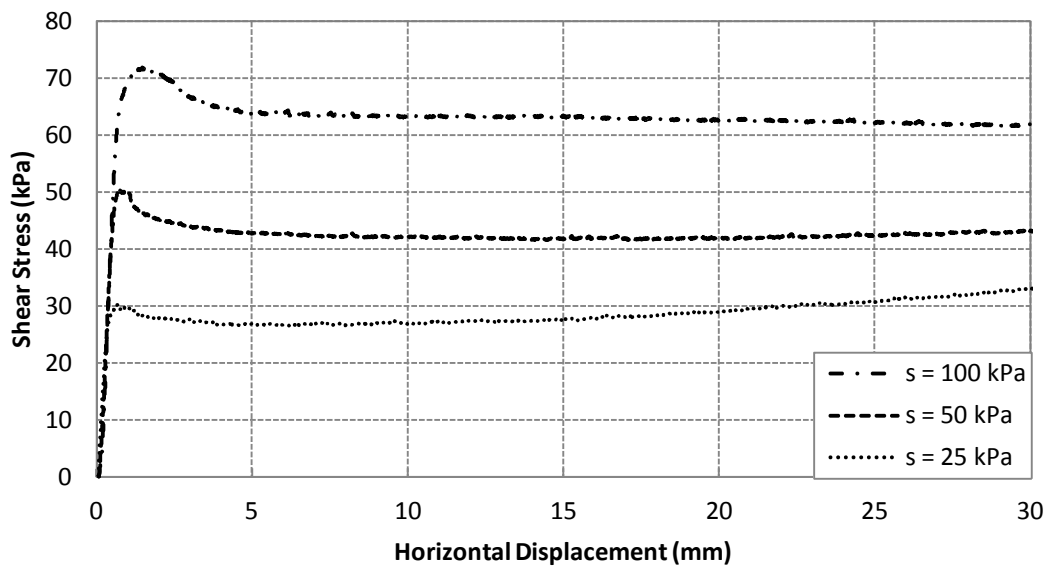
Figure 4.28 Results from multi-stage RS test under matric suction, $(u_a - u_w)$ = 25, 50 and 100 kPa and net normal stress, $(\sigma_n\text{-}u_a)$ = 25 kPa
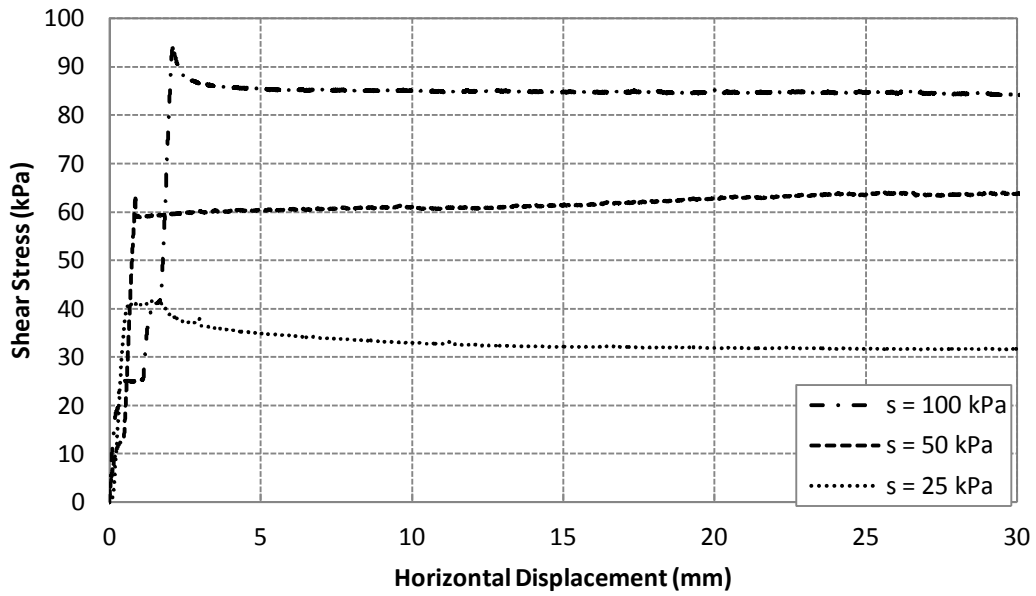
Figure 4.29 Results from multi-stage RS test under matric suction, $(u_a - u_w) = 25, 50$ and 100 kPa and net normal stress, $(\sigma_n\text{-}u_a) = 50$ kPa
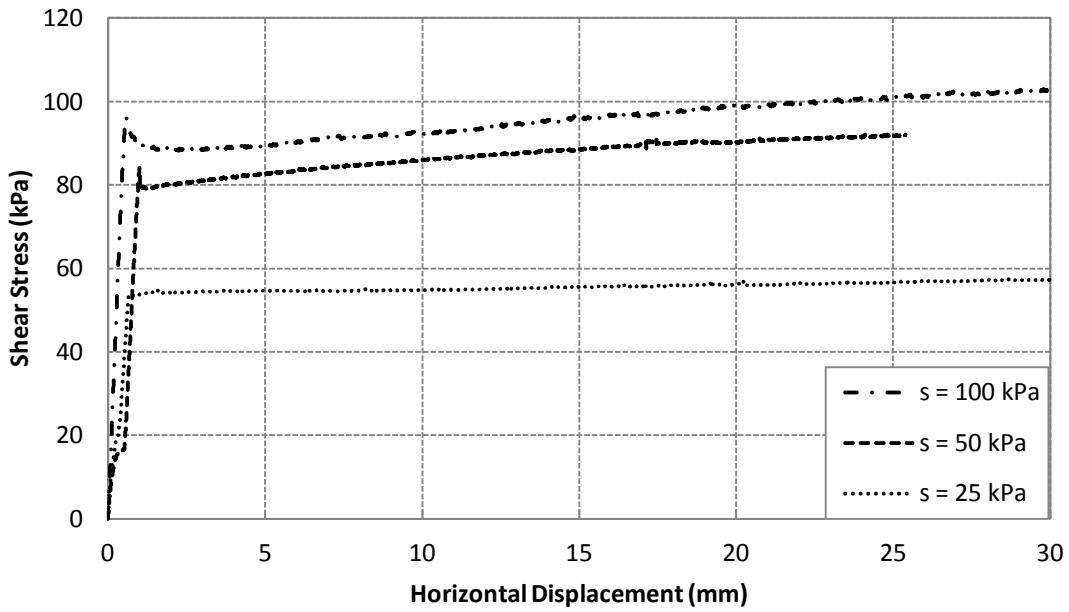
Figure 4.30 Results from multi-stage RS test under matric suction, $(u_a - u_w) = 25, 50$ and 100 kPa and net normal stress, $(\sigma_n\text{-}u_a) = 100$ kPa

4.4.1 Peak Failure Envelope

Figure 4.31 shows the effect of matric suction on both the position and slope of unsaturated peak failure envelope of compacted high PI expansive clay. It can be observed that matric suction plays a significant influence on the position of peak failure envelope with a considerable higher position for suction value of 100 kPa. For the range of matric suction considered, the increase in peak strength with increasing net normal stress appears to be linear. However, at 100 kPa suction the failure envelope appears to be non-linear. However, an increase in both the apparent cohesion, c´ and peak friction angle, φ´ with suction was observed.

Figure 4.31 Effect of matric suction on peak failure envelope of expansive clay

The variation of peak friction angle as well as cohesion intercept with suction is presented in Figure 4.32. It can be observed that, most of the increase in cohesion occurs between suction 25 and 50 kPa. The effect of suction on c´ becomes smaller for suction value of

100 kPa. On the other hand, the variation of friction angle with suction exhibits a different behavior. It can be noted that, the increase in φ´ is more prominent with the increase in suction with a much higher value at 100 kPa suction as compared to 25 and 50 kPa suction. This phenomenon suggests that the increase in peak strength is due to both capillary cohesion and friction angle.

Figure 4.32 Variation of peak friction angle and cohesion intercept with suction

Figure 4.33 shows the effect of net normal stress on both the position and slope of the peak failure envelope projected on to the peak shear stress versus matric suction plane. It can be observed that the increase in peak shear strength with increasing suction appears to be linear. However, the failure envelope at 100 kPa net normal stress shows a significant non-linearity with respect to matric suction. The φ^b value commences a value of 48.99° at matric suctions close to zero and decreases significantly at matric suctions in the range of 50 and 100 kPa and reaches to an asymptotic value. Similar results were also reported by Gan et al., (1988) and Zhan et al.,

(2006) from direct shear tests on unsaturated soils. The above phenomenon indicates that increase in suction at large value proves not to be so effective in increasing shear strength of soil. This can be attributed due to very little water filled pores in the soil skeleton to be sufficient enough to exert significant contribution in increasing strength of soil as effective as an increase in net normal stress. The variation of φ^b with net normal stress is also presented in Figure 4.34. It can be observed that φ^b increases with increase in net normal stress. Similar trend was also observed for φ' when it was compared with matric suction in Figure 4.30.

Figure 4.33 Effect of net normal stress on peak failure envelope of expansive clay

Figure 4.34 Variation of φ^b with net normal stress

In order to identify the effect of matric suction on the peak shear strength, values of angle φ^b are plotted in Figure 4.35 with respect to matric suction at different net normal stress. It can be

Figure 4.35 Variation of φ^b with suction and net normal stress

131

observed that, φ^b angle remains constant at low net normal stresses for all values of matric suction considered. On the other hand, for higher net normal stress (i.e. at 100 kPa) the contribution of matric suction toward the increase in peak shear strength is reduced as matric suction increases.

According to Vanapalli et al., (1996), there is a direct correspondence between the nonlinear nature of the peak shear strength envelope with respect to increasing matric suction and the behavior of the SWCC. At relatively low matric suction, and prior to the air-entry pressure, the soil pores remain essentially saturated. The shear strength envelope is approximately linear at this stage, and φ^b is effectively equal to the angle of internal friction φ'. The geometries of the interparticle pore water menisci dramatically change as the soil becomes unsaturated, which affects the resultant interparticle forces contributing to effective stress on the soil skeleton and, in turn, to shear strength. The reduction in the volume of pore water within this regime effectively reduces the contribution that matric suction has toward increasing shear strength. This effect is more noticeable at high net normal stresses.

4.4.2 Residual Failure Envelope

Figure 4.36 shows the effect of matric suction on both the position and slope of unsaturated residual failure envelope of compacted high PI expansive clay. It can be observed that matric suction plays a significant influence on the position of residual failure envelope with a considerable higher position for suction value of 100 kPa. For the range of matric suction considered, the increase in peak strength with increasing net normal stress appears to be linear. However, at 100 kPa suction the failure envelope appears to be non-linear. However, an increase

132

in both the apparent residual cohesion, c'_r and residual friction angle, φ'_r with suction was observed.
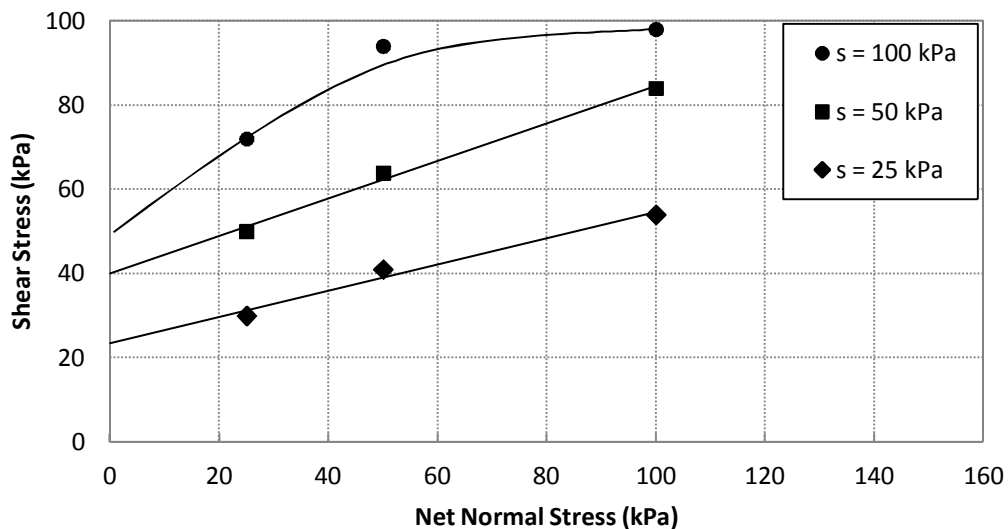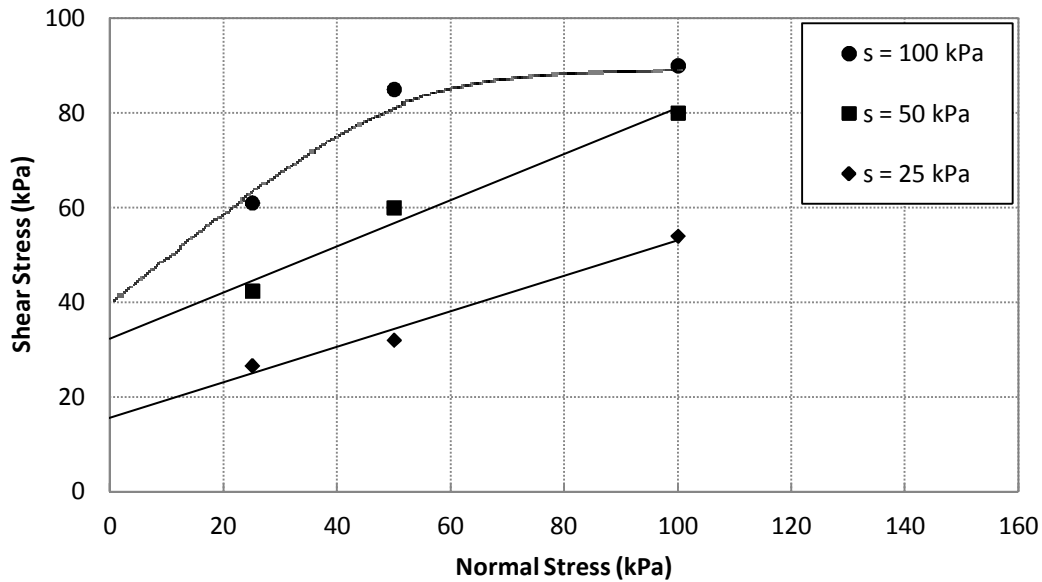

Figure 4.36 Effect of matric suction on residual failure envelope of expansive clay

The variation of residual friction angle as well as cohesion intercept with suction is presented in Figure 4.37. It can be observed that, most of the increase in cohesion occurs between suction 25 and 50 kPa. The effect of suction on c'_r becomes smaller for suction value of 100 kPa. On the other hand, the variation of residual friction angle with suction exhibits a different behavior. It can be noted that, the increase in φ'_r is more prominent with the increase in suction with a much higher value at 100 kPa suction as compared to 25 and 50 kPa suction. Similar trend was also observed for peak shear strength values with respect to suction (Figure 4.30). However, Merchán et al., (2008) reported only an increase residual friction angle with respect to suction for low to medium plasticity clay and found that residual cohesion intercept is independent of suction.
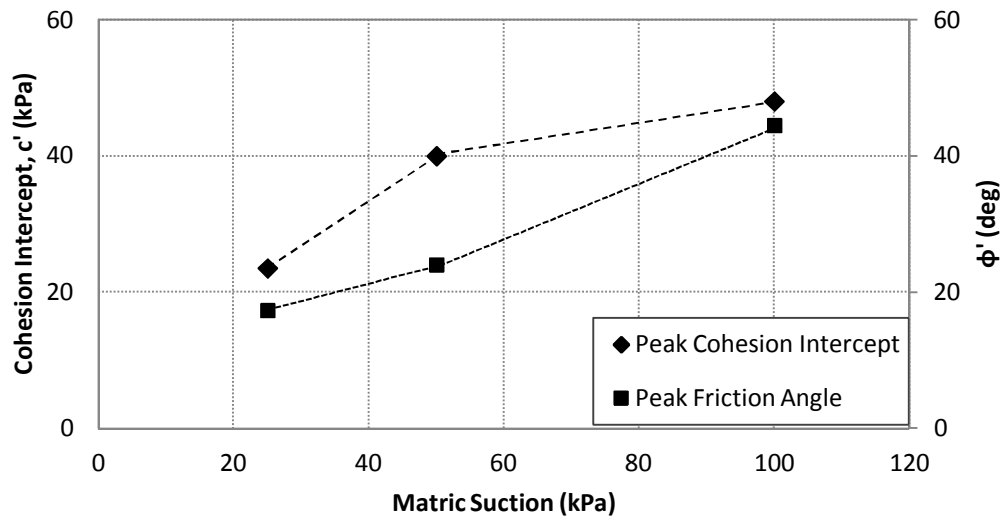
133
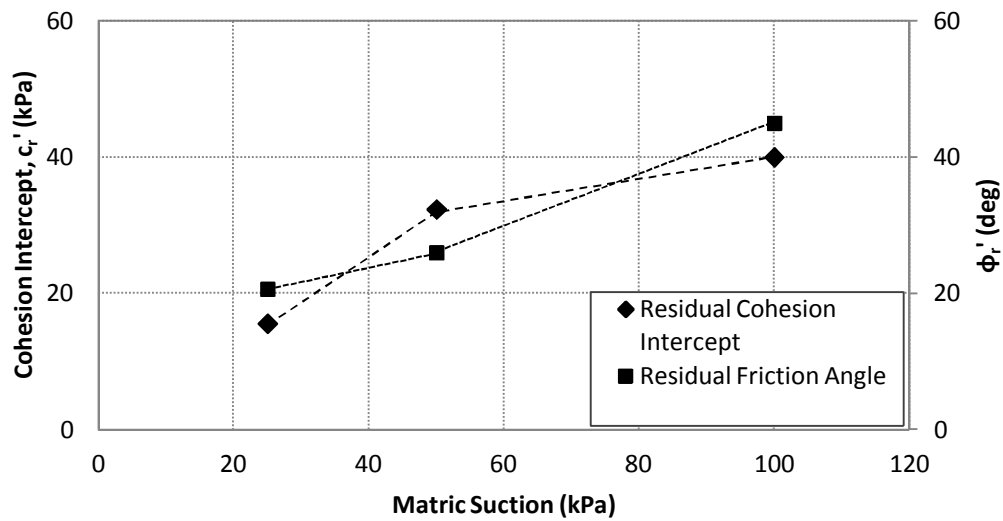
Figure 4.37 Variation of residual friction angle and cohesion intercept with suction

Figure 4.38 shows the effect of net normal stress on both the position and slope of the residual failure envelope projected on to the residual shear stress versus matric suction plane. It can be observed that the increase in residual shear strength with increasing suction appears to be linear. However, the failure envelope at 100 kPa net normal stress shows a significant non-linearity with respect to matric suction. The φ^b_r value commences a value of 48.99° at matric suctions close to zero and decreases significantly at matric suctions in the range of 50 and 100 kPa and reaches to an asymptotic value. Similar results were also observed for φ' with respect to matric suction. The variation of φ^b_r with net normal stress is also presented in Figure 4.39. It can be observed that φ^b_r increases with increase in net normal stress. Similar trend was also observed for φ^b when it was compared with net normal stress in Figure 4.34.
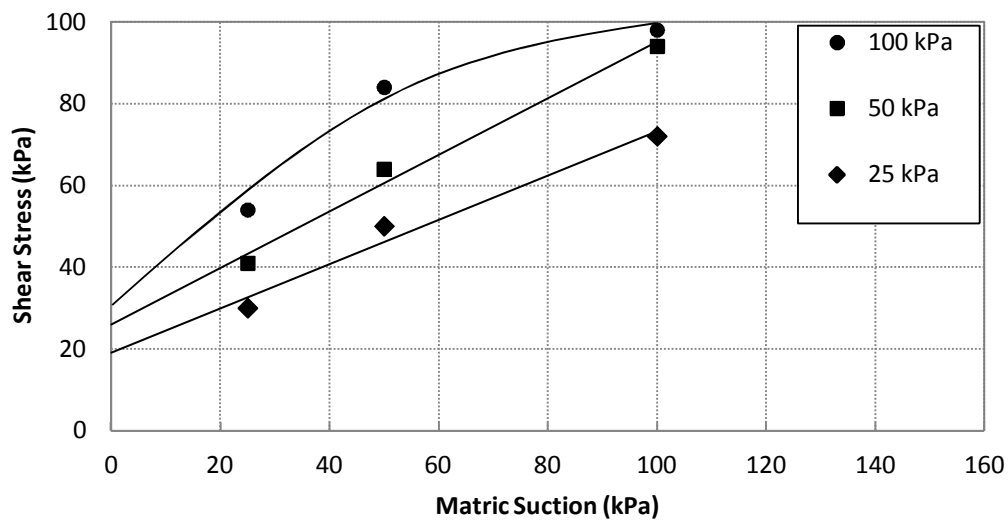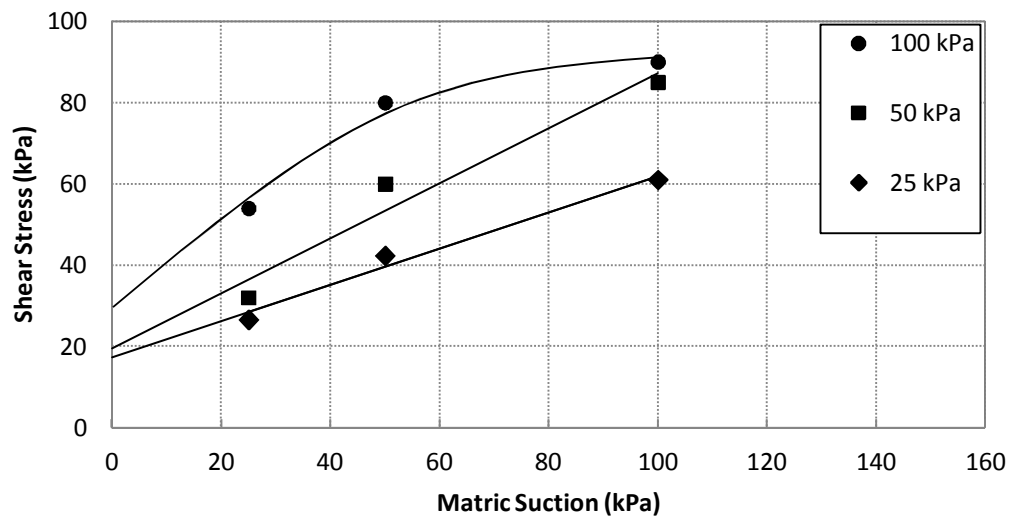
Figure 4.38 Effect of net normal stress on residual failure envelope of expansive clay
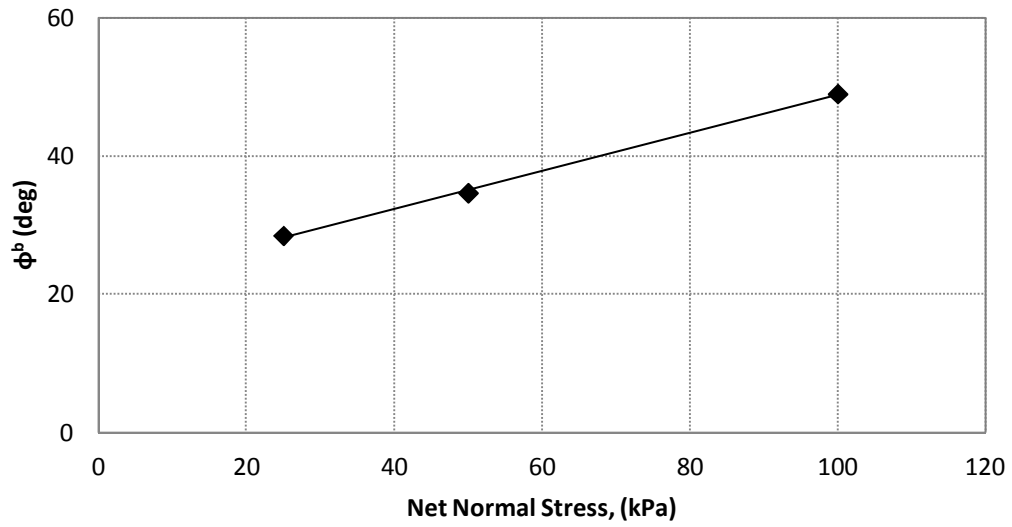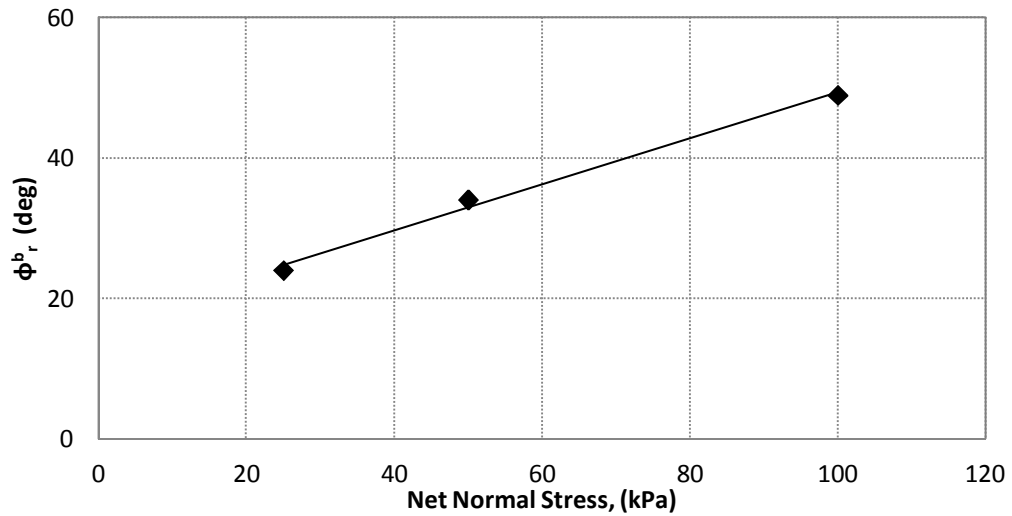

Figure 4.39 Variation of φ^b_r with net normal stress

In order to identify the effect of matric suction on the residual shear strength, values of angle φ^b_r are plotted in Figure 4.40 with respect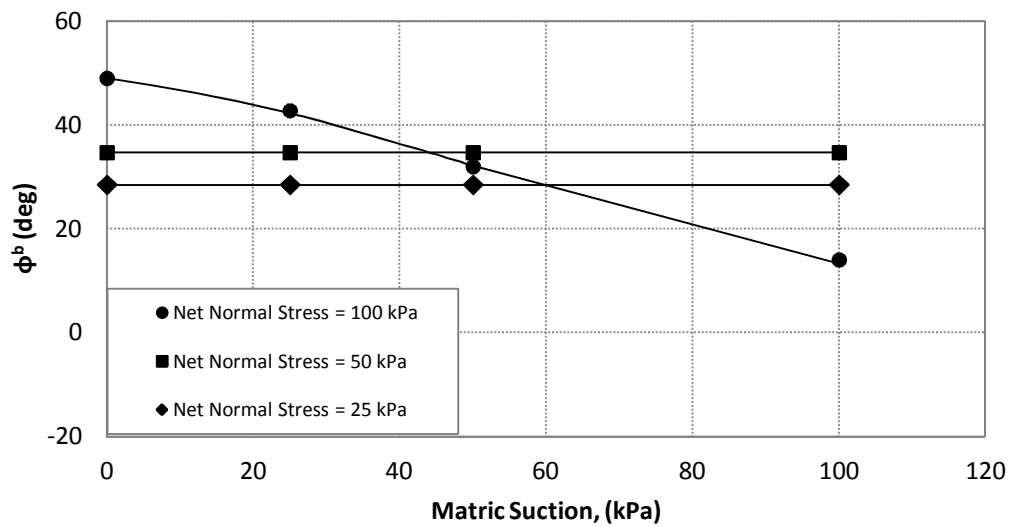 to matric suction at different net normal stress. It can be observed that, φ^b_r angle remains constant at low net normal stresses for all values of
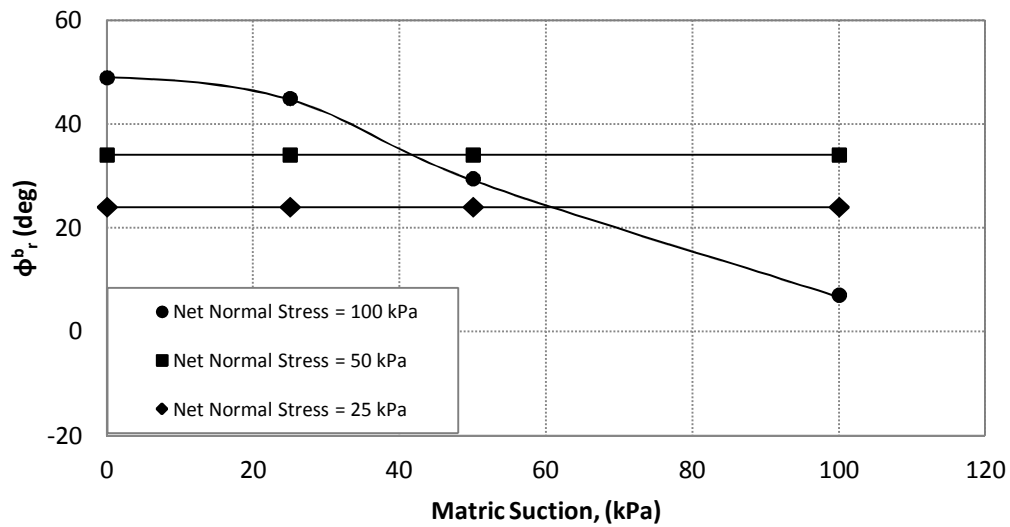
Figure 4.40 Variation of φ^b_r with suction and net normal stress

matric suction considered. On the other hand, for higher net normal stress (i.e. at 100 kPa) the contribution of matric suction toward the increase in residual shear strength is reduced, even becomes a negative value, as matric suction increases. Similar behavior has also been observed for φ^b angle with matric suction at different net normal stresses which was presented in Figure 4.35.

4.5 Direct Shear Test Results

Multi-stage direct shear tests have been performed on saturated specimen to study the effect of softening behavior due to wetting and drying. However, during the tests, no clear residual condition was observed and only the peak shear strength parameters have been obtained. The failure envelopes for the three tests performed under different conditions are presented in

Figure 4.41. From figure it can be observed that, Test 1 and 3 have almost identical failure envelope. On the other hand, reduction in shear strength parameter has been observed for Test 2.
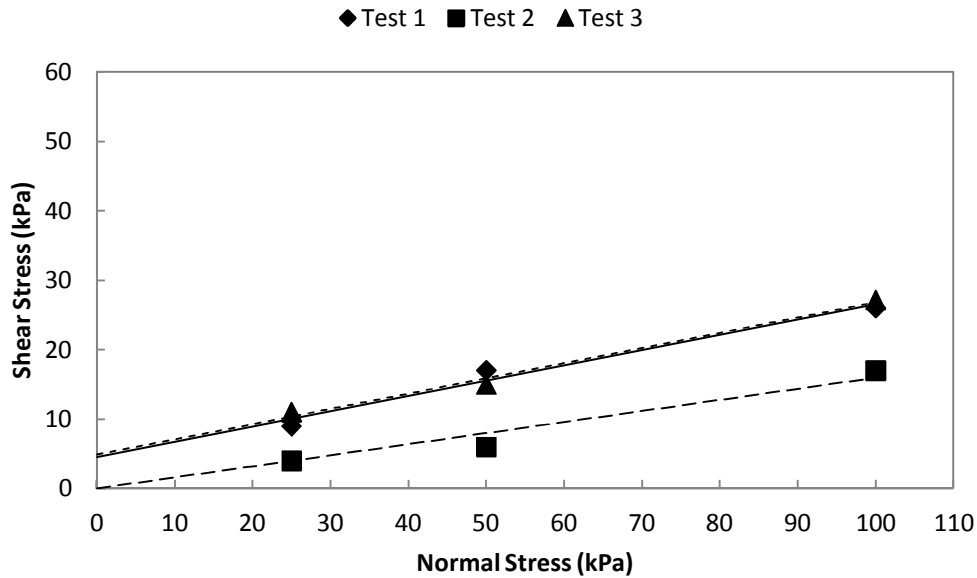
Figure 4.41 Effect of wetting and drying on peak failure envelope of expansive clay

Table 4.6 presents the estimated shear strength parameters for the three multi-stage tests performed under different condition. From table it can be noted that, Test 2 which has been performed with one cycles of wetting and drying allowing no volume change shows a decrease in both cohesion intercept and angle of internal friction. On the other hand, no change in shear strength is observed for Test 3 which was also subjected to one cycles of wetting and drying and allowing volume to change as compared to Test 1 which was performed without subjecting to wet-dry cycle.

Table 4.6 Peak Shear Strength Parameters for Multi-stage Direct Shear Tests

Soil	Test No.	σ, kPa	Wet-Dry Cycle	No. of Stages	Condition	c´(kPa)	φ´
CH	1	25 50 100	No	3	Conventional	4.515	12.41
	2	25 50 100	1	3	No volume change	0	9.09
	3	25 50 100	1	3	Volume change	4.92	12.37

Based on the test results, it can be observed that, the reduction in cohesion due to cycles of wetting and drying is more significant as compared to reduction in friction angle. Shear strength of soil derived from cohesion is completely lost after wet-dry cycles. Rogers and Wright (1984), Kayyal and Wright (1991) and Zornberg et al., (2007) also reported that reduction in cohesion is more significant due to cycles of wetting and drying. Therefore, the changes in shear strength of a slope constructed on high PI expansive clay, is attributed due to two different physical processes: reduction in shear strength due to wet dry cycle and reduction in matric suction during rainwater infiltration.

CHAPTER 5

NUMERICAL MODELING

5.1 Introduction

In this section a two dimensional numerical study on the pore pressure response in an initially unsaturated soil slope constructed on expansive clay subjected to various rainfall conditions is conducted. Finite element software PLAXIS has been used to perform the numerical study of rain infiltration and subsequent slope stability. The main objective of this numerical study is to compare the pore pressure distribution in the field with the numerical study and also to investigate the influence of SWCC of expansive clay and rainfall intensity and duration on pore pressure response as well as stability of slope.

5.2 Background

In this study, the finite element program PLAXIS was used which incorporates the soil water characteristic curve (SWCC) and permeability function to simulate the flow of water through unsaturated soil. Water flow through unsaturated soil is governed by the same concept which is known as Darcy's law but the coefficient of permeability (k_w) is a function of water content in unsaturated soils which is assumed to be constant in saturated soils.

The flow of water in unsaturated soil can be modeled by Richard's equation (Dogan and Motz, 2005);

$$\left\{\frac{\partial}{\partial x}\left[k_x(h)\frac{\partial h}{\partial x}\right] + \frac{\partial}{\partial y}\left[k_y(h)\frac{\partial h}{\partial y}\right] + \frac{\partial}{\partial z}\left[k_z(h)(\frac{\partial h}{\partial z} + 1)\right]\right\} = [C(h) + S.S_s]\frac{\partial h}{\partial t} \qquad (5.1)$$

where k_x, k_y, and k_z are permeability coefficients in x, y and z directions respectively, $C(h)$ is the specific moisture capacity (1/L) and S_s is the specific storage (1/L). The equation states that the sum of the rates of change of flows in the x-direction and y-direction is equal to the rate of change of the head with respect to time. For steady state flow, water entering and leaving a soil element is same at all times and thereby the right hand side of the equation vanishes.

In unsaturated flow, the hydraulic conductivity is highly dependent on the degree of saturation of a soil. As saturation decreases, the volumetric water content of the soil also decreases which affects the movement of water through the soil because there are less water filled spaces available for water flow (Gasmo et al. 2000). According to Ng et al. (1998), water flows along a web of interconnected conduits in soils. The size and number of the interconnected pores increases with the increase in moisture content which enhances the ability to flow water. Therefore, the hydraulic conductivity is highest at the saturated condition but keeps decreasing as more water is expelled from the pores through the disappearance of the continuous water-filled conduits.

However, the coefficient of permeability is not constant in unsaturated soils but is a function of matric suction. Estimates of the unsaturated water coefficient of permeability are difficult to obtain because measuring this parameter is time consuming and expensive. Several

investigators, therefore, used models for calculating unsaturated water coefficient of permeability from the more easily measured soil-water characteristic curve (Brooks and Corey, 1964; Maulem 1976; Van Genuchten, 1980; Fredlund et al., 1994).

5.3 Numerical Study of Slope Infiltration

The numerical study of infiltration of rainwater into the slope was performed using the finite element program PLAXFlow. The purpose of the study was to determine the pore pressure distribution in the slope due to varying rainfall intensity and duration. The study also focuses on the influence of SWCC on the pore pressure distribution in the slope.

5.3.1 Finite Element Model

The finite element model was constructed based on the site condition along US 287 S Hwy under this study. The existing embankment is about 9.2 m high with a side slope of 3 (H): 1(V). The slope was divided into three different soil layers according to their approximate stress state and permeability condition which is presented in Figure 5.1.
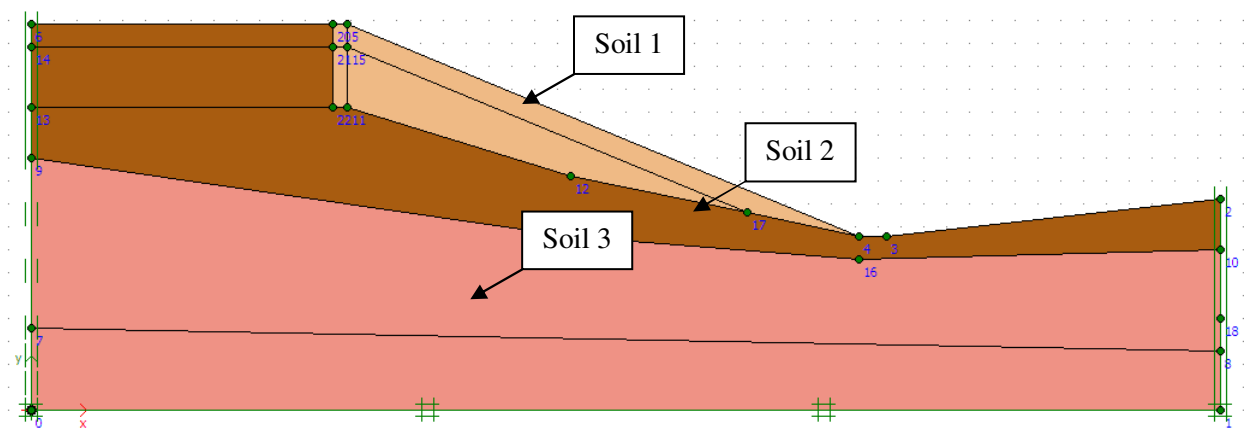
Figure 5.1 Soil Slope Model

141

To carry out a finite analysis using PLAXIS, a finite element mesh has been created and the material properties and boundary conditions are specified. This is done during pre-processing of data. To set up a finite element model, a two-dimensional geometry model composed of points, lines and other components has been created in the XY-plane. The generation of an appropriate finite element mesh and the generation of properties and boundary conditions on an element level are automatically performed by the PLAXIS mesh generator based on the input of the geometry model. The final part of the input comprises the generation of water pressures and initial effective stresses to set the initial state.

Finite element model used in this analysis is plain strain model. A plain strain model is used for geometries with a (more or less) uniform cross section and corresponding stress state and loading scheme over a certain length perpendicular to the cross section (z direction). Displacements and strains in z-direction are assumed to be zero. However, normal stresses in z direction are fully taken into account. The 15-node triangle, used in this study, is a very accurate element that has produced high quality stress results for difficult problems. Standard fixities were used as boundary condition. The two vertical boundaries were free to move vertically and were considered to be fixed in the horizontal boundary direction. The bottom boundary was modeled as fixed boundary.

The boundary conditions for the steady state and transient condition in the seepage model were defined as shown in Figure 5.2. The conditions along the left and right vertical boundaries were defined as no flow boundary. The bottom boundary was specified as closed boundary and the top boundary as a flux boundary. Rainfall was simulated by specifying a pressure head ($\psi_{min} =0$) equal to zero at the surface which simulates non-infiltrating water

running off the slope. The presence of positive pressure head at the top surface is analogous to having a ponding situation. But the ponded water will run off an inclined slope and the maximum rainfall that can infiltrate into a slope will be a rainfall that will maintain a pressure head equal to zero at the top surface.
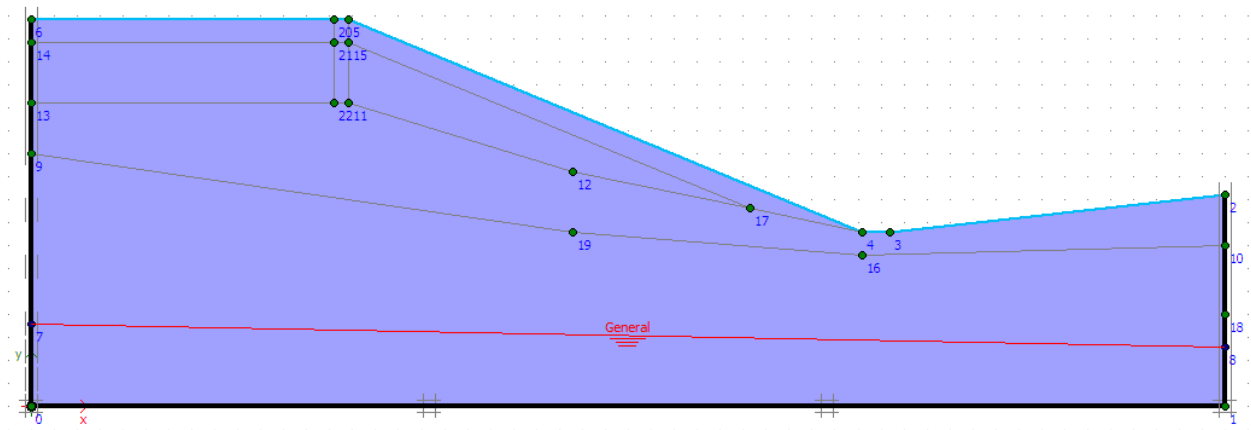
Figure 5.2 Boundary conditions of the soil slope model

5.3.2 Input Parameters for Seepage Analyses

The two dimensional finite element program PLAX Flow makes use of the permeability function proposed by Maulem (1976) based on the best fitting parameters obtained from Van Genuchten equation (1980) for SWCC to perform the steady state and transient seepage analysis. The best fitting parameters obtained from the stress dependent soil water characteristic curve using Tempe pressure cell along with saturated permeability which has been discussed in Chapter 3, were used as a input parameter for flow analyses. SWCC parameters considering volume change behavior obtained from the specimens compacted wet of optimum has been used for the current study which is presented in Table 5.1.

Table 5.1 Input Parameters for Predicting Permeability Function

Identification	Net Normal Stress, (kPa)	α (1/m)	n	m	Saturated Permeability, k_s (m/s)
Soil 1	25 and 50	0.064	1.219	0.1797	
Soil 2	100	0.064	1.2357	0.1908	3.54E-09
Soil 3	100	0.064	1.2357	0.1908	

5.3.3 Comparison with Field Data

Based on the information obtained from laboratory, the instrumented slope was used to compare the field pore pressure values at the end of a rainfall event with numerical simulation. For the current study, rainfall event observed on April 11, 2011 was used to compare with numerical study. Figure 5.3 shows the pore pressure profile at the end of the rainfall event on April 11, 2011 from field instrumentation.

(a)   (b)
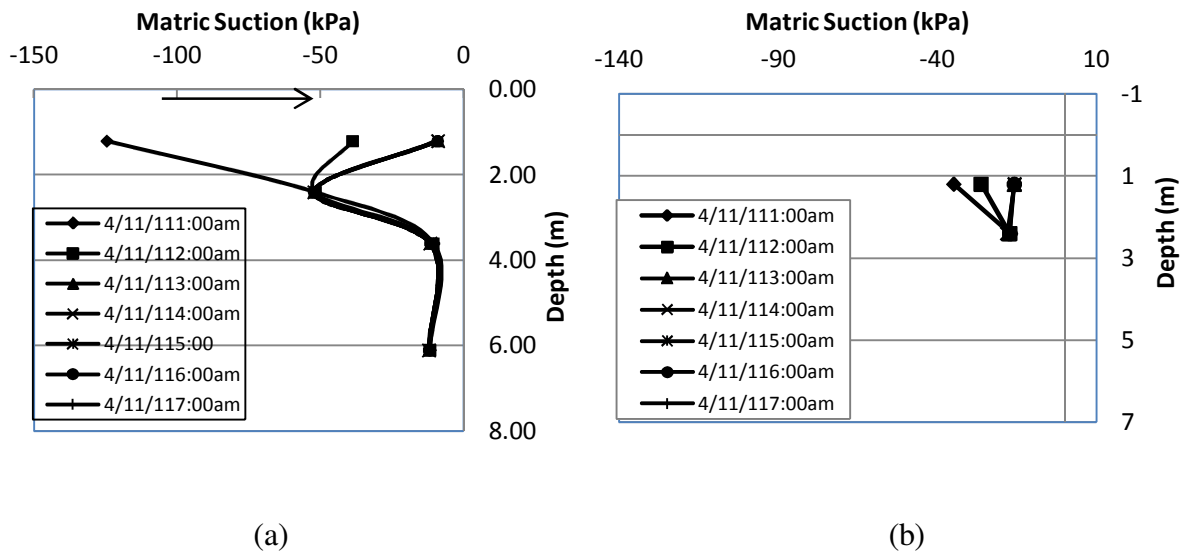
Figure 5.3 Pore pressure profile (a) at the crest and (b) at the middle of instrumented slope on April 11, 2011 rainfall event

In order to simulate the field condition, it was necessary to obtain the initial pore pressure condition on April 11, 2011 prior to rainfall. This was achieved by applying a negative flux of (0.195E-3 m/h) at the surface for a sufficient period of time. However, during the evaporation simulation, suction along the depth increased which could not be controlled. Although the pore pressure distribution on the top 2 m of soil was brought close to the field condition, the pore pressure distribution at depth below 2 m was high compared to the initial pore pressure distribution observed in the field. After achieving the field pore pressure condition on April 11, 2011, the transient seepage analyses were performed. The rainfall that occurred on April 11, 2011, lasted for 7 hours with the highest rainfall amount of 45.4 mm/h and a total rainfall amount of 54.2 mm which was given as a input in the seepage module (Figure 5.4).
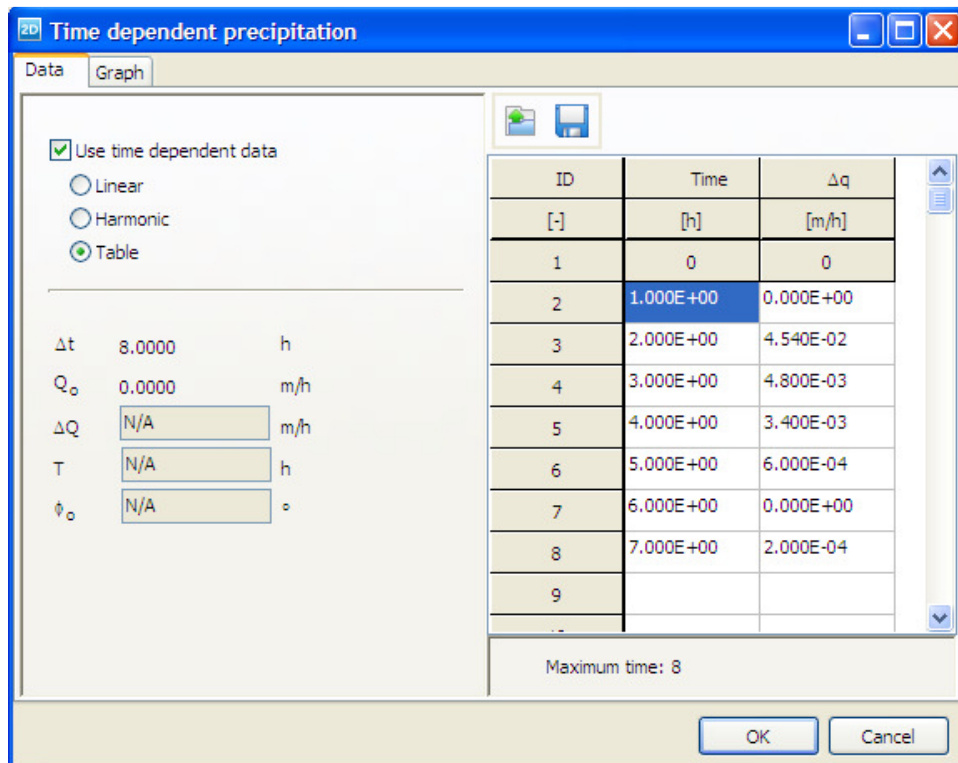
Figure 5.4 Input table for rainfall event on April 11, 2011

The pore pressure profiles both at the crest and bottom of slope from the numerical model are presented in Figure 5.5 (a) and (b). From the numerical model results, it can be seen that, there was no significant change in pore pressure distribution occurred after the rainfall event. The discrepancies between the field and the numerical results are believed to be due to low permeability used in the numerical analysis. Laboratory measurement of saturated permeability indicates a value of 3.54E-9 m/s which seldom exists in the field due to presence of cracks and fissures. Based on the field infiltrometer test, Zhan et al., (2007) reported that infiltration rate can increase on the three order of magnitude in areas of open cracks due to rapid ingress of water through the cracked portion.
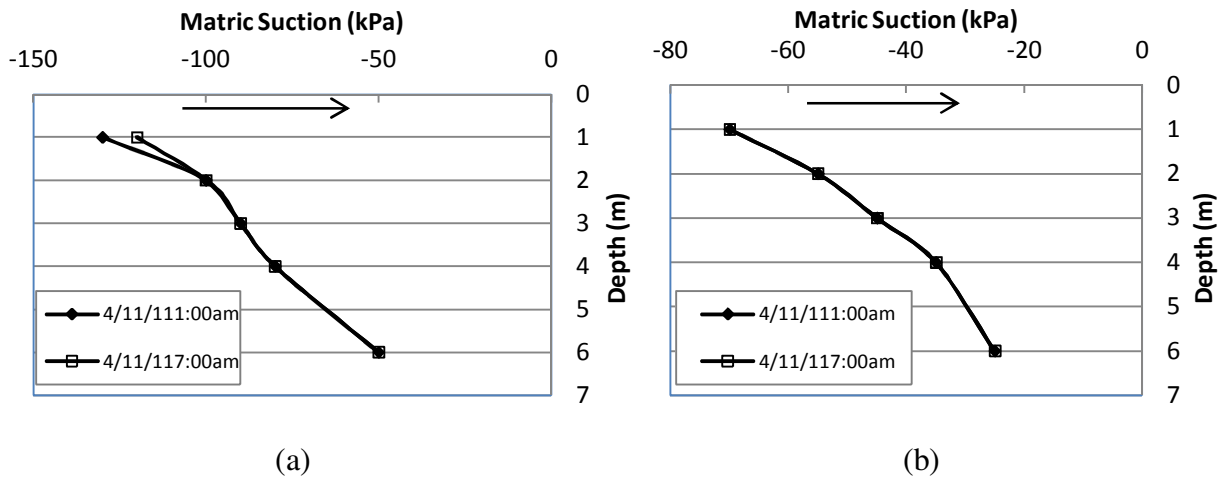
Figure 5.5 Pore pressure profile (a) at the crest and (b) at the middle of slope from numerical model

Aubeny and Lytton (2003) estimated 10 times increase in rate of moisture changes due to formation of cracks on high PI clays. Therefore, a high saturated permeability (k_s = 3.54E-6 m/s) value was adopted for top 3.6 m soil which is susceptible to weathering and cracking due to changes in climatic condition. The distribution of pore pressure profile with the revised saturated permeability is presented in Figure 5.6. The model shows a decrease in suction over time due to

applied rainfall. The shifting of the curve to the right shows the downward progression of the infiltration. However, it can be seen that, the modeling results over predicts the field infiltration rate which is clear through the formation of positive pressure at the middle of the slope at 2 m depth. From the field instrumentation, no change in pore pressure was observed at this depth due to the rainfall event on April 11, 2011.
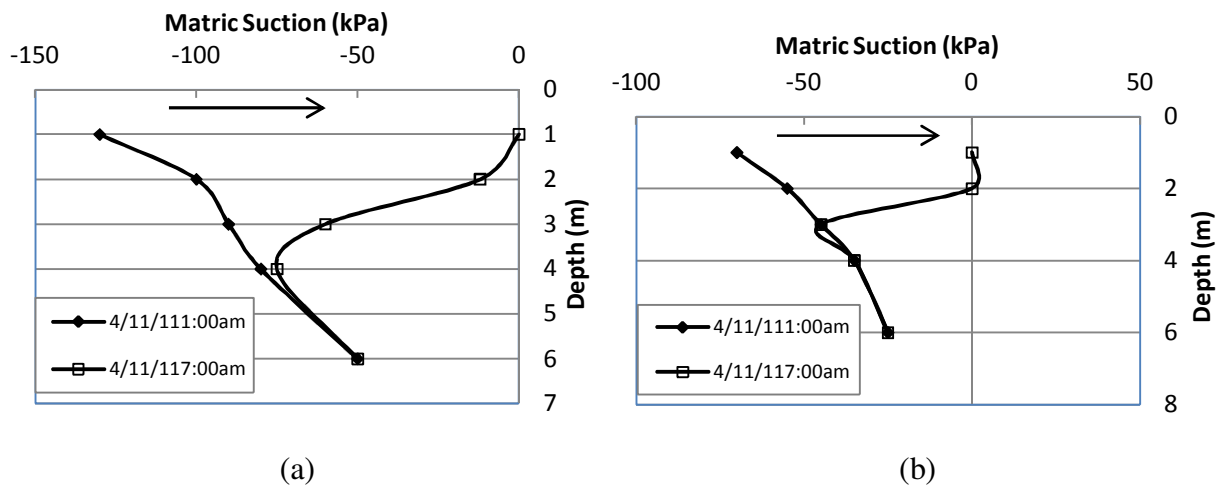
Figure 5.6 Pore pressure profile (a) at the crest and (b) at the middle of slope from numerical model with $k_s = 3.54E-6$ m/s

Due to crack formation in the field, the infiltration rate may be higher at the crest of the slope but field infiltration test data on cracked soil showed a decrease in infiltration rate with time in the cracked soil. Zhan et al. (2007) reported a decrease in field infiltration rate from field infiltrometer test on a slope constructed on expansive clay in the cracked region which is presented in Figure 5.7.Favre et al. (1997) also reported that high intensity rain falling onto a dry cracked soil resulted in rapid crack closure at the surface within 4.5 h because of swelling of unsaturated soils. Therefore, a saturated permeability ($k_s = 3.54E-7$ m/s) value in between the laboratory measurement and high permeability value was adopted for top 3.6 m soil. The

distribution of pore pressure profile with the revised saturated permeability is presented in Figure 5.8.
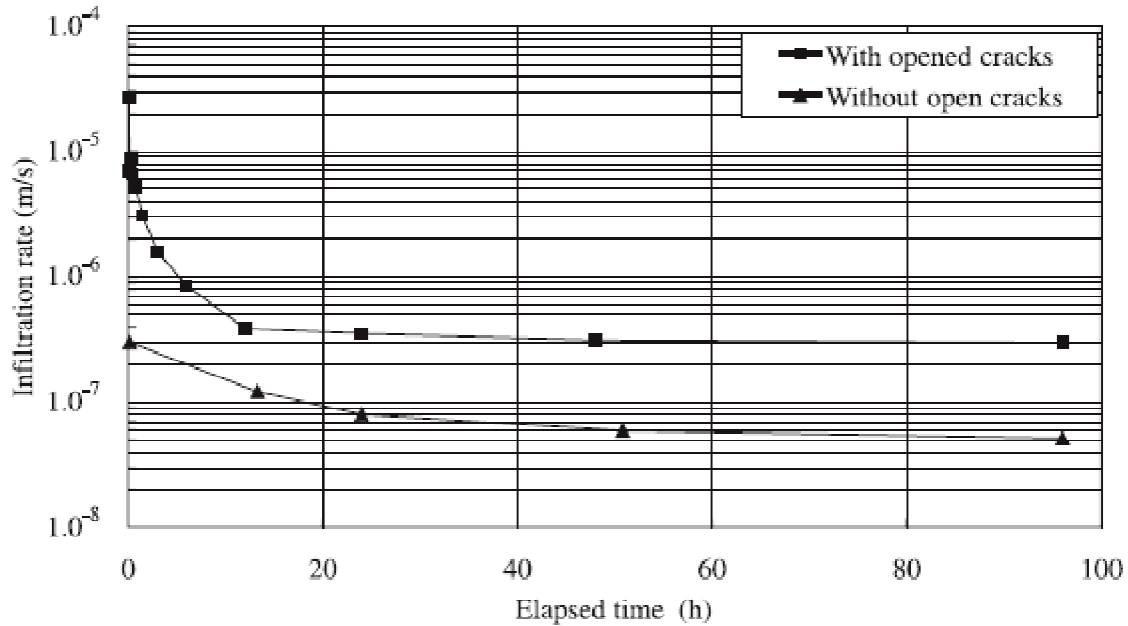
Figure 5.7 Change in infiltration rate with time from double-ring infiltration tests (Zhan et al., 2007)

The model shows a decrease in suction over time due to applied rainfall. The shifting of the curve to the right shows the downward progression of the infiltration. The results obtained from the revised value of permeability shows a similar trend as observed from the field but under predict the field infiltration value which is reflected through the suction value obtained at the end of rainfall period. Therefore, top 3 m of soil was divided into 3 layers with permeability of 3.54E-6, 3.54E-7 and 3.54E-8 m/s in order to account for high permeabiity due to crack formation. The distribution of pore pressure profile with the revised saturated permeability is presented in Figure 5.9. The model shows a decrease in suction over time due to applied rainfall. The shifting of the curve to the right shows the downward progression of the infiltration. The pore pressure profile obtained from the numerical modeling is believed to be an acceptable

match for the field condition and therefore the current model was used throughout the parametric study.
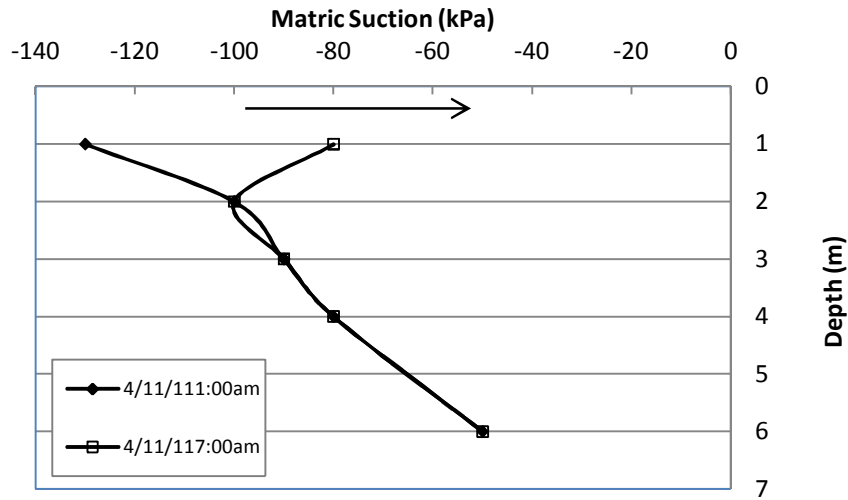
(a)
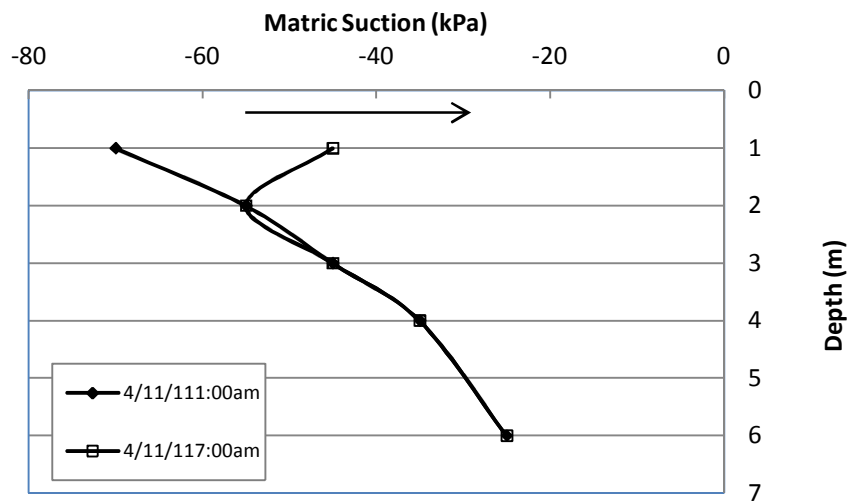
(b)

Figure 5.8 Pore pressure profile (a) at the crest and (b) at the middle of slope from numerical model with $k_s = 3.54E-7$ m/s
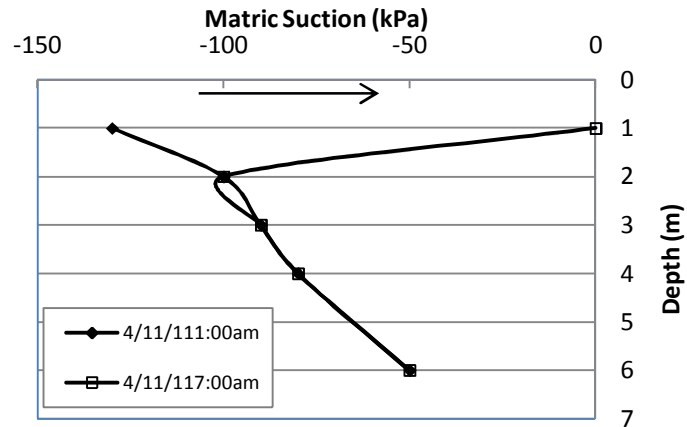
(a)
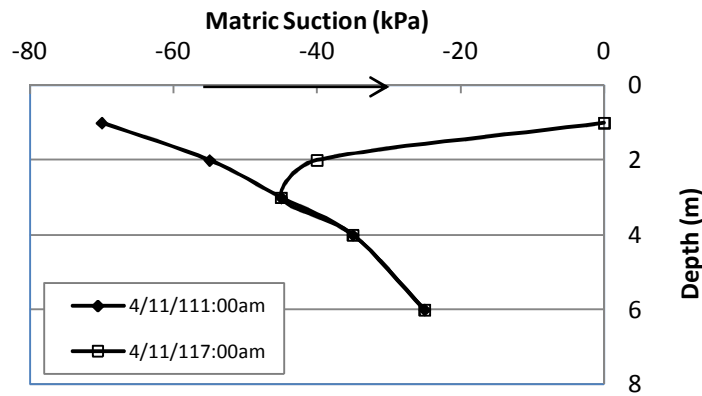
(b)

Figure 5.9 Pore pressure profile (a) at the crest and (b) at the middle of slope from numerical model with $k_s = 3.54E-7$ m/s

5.3.4 Simulated Rainfall Condition

In order to investigate the effect of rainfall on slope stability, rainfall events with 3 different return period were adopted (Table 5.2) based on the Texas rainfall data collected from National Oceanic and Atmospheric Administration (NOAA). Peck (1967) and Lumb (1975) suggested that rainfall duration of 10-day and 15-day affects slope stability most. On the other hand, Ng et al. (1998) suggested that the critical duration of antecedent rainfall varies between 2 to 7 days for Clayey Sandy Silt in Hong Kong with a 10 year return period. On the other hand,

according to Alonso et al. (1995), the risk of failure is controlled by the varying rates of infiltration, which in turn depend on rainfall intensities, the slope geometry and soil characteristics. Therefore, for a given rainfall event and slope geometry these properties control the evolution of factor of safety.

For the current study, rainfall duration was varied from 1 day to 5 day to identify the effect of prolonged rainfall period as well as rainfall intensity on stability of slope. From Table 5.2 it can be noted that, rainfall intensity decreases with the increase in rainfall duration. To identify the effect of total amount of rainfall on slope stability three different return period; 2, 5 and 10 years were considered for rainfall duration of 1 day to 5 day. A higher return period corresponds to a larger total rain amount which can be noted in Table 5.2.

Table 5.2 Summary of Various Rainfall Condition Simulated (NOAA)

Duration (day)	Return Period		
	2 year	5 year	10 year
	Rainfall (mm)		
1	101.6	165.1	190.5
2	120.65	177.8	203.2
3	136.2	190.5	215.9
4	152.4	203.2	228.6
5	161.2	215.9	241.3

5.3.5 Initial Steady State Condition

Prior to simulation of different rainfall events, an initial steady state condition was simulated to obtain similar ground water condition. Initial steady state condition was obtained by

applying a ground water table at a depth of 13.2 m from the crest which was observed during site investigation. The initial pore water pressure distribution of the slope after the steady state analysis is presented in Figure 5.10. From figure it can be observed that, initially the slope is unsaturated with a maximum matric suction (-140 kPa) observed at the crest of the slope which decreases with depth. Similar decreasing trend of matric suction with depth was also observed from the field instrumentation results. However, maximum suction of -500 kPa was observed during dry period and minimum suction of -10 kPa was observed after the rain at 1.2 m depth at the crest. Due to the limitation of the torque capacity, unsaturated shear strength of the soil could not be measured at suction more than -100 kPa. Therefore, the initial suction condition was simulated to have a maximum suction close to -100 kPa for the current study.
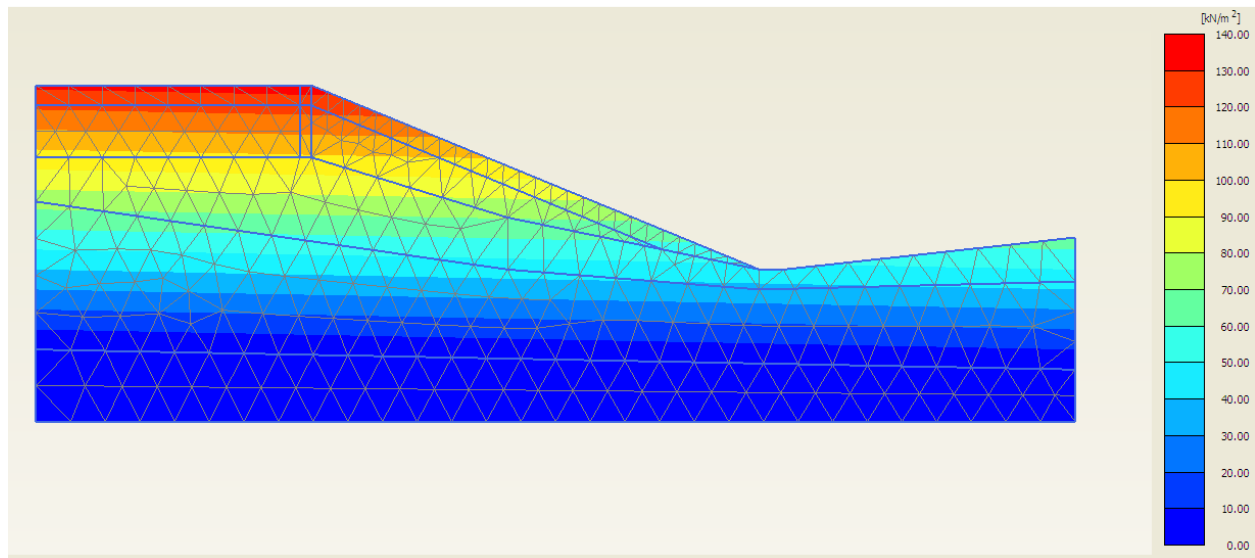
Figure 5.10Initial Matric Suction Distribution Prior to Rainfall Simulation

5.3.6 Effect of Rainfall Duration on Pore Pressure Distribution

To investigate the effects of rainfall duration on pore water pressure distribution, rainfall events with 2, 5 and 10 year return period were adopted which is presented in Figure 5.11. From figure it can be observed that, intensity of rainfall decreases with an increase in rainfall duration. The distribution of pore water pressure profile after 1 day rainfall is presented in Figure 5.12. In PLAXIS, negative pore pressure or matric suction is taken as positive and positive pore pressure is presented as negative value. However, when the computed distribution of pore pressure is presented in graph, the reverse sign convention is adopted for the current thesis due to easy of understanding. Figure 5.13 and 5.14 presents the computed pore pressure distribution at the crest and middle of slope after 1 day to 5 day rainfall period.
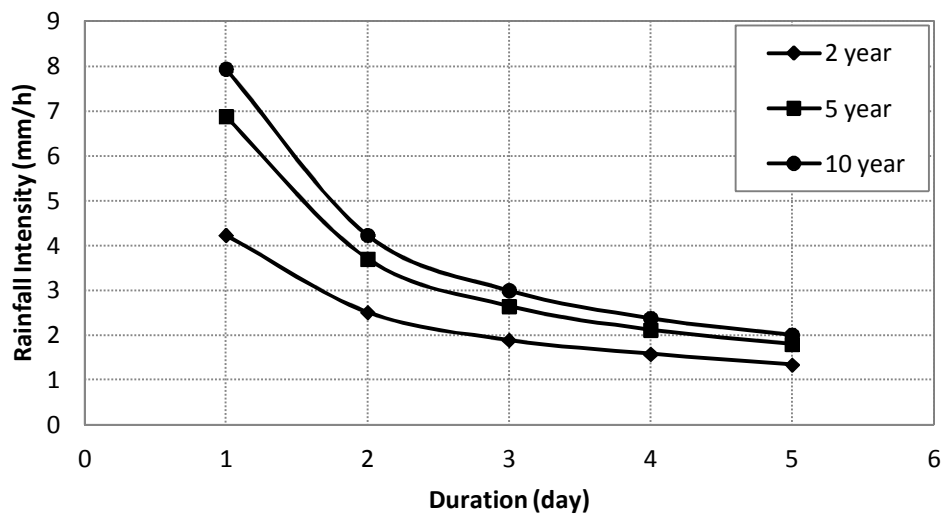
Figure 5.11 Relationship between rainfall intensity and duration for different return period
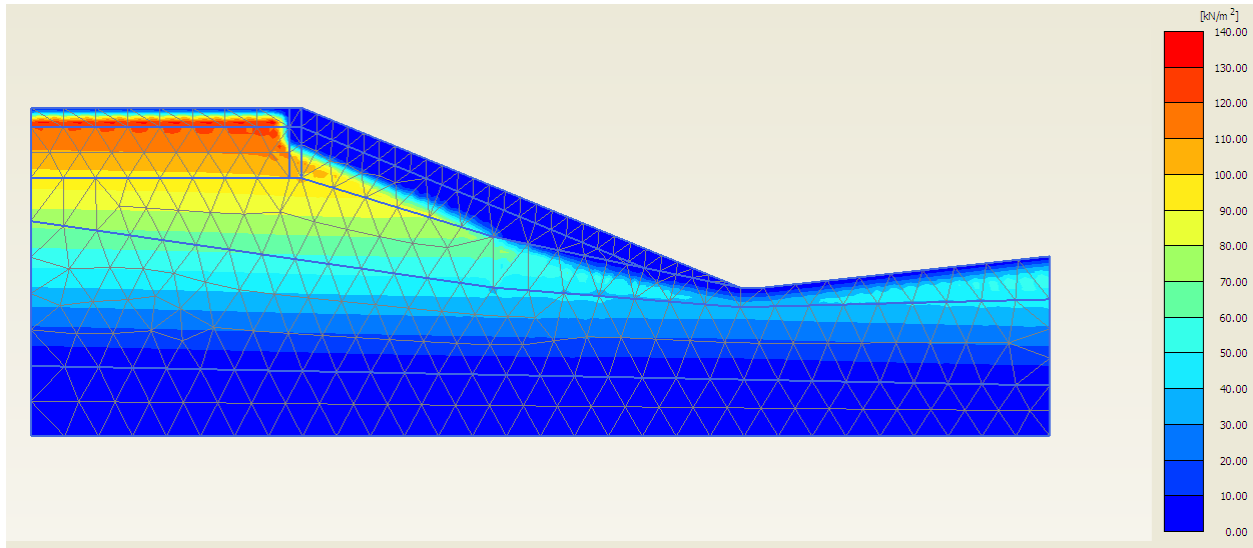
Figure 5.12 Pore Water Pressure Profile after 1 Day Rainfall

It is clear that matric suction reduces from 135 kPa to 0 kPa at the slope surface at the end of each rainfall. On the other hand, this reduction varies at different depth for different rainfall duration. Due to low permeability of the clay, a relatively shallow advancing wetting front is developed as most of the rainfall cannot infiltrate into the soil. On the other hand, pore pressure distribution is completely different after 5 day low intensity prolonged rainfall. The matric suction is completely destroyed at the top 3 m depth both at the crest and middle of the slope.
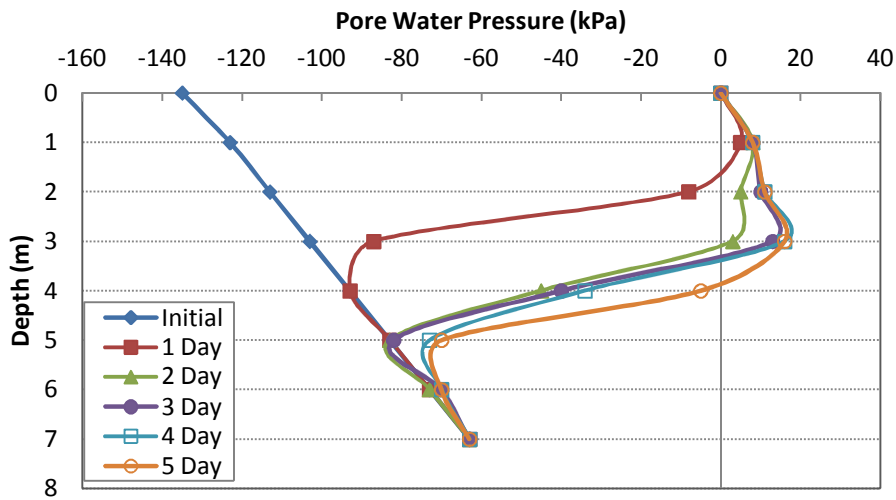
Figure 5.13 Distribution of Pore Water Pressure at the end of each rainfall event for 2 year return period (at the crest)
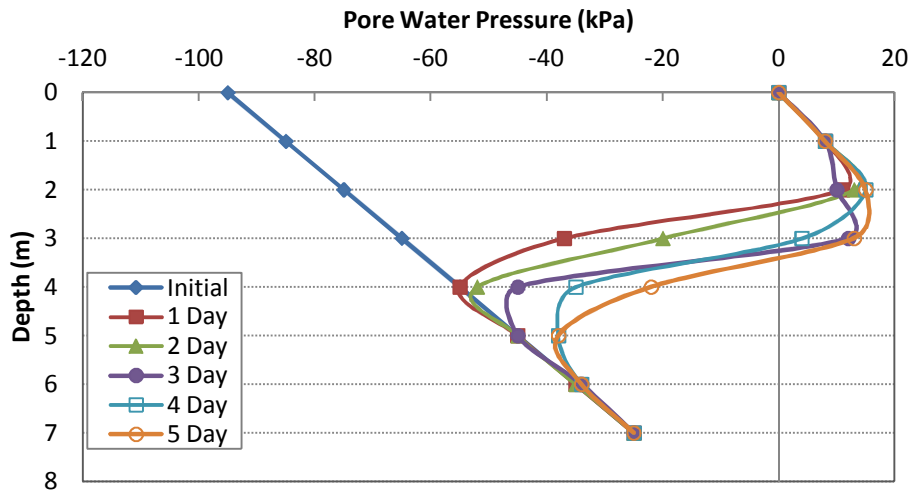
Figure 5.14 Distribution of Pore Water Pressure at the end of each rainfall event for 2 year return period (at the middle)

The generation of positive pressure can be explained by interflow within the slopes which flowed down towards the toe of the slope. From Figure 5.15, it can be seen that, the highest amount of infiltration occurs at the crest of the slope because most of the infiltration at the crest flowed vertically downwards. Gasmo et al. (1999) also observed highest infiltration rate at the crest of the slope followed by the face and then the toe of the slope. The amount of water that did

155

enter the slope face was combined with the interflow from the crest and flowed down toward the toe. Due to low permeability of the intact clay below the top weathered layer, the infiltrated water accumulates at the interface and positive pore water pressure developed. The highest infiltration at the crest can also be validated from the vertical deformation after the rainfall period. Figure 5.16 shows the vertical deformation at the end of 1 day rainfall event. It can be seen that, the additional deformation caused by the rainfall is highest at the crest of the slope.
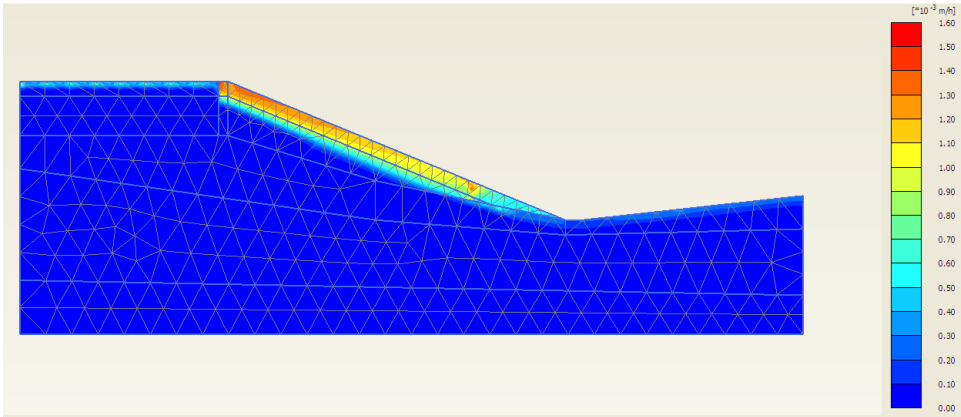
Figure 5.15 Ground Water Flow due to Rainfall Infiltration after 1 Day
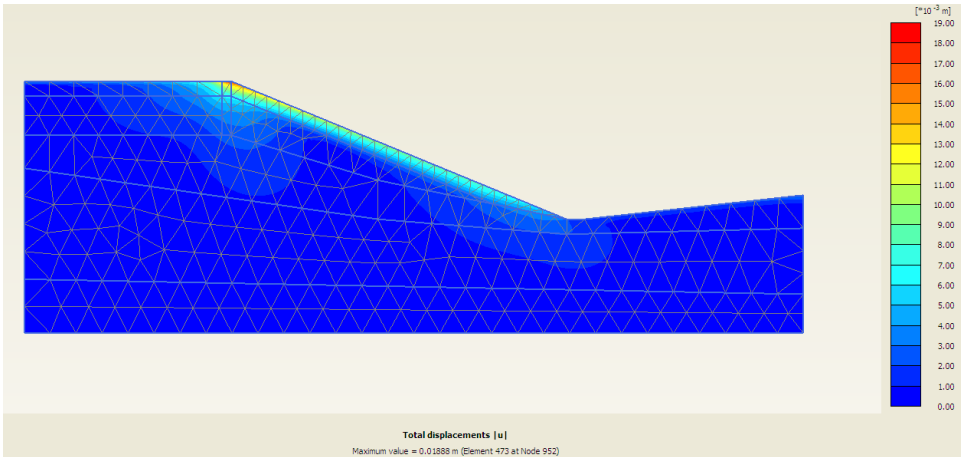
Figure 5.16 Vertical Displacement at the end of 1 Day Rainfall

5.3.7 Effect of Return Period

From Table 5.2, it can be noted that, a higher return period would correspond to a higher total rain amount and corresponding average rainfall intensity for a given duration. In this study, 1 and 5 day rainfall for 2 year and 5 year return period are considered to investigate the effect of rainfall amount on pore water pressure distribution on the study slope. The pore pressure distribution at the crest of the slope after 1 day and 5 day for two different return period is presented in Figure 5.17. From Figure it can be observed that, pore water pressure profiles for the two rainfall amounts overlap which indicates that the excess amount of rainfall resulting from 5 year higher rainfall will be the surface runoff. Ng et al. (2001) suggested that there should be a critical rainfall return period above which no significant increase in pore water pressure will be induced.
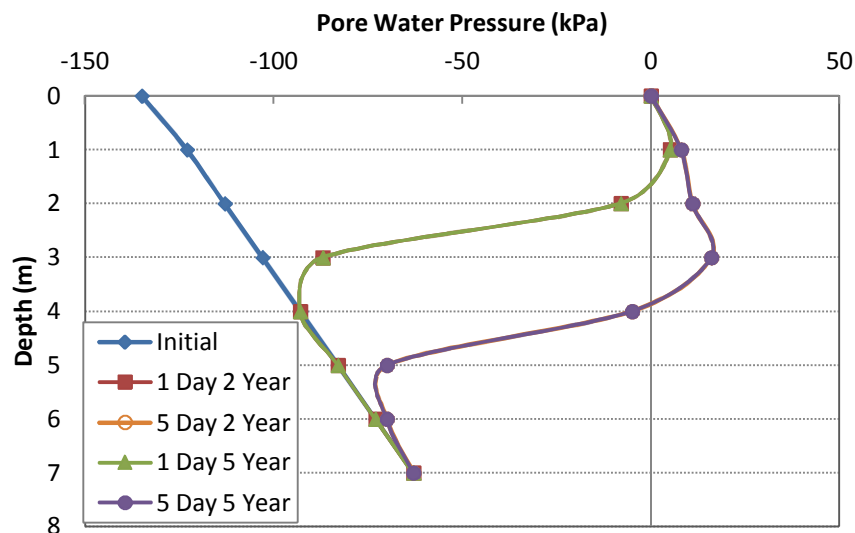
Figure 5.17 Pore pressure distribution with depth for 1 day and 5 day rainfall with 2 year and 5 year return period (at the crest)

Similar results were also observed for the pore pressure distribution at the middle of the slope which is presented in Figure 5.18. This phenomenon can be explained by the darcy's law

157

where infiltration is dependent on water permeability and hydraulic gradient. Each material has its highest limit of coefficient of permeability which is the saturated permeability. Even a high intensity of rainfall is applied, not all the rainwater can actually infiltrate and there may not be any significant difference in pore pressure distribution.
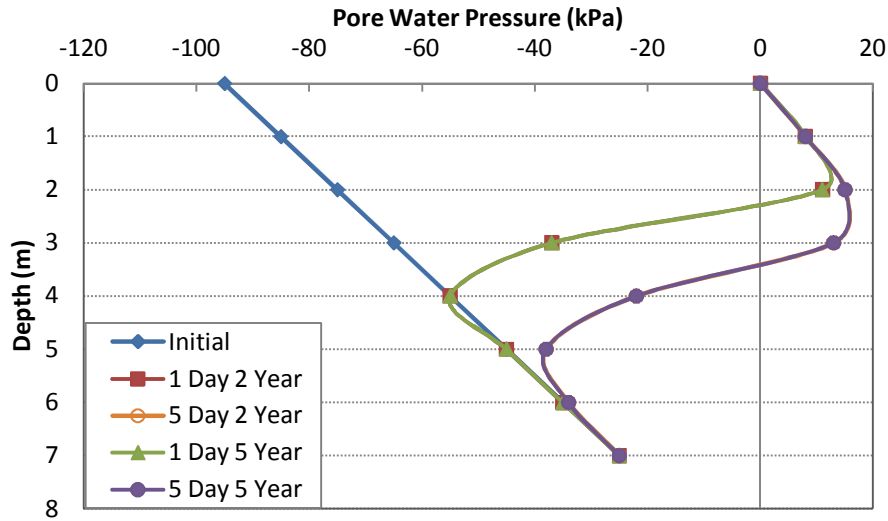
Figure 5.18 Pore pressure distribution with depth for 1 day and 5 day rainfall with 2 year and 5 year return period (at the middle)

5.3.8 Effect of Volume Change Behavior

Figure 5.19 and 5.20 presents the computed pore pressure distribution with depth at the crest and middle of slope. The pore pressure distribution was computed with the best fitting parameters and permeability functions considering with and without volume change behavior for 1 day and 5 day rainfall period with a 2 year return period. It can be readily observed that there is a significant difference between the pore pressure distribution with and without considering volume change behavior. The SWCC without considering volume change behavior predicts higher soil suction profile than computed considering volume change behavior. SWCC constructed considering no volume change behavior has a low air entry value and higher

158

desaturation rate compared to the one considering volume change behavior. Therefore, the former one predicts low water permeability for a given suction and the infiltration rate will be low. On the hand, the later one has high air entry value and lower desaturation rate and thereby has flatter shape and has high coefficient of permeability at a given suction. This will induce faster advancement of wetting front which can be observed from both Figure 5.19 and 5.20.
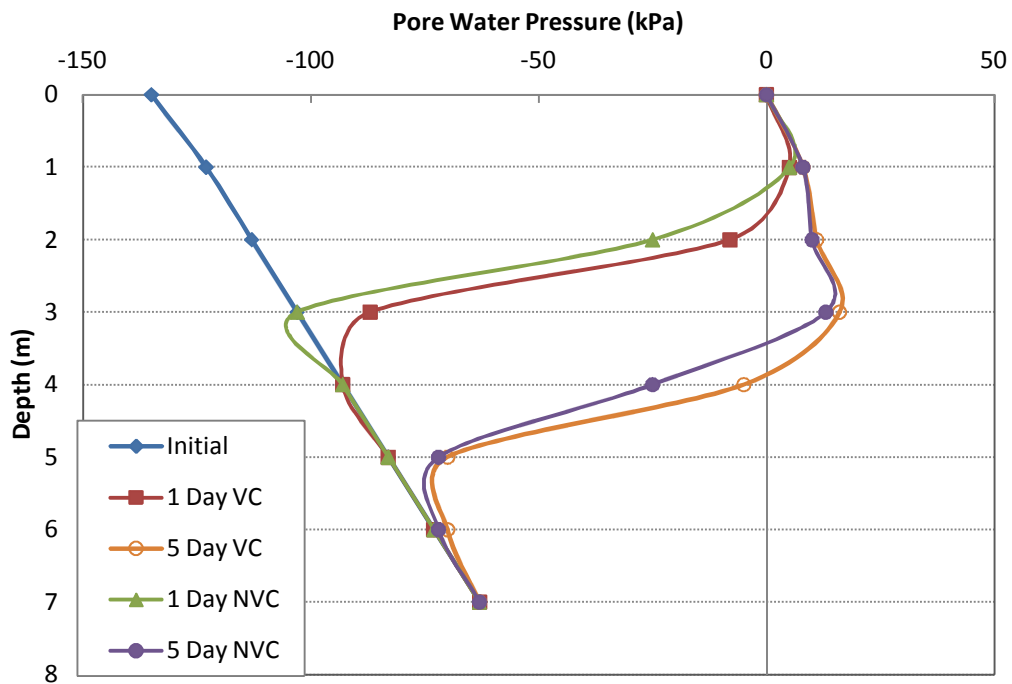
Figure 5.19 Pore water pressure distribution for 1 and 5 day rainfall condition with and without considering volume change behavior (at the crest)
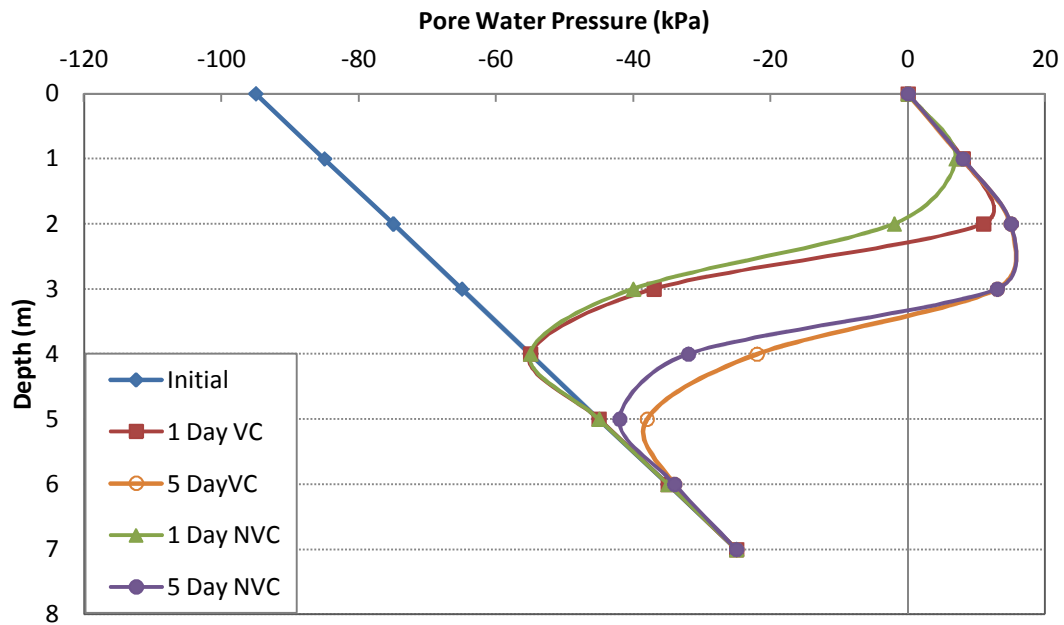
Figure 5.20 Pore water pressure distribution for 1 and 5 day rainfall condition with and without considering volume change behavior (at the middle)

5.4 Slope Stability Analyses

After the generation of pore pressure in transient analyses, stability analyses have been carried out for each of the case considered in the previous sections using PLAXIS. The model in PLAXIS makes use of the Bishop's effective stress concept to calculate unsaturated response of soils and for performing fully coupled hydro-mechanical behavior of soils. Bishop's effective stress equation used by PLAXIS is defined by,

$$\sigma = \sigma' + S_e . \sigma_w \qquad (5.2)$$

The above equation has been simplified for practical application assuming that the pore air pressure is constant and is small enough to be neglected. The coefficient of matric suction (χ)

is assumed to be equal to the effective saturation in PLAXIS which is a function of suction pore pressure. However, there is a significant uncertainty about using single stress state for unsaturated soil as was discussed in chapter 2. Slopes constructed in arid and semi-arid region remain in unsaturated condition above the ground water table. To accurately predict the mechanical behavior of unsaturated soil, two stress state variables are required of which the most widely used, is the combination of net normal stress $(\sigma - u_a)$ and matric suction $(u_a - u_w)$. Based on these two stress state variables, Fredlund et al. (1978) proposed the following equation which is an extension of M-C theory to describe the shear strength of unsaturated soil:

$$\tau = c' + (\sigma - u_a)tan\varphi' + (u_a - u_w)tan\varphi^b \qquad (5.3)$$

Where,

$(\sigma - u_a)$ = net normal stress

$(u_a - u_w)$ = matric suction

φ' = angle of internal friction associated with the change in net normal stress

φ^b = angle representing the rate of change in shear strength relative to matric suction change

The above equation can also be written as,

$$\tau = c_{app} + (\sigma - u_a)tan\varphi' \qquad (5.4)$$

Where,

$c_{app} = c' + (u_a - u_w)tan\varphi^b$

Since, the calculation kernel used in PLAXIS cannot accommodate for two stress state variables, shear strength parameters were changed manually after every rainfall simulation based on the generated pore pressure. Based on the site investigation, it was identified that, the slope under this study is constructed on Eagle Ford Clay. Therefore, both Soil 1 and Soil 2 (Figure 5.1) were assigned similar shear strength parameters which were determined from suction controlled ring shear test. Soil 3 is the insitu eagle ford shale with high shear strength parameter. Mohr-Coulomb model has been used to perform the stability analyses which have five basic input parameter. The soil parameter used for this current study is presented in Table 5.3.

Table 5.3 Soil Data Set Parameters

Soil	φ'	c_{app} (kPa)	γ (kN/m^3)	E (kN/m^2)	ν
1	Fig. 5.21	Fig. 5.21	18.5	7182	0.3
2	Fig. 5.21	Fig. 5.21	20	9500	0.25
3	35	143	20	12000	0.2

Slope stability analyses were performed using PLAXIS by phi-c reduction method. In this approach the tanφ and c of the soil are successively reduced until failure of the structure occurs. Once the pore pressure is generated for a particular rainfall event, the soil profile was divided based on the pore pressure profile. Then shear strength parameter presented in Figure 5.21 was assigned to the soil profiles. In this case, instead of applying c´, c_{app} is incorporated to take the effect of suction into account. Therefore, the extended M-C equation proposed by Fredlund (1978) takes the form of general M-C equation which is presented in Equation 5.4. The above procedure is presented through an example below for better clarification and also validation.
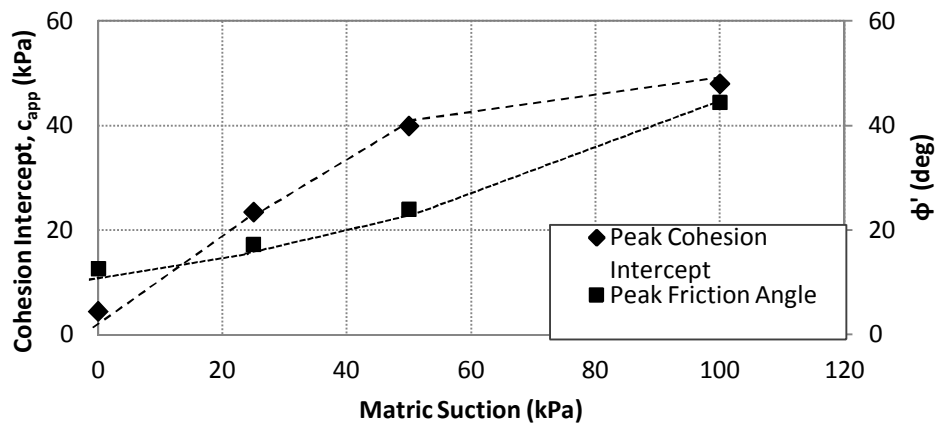
Figure 5.21 Variation of peak friction angle and cohesion intercept with suction

The effect of net normal stress on peak failure envelope and also the variation of φ^b with net normal stress are presented in Figure 5.22 and 5.23 which were obtained from suction controlled ring shear test and were also discussed in Chapter 4.
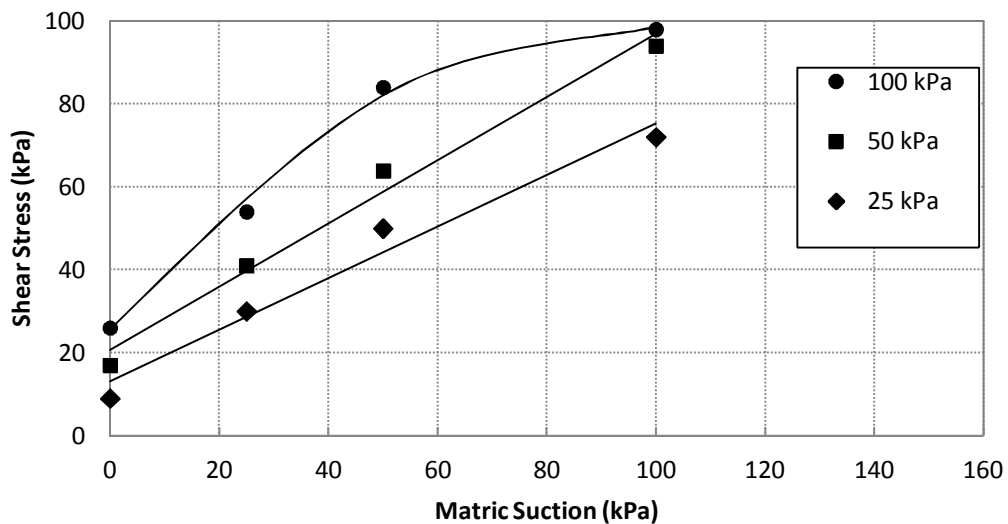
Figure 5.22 Effect of net normal stress on peak failure envelope
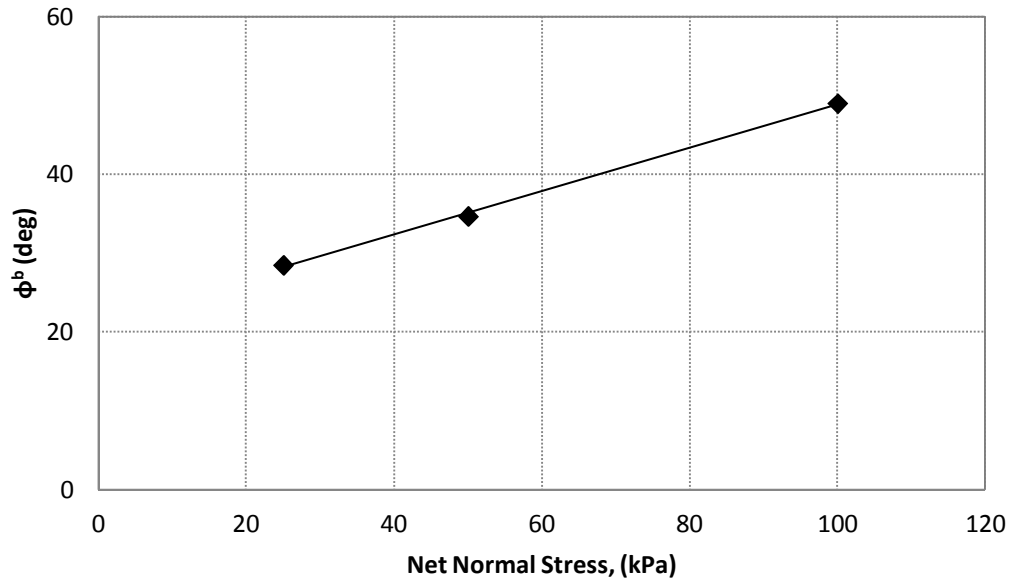
Figure 5.23 Variation of φ^b with net normal stress

Let, a soil layer has a suction of 50 kPa after a certain rainfall. Therefore, to perform the analyses, the layer was assigned the following values of c_{app} and φ from Figure 5.21.

$c_{app} = 39.95 \, kPa$, and $\varphi = 24.03°$

Now,

$c_{app} = c' + (u_a - u_w)tan\varphi^b$

$c_{app} = 4.52 + 50 * tan34.67°$ (where, c´ is saturated cohesion intercept and φ^b is from

Figure 5.23)

$c_{app} = 39.1 \, kPa$ which is close to the value taken from Figure 5.21.

Now, if the normal stress at the depth of soil layer is 50 kPa than the shear strength will be,

$\tau = c_{app} + (\sigma - u_a)tan\varphi'$

$$\tau = 39.95 + 50 * tan24.03°$$

$$\tau = 62.24 \, kPa$$

which is close to shear strength value, $\tau = 63.89 \, kPa$ obtained from Figure 5.22.

However, the measurement of unsaturated shear strength of expansive clay due to cycles of wetting and drying could not be made and only the saturated shear strength was obtained from drained direct shear test. In order to incorporate the effect of suction on the shear strength at fully softened state, equation proposed by Aubeny (2003) was used which is presented in Equation 5.5.

$$c_{app} = -h_m f\theta sin\varphi'/[1 - sin\varphi'] \qquad (5.5)$$

where,

φ' = mechanical stress internal friction angle

θ = volumetric water content

f = factor ranging 1 to $1/\theta$

h_m = matric suction

The apparent cohesion due to matric suction was measured for different values of suction observed in the field and was incorporated during the stability analyses based on the pore pressure distribution, similar way discussed previously. The values of apparent cohesion and friction angle calculated from Equation 5.5 are presented in Figure 5.24.
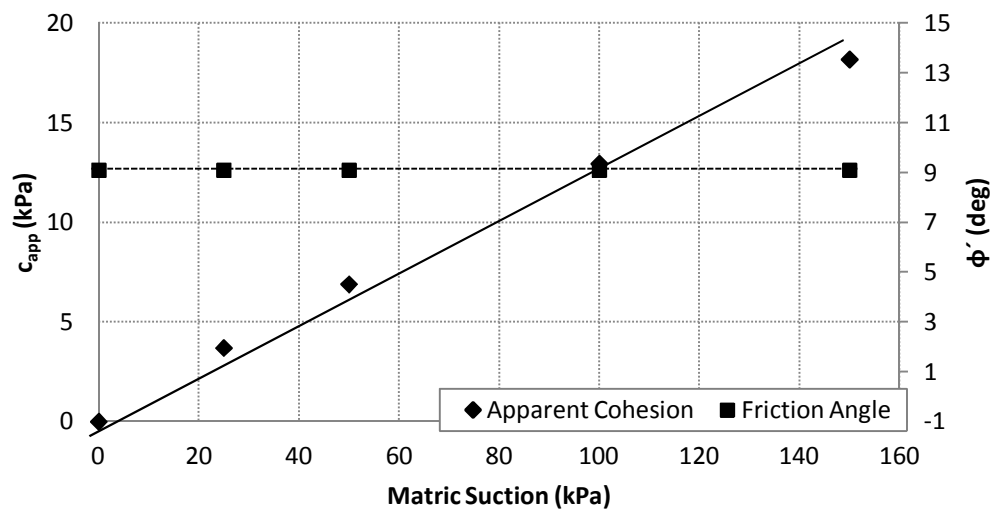
Figure 5.24 Variation of apparent cohesion and friction angle with suction at fully softened state

5.4.1 Effect of Rainfall Duration

Figure 5.25 and 5.26 shows the deformation pattern of the soil after the stability analysis for 1 day rainfall period when using the as compacted unsaturated shear strength from ring shear tests. The failure pattern observed after 1 day rainfall can be explained from the pore pressure distribution after the rainfall period. Before, the rainfall simulation, matric suction of in the soil decreases with increasing depth which was observed in the field and also in the model. After 1 day rainfall period, depth to which matric suction decreased was not sufficient enough to generate a failure and thereby the failure surface passes through the low suction state observed at deeper depth with high factor of safety.
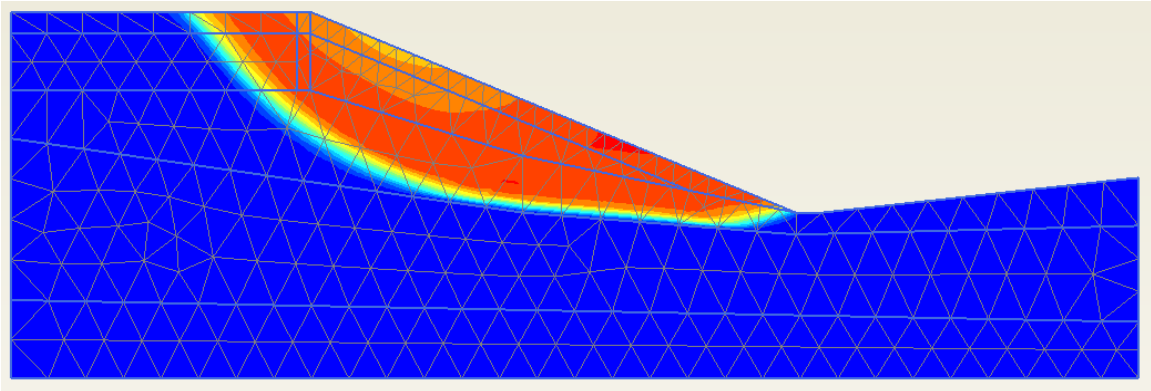
Figure 5.25 Deformation of soil after stability analysis for 1 day rainfall (FS = 2.7)
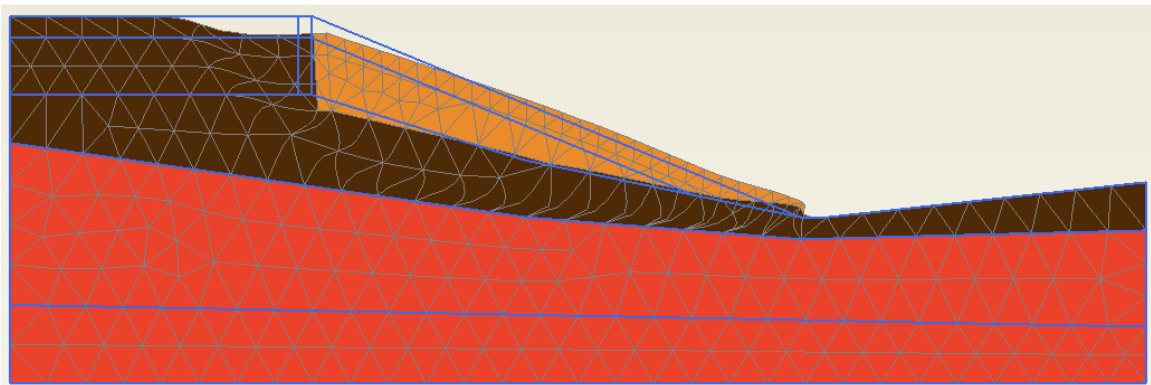
Figure 5.26 Deformed mesh of soil after stability analysis for 1 day rainfall (FS = 2.7)

On the other hand, when the rainwater infiltrated to a sufficient depth after a prolonged 5 day rainfall, the depth of failure surface decreased which can be observed in Figure 5.27 and 5.28. The value of factor of safety also decreased to 1.65 from 2.7. During the prolonged rainfall period, suction was totally destroyed up to a depth of 2 m at the crest and formation of positive pore pressure was also observed at the middle of the slope at 2 m depth. Due to decrease in suction, the soil did not have sufficient strength to resist the sliding mass which in turn resulted in a failure of the slope with low factor of safety at shallow depth.

167
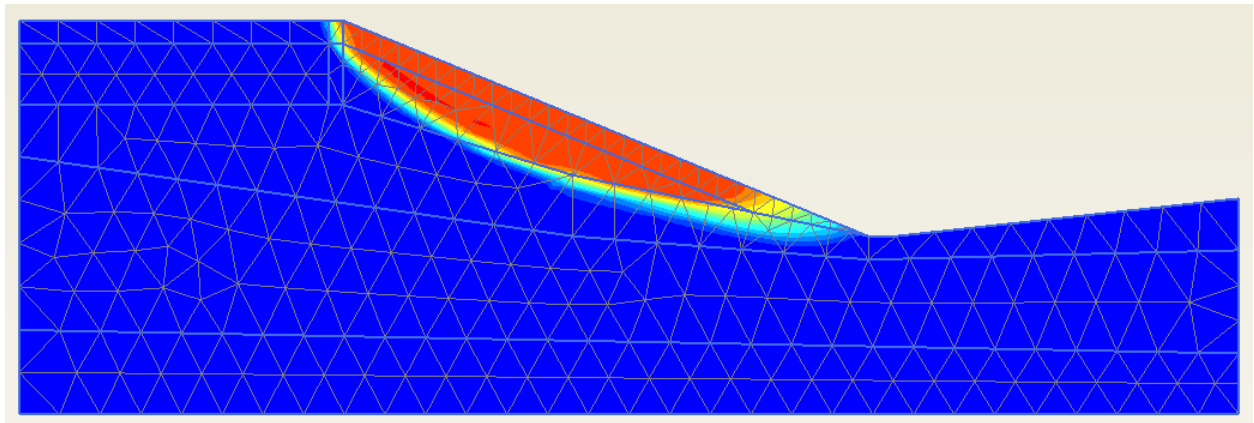
Figure 5.27 Deformation of soil after stability analysis for 5 day rainfall (FS = 1.65)
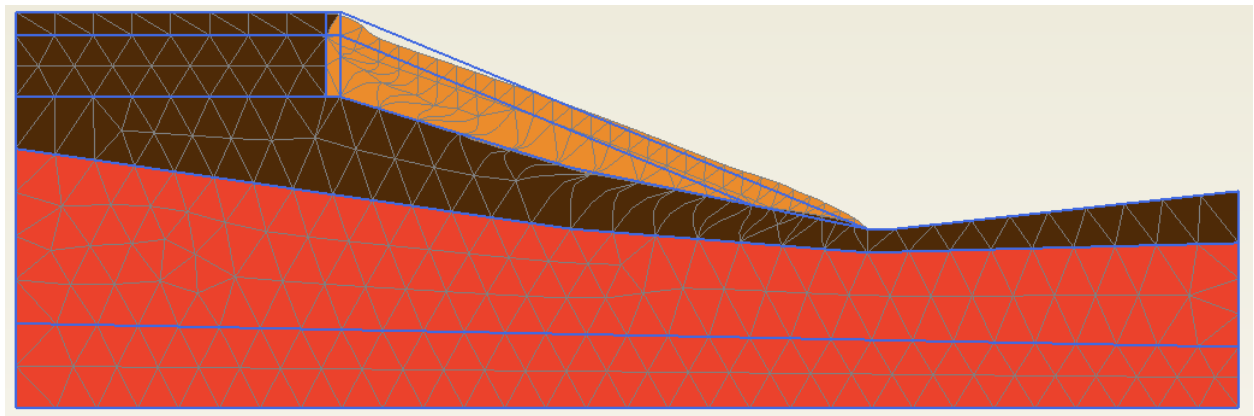
Figure 5.28 Deformed mesh of soil after stability analysis for 5 day rainfall (FS = 1.9)

The change in factor of safety with rainfall duration for 2 year return period is presented in Figure 5.29. During the stability analyses, both as compacted strength and fully softened strength were considered for Soil 1 which is susceptible to strength degradation. From Figure it can be observed that, lowest factor of safety was observed after 5 day prolonged rainfall period with low intensity. Since, expansive clay has low water coefficient of permeability, the high intensity of rainfall did not infiltrate into the soil to a deeper depth and significant decrease in factor of safety was also not observed. On the other, low intensity long duration rainfall caused

larger infiltration of rainwater for a sufficient time period and resulted in lowest factor of safety. Based on the transient seepage analyses and factor of safety evaluation, Rahimi et al., (2011) suggested that, high conductivity soil produces lowest factor of safety within a short period of rainfall and low conductivity soil shows lowest factor of safety after a long duration compared to the low conductivity soil.
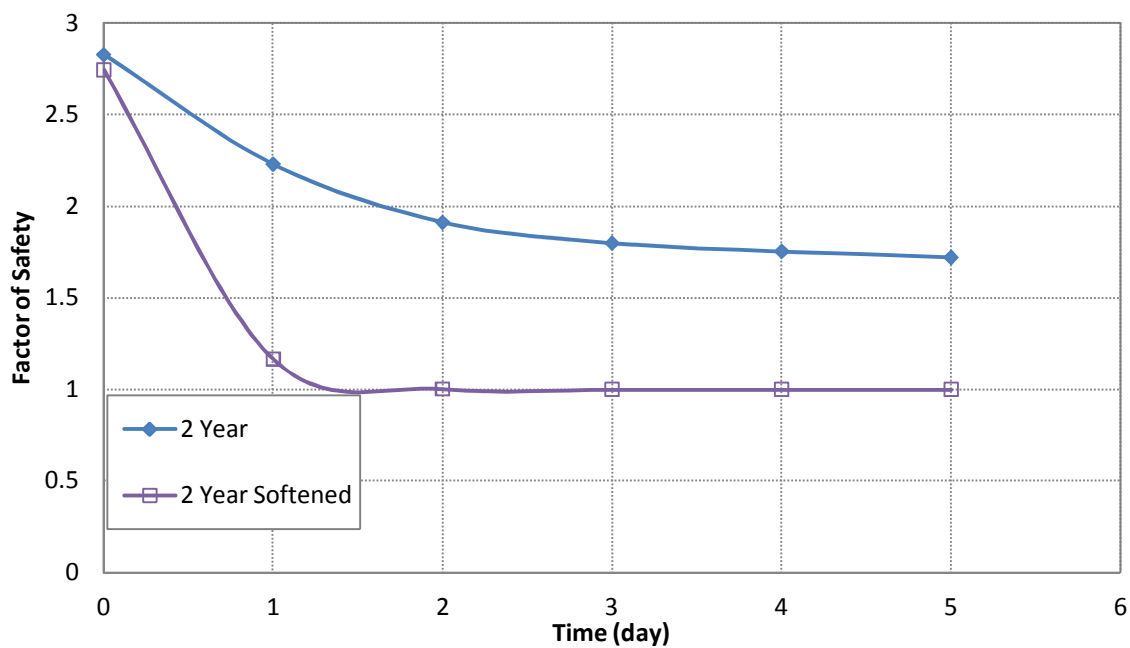
Figure 5.29 Variation of factor of safety with rainfall duration

From Figure 5.29, it can also be observed that, factor of safety can be underestimated if softening behavior of expansive clay due to wet dry cycle is ignored. The as compacted specimen produced a factor of safety of 1.65 after 5 day rainfall period. On the other hand, when the softening behavior of top soil was considered, it produced a factor of safety of 0.99 which indicates the failure of slope.

5.4.2 Effect of Rainfall Return Period

Figure 5.30 shows the change in factor of safety with the change in rainfall return period for 1 day to 5 day rainfall period. It can be noted that, higher return period would correspond to a higher total rain amount and corresponding high average rainfall intensity for a given duration.
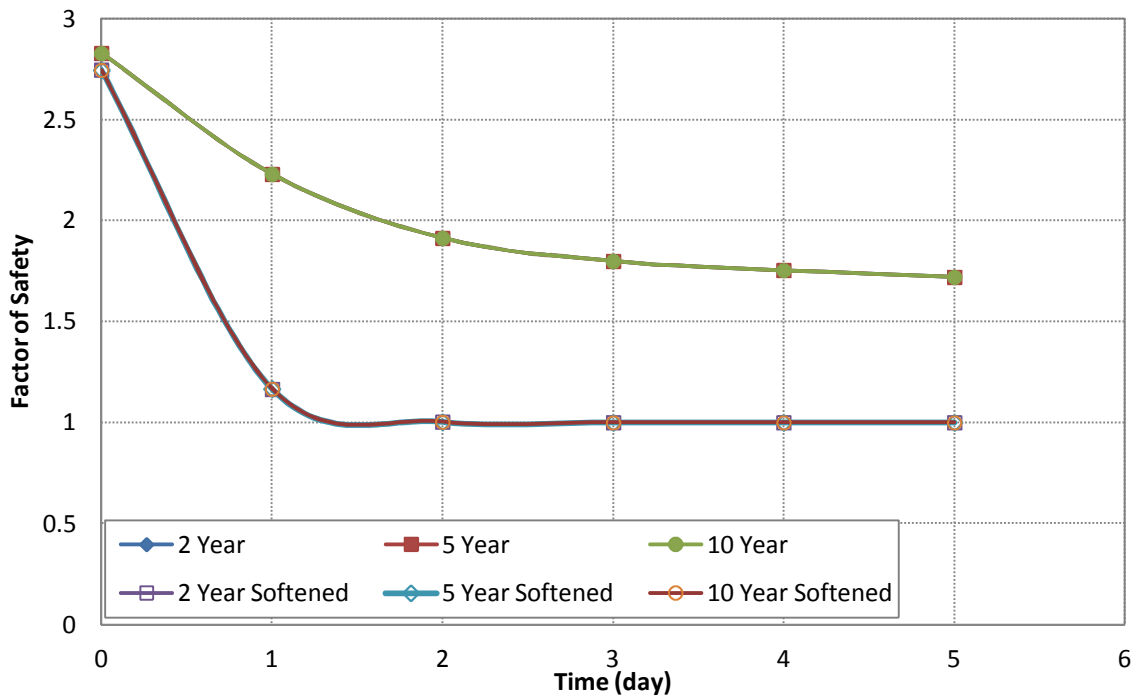
Figure 5.30 Variation of factor of safety with rainfall return period

But no significant change in factor of safety was observed due to applied higher total rainfall amount. This phenomenon can be explained by the Darcy's law where infiltration is dependent on water permeability and hydraulic gradient. Each material has its highest limit of coefficient of permeability which is the saturated permeability. Even a high intensity of rainfall is applied, not all the rainwater can actually infiltrate and there may not be any significant difference in pore pressure distribution which leads to similar factor of safety evolution of the slope.

5.4.3 Effect of Volume Change

Figure 5.31 presents the computed factor of safety of the slope with and without considering volume change behavior of soil during infiltration analyses. From figure it can be seen that, the assumption considering no volume change behavior leads to a higher factor of safety for certain duration of rainfall as compared to the one considering volume change. When no volume change was considered, the predicted coefficient of permeability was low for a given soil suction and therefore produces lower infiltration rate and low factor of safety. On the hand, when volume change is considered the soil possesses high coefficient of permeability at a given suction. This will induce faster advancement of wetting front which will lead to low factor of safety.
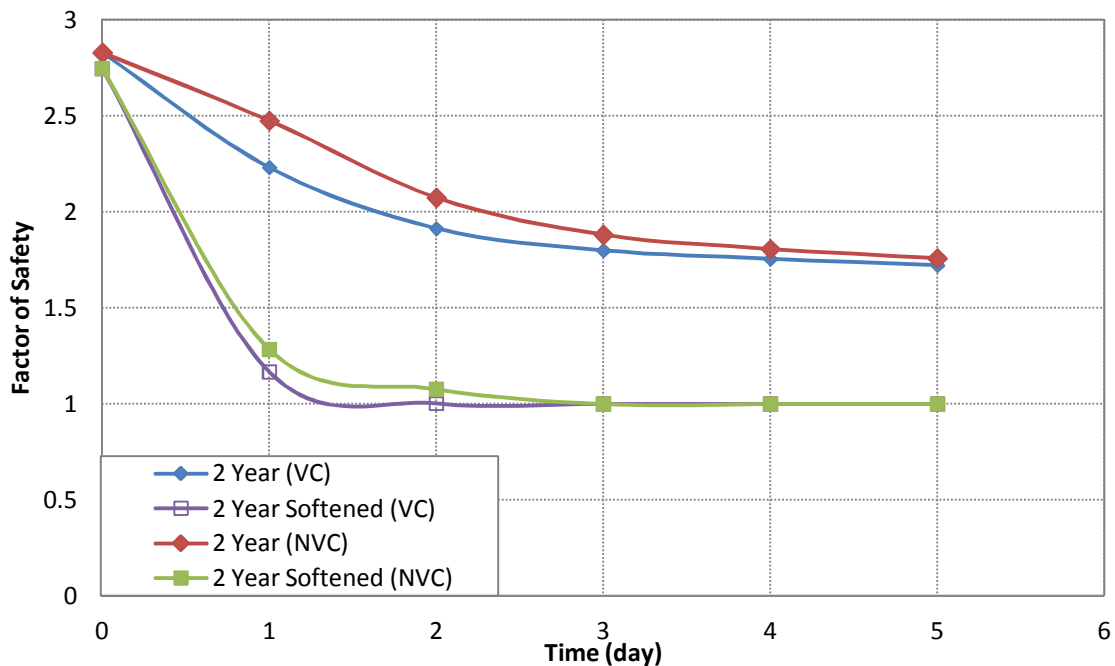
Figure 5.31 Variation of factor of safety with and without considering volume change behavior.

5.5 Geo-hazard Potential Model

It is important to understand the behavior of expansive clay in order to develop a early hazard prediction system of slope failure based on weather forecast which has led to the initiation of current research work. Based on the current research work, the following methodology can be adopted to design the early hazard warning system based on the rainfall forecast data which is presented in Figure 5.32.

Based on the current research, the key informations required for analyzing the geo-hazard potential due to rainfall induced slope failure are: (1) Rainfall events, which can be obtained from installed raingauges at different site locations or based on the sattelite data, (2) Existing soil moisture or suction condition which can influence the infiltration behavior. This information can be obtained by installing moisture sensors and tensiometers at different locations of slope and
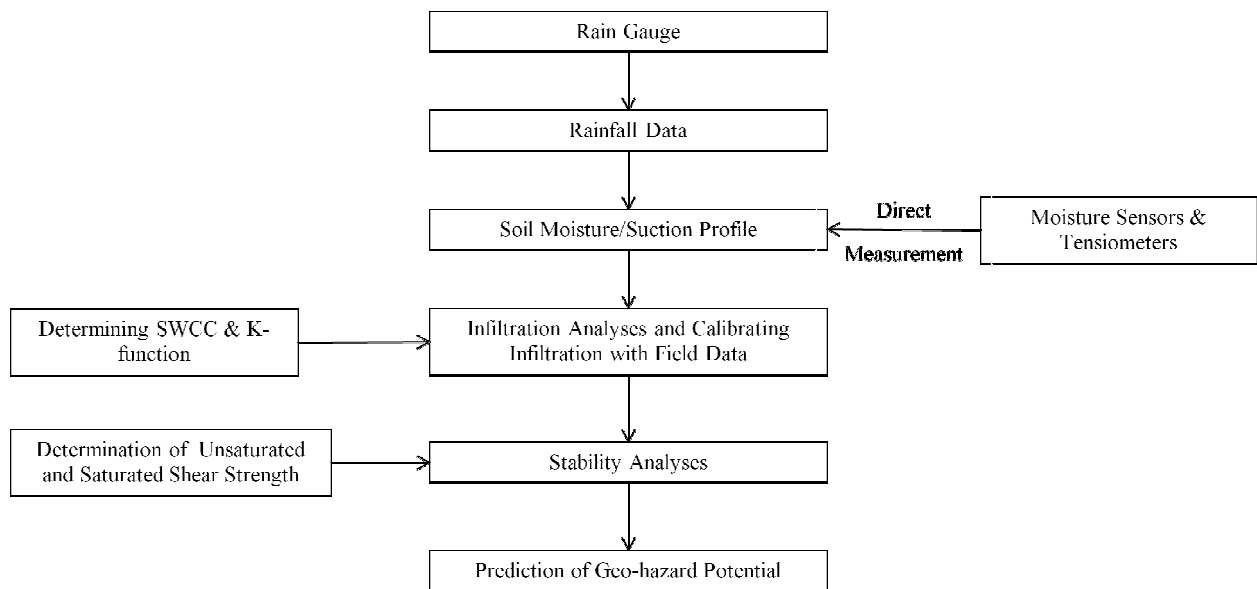
Figure 5.32 Flow chart for geotechnical analyses of rainfall hazard warning system for slope failure

collecting data using dataloggers, (3) Soil water characteristic curves (SWCC) of the soil samples which can be used to determine permeability function in order to input in infiltration analyses to obtain soil moisture profile or suction profile after a rainfall event. Changes in volume should be considered during SWCC construction to represent accurate water retention characteristic of expansive clay. The infiltration analyses need to be calibrated using field data due to possible variation of in situ permeability condition which results from the presence of cracks and fissures in the field (4) The changes in shear strength characterisitic due to changes in soil moisture condition (or matric suction) determined in the laboratory can be used as an input to the non-linear analyses or limit equilibrium analyses in order to investigate the changes in factor of safety for a rainfall event and finally (5) Prediction of the geo-hazard potential based on the factor of safety obtained. If the factor of safety is less than 1, the slope is susceptible to failure and precautions should be taken.

CHAPTER 6

CONCLUSIONS AND RECOMMENDATIONS

Rainfall-induced slope failure is a common problem in areas with slope constructed on high plasticity clays. Such slopes are stable within a certain range of water saturation and when the saturation exceeds a critical value, the slope becomes unstable leading to failure. Most of these failures involve shallow surface slides with depth less than 10 ft and require periodic maintenance which can become costly for state and Federal Agencies. These post failure costs can be significantly reduced if precautions are taken ahead of time. Development of an early hazard warning system based on weather forecast data can help identify potential slopes susceptible to failure due to rainfall. But development of such system will require a better understanding of the in situ behavior of soil due to rainwater infiltration as well as changes in shear strength characteristics of the soil. From these information, stability analyses of slope can be performed for a certain rainfall forecast to determine the geo-hazard potential of that slope. The overall objective of this research was to develop a methodology which can be used to determine geohazard potential of rainfall induced slope failure on expansive clay based on the weather forecast.

6.1 Summary and Conclusions

Based on the current study, main results and conclusions can be summarized as follows:

1. Results obtained from field instrumentation indicate that the variation in the moisture content and matric suction were different at different depths. The maximum variation often occurred near the ground surface (i.e. at 1.2 m depth) and the magnitude of variation decreased with increase in depth.

2. Matric suction as high as -700 kPa was observed at 1.2 m depth during relatively dry summer period which subsequently decreased to a value of -10 kPa during rainfall events.

3. Highest infiltration often occurred near the crest of the slope due to flow of water in the vertical direction which then becomes interflow within the slope. Presence of cracks at the crest also accelerated the ingress of water into the slope during rainfall events.

4. The depth of active zone up to which moisture variation occurs was observed to be 3.6 m. Therefore, reduction in soil shear strength due to cyclic variation of weather condition is limited to a depth of 3.6 m, which also matches close to the observed failure depth (3.04 m) on slopes constructed on high PI clay. Based on the swell tests under different normal stress for expansive clay in this study, it was observed that swelling can occur up to a depth of 3.8 m upon wetting, which also indicates the depth to which strength reduction can occur due to cyclic swell shrink phenomenon of expansive clay.

5. Low intensity long duration rainfall resulted in delayed penetration of rainwater as compared to the high intensity rainfall.

6. Infiltration behavior depends on the initial distribution of matric suction profile. Initial high suction can result in lower infiltration of rainwater due to low permeability of unsaturated soil.

7. Soil water characteristic curve of expansive clay yields higher air entry value and lower desaturation rate when compared with no volume change assumption during SWCC determination. Based on the experimental results, it can be observed that, for a certain value of matric suction, permeability of soil without considering volume change has lower value as compared to the volume change consideration. According to this behavior, permeability function predicted from no volume change assumption will under predict the infiltration rate and subsequently produce higher factor of safety.

8. Specimens compacted wet of optimum do not strongly depend on the applied stress history due to identical micro-structure formation. On the other hand, SWCC of expansive clay, compacted dry of optimum water content shows a shift to the right with high net normal stresses which indicates increase in air entry value. The increase in air entry value indicates that higher suction is required to desaturate the specimen due to smaller pore size distribution. Therefore, with the increase in normal stress the rate of reduction in water content decreases.

9. SWCC of expansive clay strongly depends on the initial molding water content. Specimens compacted wet of optimum yield high air entry value and lower desaturation rate as compared to the specimens compacted dry of optimum. The difference in the observed behavior for specimens on the wet and dry side of optimum water content, may be due to formation of different macro-structure. The specimens compacted dry of optimum contain large pore spaces between the clods of soil. On the other hand,

specimens compacted wet of optimum do not contain inter connected pore spaces and offer more resistance to desaturation as compared to the specimens compacted dry of optimum.

10. Results obtained from suction controlled ring shear tests indicate that both net normal stress and matric suction has significant influence on peak and residual strength of expansive clay. Both peak and residual strength increases with increase in net normal stress and matric suction. Expansive clay under this study shows a hardening-softening behavior with increase in matric suction.

11. Both peak and residual failure envelope were found to be linear in the shear stress vs net normal stress plane at suction of 25 and 50 kPa. However, the failure envelope showed a non-linear trend for 100 kPa suction. Both the cohesion intercept and friction angle in the peak and residual state increases linearly with increase in suction for the range of net normal stress and matric suction considered for this study.

12. The increase in both peak and residual shear strength with suctions in shear stress vs matric suction plane appears to be linear for 25 and 50 kPa net normal stress but becomes non linear at 100 kPa net normal stress.

13. Both φ^b and φ^b_r angles which represent the change in shear strength with suction tend to decrease with an increase in suction.

14. Shear strength of high PI expansive clay decreases when subjected to cycles of wetting and drying. The value of cohesion completely disappears due to wet dry cycles leading to shear strength condition at normally consolidated state.

15. Based on the laboratory test results, numerical modeling was performed to compare the field infiltration measurement for rainfall event on April 11, 2011 with modeling results.

The estimated suction profile was higher compared to the field measurement which indicates less infiltration during numerical analyses. The above phenomenon can be explained due to the presence of large cracks observed during field investigation which made easy passage of water into the slope thereby increasing the permeability of soil.

16. Low intensity long duration rainfall was found to be most critical for expansive clay under current study which is consistent with the results previously reported for soils with low permeability.

17. Effect of rainfall return period was found to be insignificant for the current study. The amount of rainfall considered for current study indicates the highest rainfall amount for that particular return period. There was no significant increase in pore pressure observed for the three return period considered for this study.

18. No volume change assumption underestimates the infiltration amount as compared to volume change behavior for expansive clay which results in prediction of higher factor of safety for a particular rainfall event.

19. Stability analyses performed for different rainfall event show that the use of fully softened shear strength within the active zone can reduce the factor of safety as low as twice the value as compared to the as compacted strength.

6.2 Recommendations for Future Work

Based on the current study, the following recommendations are given for future studies:

1. Most of the rainfall induced slope failures are shallow in nature and the failure surface are limited to the top few meters of active zone or moisture variation

zone. Therefore, studies on the effect of wetting and drying on the SWCC under different net normal stresses are recommended.

2. Hysteresis of SWCC has not been taken into account for the current study. Infiltration of rainwater is a wetting process and therefore, a study on the behavior of SWCC under wetting process is recommended.

3. The study of the effect of swelling potential of expansive clay during wetting on SWCC is recommended for future study.

4. During relatively dry summer period, the matric suction is higher in the slope and therefore, it is recommended to study the changes in shear strength of expansive clay at high suction state.

5. The effect of wetting and drying on shear strength of expansive clay has been performed under saturated condition for the current study. It is recommended to study the fully softened strength in unsaturated condition.

6. Rainfall pattern can significantly influence the infiltration behavior and subsequently the stability of slope for same duration and amount of rainfall. Therefore, investigations on the changes in infiltration behavior and stability of slope for different rainfall pattern are recommended.

REFERENCES

Alonso, E., Gens, A., Lloret, A., and Delahaye, C., (1995) "Effect of Rain Infiltration on the Stability of Slopes" Proceedings of the First International Conference on Unsaturated Soils, UNSAT'95, Paris, France, Vol. 1, pp. 241-249.

Aubeny, C. P., and Lytton, R. L. (2003). "Long term strength of compacted high PI clays." *Federal Highway Rep. TX03/2100-1.*

Aubeny, C. P., and Lytton, R. L. (2004). "Shallow slides in compacted high plasticity clay slopes." *J. Geotech. Geoenviron. Eng.,* 130(7), 717-727.

Benson, C.H., and Daniel, D.E. (1990) "Influence of clods on hydraulic conductivity of compacted clay." *J. Geotech. Eng.,* 116(8), 1231-1248.

Brooks, R.H., and Corey, A.T. (1964). "Hydraulic properties of porous media." Hydrology paper no. 3, Civil Engineering Dept., Colorado State University, Fort Collins, Colo.

Bao, C.G., Gong, B.W., and Zhan, L.T. (1998). "Properties of unsaturated soils and slope stability for expansive soil." Proc., 2nd Int. Conf. on Unsat. Soils, Vol. 2, Beijing, 71-98.

Bulut, R., Lytton, R.L., and Wray, W.K. (2001) "Soil suction measurements by filter paper" Proceedings of GSP 115, ASCE, Geo-Institute, Houston, Texas, 2001.

Collins, B. D., and Znidarcic, D. (2004). "Stability analyses of rainfall induced landslides." *J. Geotech. Geoenviron. Eng.,* 130(4), 362-372.

Duncan, J. M. and Wright, S. T., (2005). *Soil strength and slope stability*, Wiley, New Jersey

180

Escario, V. (1980). "Suction-controlled penetration and shear tests." In Proceedings of 4th International Conference on Expansive Soils, Denver, CO, 781-787.

Escario, V., and Saez, J. (1986). ''The shear strength of partly saturated soils,'' Geotechnique, 36(3), 453–456.

Esteban, V., and Saez, J. (1988). "A device to measure the swelling characteristics of rock samples with control of the suction up to very high values." *ISRM Symp. on Rock Mechanics and Power Plants*, Balkema, Madrid, Spain, Sept. 12–16.

Fredlund, D. G., and Rahardjo, H. (1993). "*Soil Mechanics for unsaturated soils.*" Wiley, Singapore.

Fredlund, D.G., Xing, A., and Huang, S. (1994). "Predicting the permeability functions for unsaturated soils using the soil-water characteristic curve." Can. Geotech. J. Ottawa, 31, 533-546.

Fredlund, D.G., and Morgenstern, N.R., (1977). "Stress state variables for unsaturated soils." J. Geotech. Eng. Vol. 103, pp. 447-466.

Fredlund, D.G., Morgenstern, N.R., Wider, R.A. (1978). "Shear strength of unsaturated soils" Canadian Geotechnical Journal, 15(3), 313-321.

Fredlund, D. G., and Rahardjo, H. (1993). "*Soil Mechanics for unsaturated soils.*" Wiley, Singapore

Fredlund, D. G, Xing, A., Fredlund, M. D., and Barbour, S. L. (1996). "The relationship of unsaturated soil shear strength to the soil–water characteristic curve." *Can. Geotech. J.,* 33, 440–448.

Fredlund, D. G. (2006). "Unsaturated soil mechanics in engineering practice." *J. Geotech. Geoenviron. Eng.,* 132 (3), 286-321.

Gamboa, C.L.V. (2011) "Unsaturated soil behavior under large deformations using fully servo/suction controlled ring shear apparatus." PhD Thesis, The University of Texas at Arlington.

Gasmo, J.M., Rahardjo, H., and Leong, E.C. (2000). "Infiltration effects on stability of a residual soil slope." Computers and Geotechnics, 26, 145-165.

Gan, J.K.M., Fredlund, D.G., and Rahardjo, H., (1988) "Determination of Shear Strength Parameters of an Unsaturated soil using the Direct Shear Test" *Can. Geotech. J.,* 25, 500-510.

Heureux, J.S.L., Høeg, K., and Høydal, A. (2006). "Numerical analyses and field case study of slope subjected to rainfall." GSP 147, Vol. 2, 2279-2290.

Hossain, Md. A., and Yin, J.H. (2010). "Behavior of a compacted completely decomposed granite soil from suction controlled direct shear tests." Journal of Geotechnical and Geoenviromental Engineering, 136(1), 189-198.

Hoyos, L.R., Velosa, C.L., and Puppala, A.J. (2012) "Residual strength of unsaturated soils using a fully servo/suction controlled ring shear apparatus" Proceedings of GSP 225, ASCE, GeoCongress, Oakland, California, 2012.

Hilf, J. (1956). "An investigation of pore-water pressure in compacted cohesive soils." PhD dissertation, Tech. Memo. No. 654, U.S. Dept. of the Interior Bureau of Reclamation, Design and Construction Dev., Denver, Colo.

Johnson, K. A., and Sitar, N. (1990). "Hydrologic conditions leading to debris-flow initiation." *Can. Geotech. J.,* 27(6), 789-801.

Jotsankasa, A., and Mairaing, W., (2010) " Suction-Monitored Direct Shear Testing of Residual Soils from Landslide-Prone Areas." *J. Geotech. Geoenviron. Eng.,* 136(3), 533-537.

Kim, Y. K., and Lee, S. R. L. (2010). "Field infiltration characteristics of natural rainfall in compacted roadside slopes." *J. Geotech. Geoenviron. Eng.,* 136(1), 248-252.

Kayyal, M.K. and Wright, S.G. (1991) "Investigation of Long-Term Strength Properties of Paris and Beaumont Clays in Earth Embankments." *Research Rep. 1195-2F*, Center for Transportation Research, Univ. of Texas at Austin.

Kibria, G. (2011). "Determination of geotechnical properties of clayey soil from resistivity imaging." Masters thesis, The Univ. of Texas at Arlington, Arlington, USA.

Lu, N., and Likos, W.J. (2004). "Unsaturated soil mechanics" John Wiley & Sons, Inc.

Lim, T. T., Rahardjo, H., Chang, M. F., and Fredlund, D. G. (1996). "Effect of rainfall on matric suction in a residual soil slope." *Can. Geotech. J.,* 33, 618-628.

Li. A. G., Yue, Z. Q., Tham, L. G., Lee, C. F., and Law, K. T. (2005). "Field-monitored variations of soil moisture and matric suction in a saprolite slope." *Can. Geotech. J.,* 42, 13-26.

Maulem, Y. (1976). "A new ,model for predicting the hydraulic conductivity of unsaturated porous media." Water Resour. Res. 12:513-522.

Morgenstern, N.R. (1979). "Properties of compacted soils." Contribution to panel discussion, Session IV, Proc., 6th Panamerican Conf. on Soil Mechanics and Foundation Engineering, Vol. 3, 349-354.

Merchán, V., Vaunat, J., Romero, E., and Meca, T. (2008). "Experimental study of the influence of suction on the residual friction angle of clays." Proceedings of the First European Conference on Unsaturated Soils, Durham, U.K., 423-428.

Melinda, F., Rahardjo, H., Han, K. K., and Leong, E. C., (2004). "Shear strength of compacted soil under infiltration condition." *J. Geotech. Geoenviron. Eng.,* 130 (8), 807-817.

Meerdink, J.S., Benson, C.H., and Khire, M.V. (1996) "Unsaturated hydraulic conductivity of two compacted barrier soils." *J. Geotech. Eng.,* 122(7), 565-576.

Ng. C.W.W., and Pang, Y.W., (2000). "Influence of stress state and soil-water characteristics and slope stability." *J. Geotech. Geoenviron. Eng.,* 126(2), 157-166.

Ng. C.W.W., and Menzies, B., (2007). "Advanced unsaturated soil mechanics and engineering." Taylor and Francis, NY.

Ng, C. W. W., Springman, S. M., and Alonso, E. E. (2008)."Monitoring the performance of unsaturated soil slopes." *Geotech. Geol. Eng.,* 26, 799-816.

Padilla, J.M, Perera, Y.Y., Houston, W.N., Perez, N., and Fredlund, D.G. (2006). Quantification of air diffusion through high air-entry ceramics disks. Proc. 4st International Conference on Unsaturated Soils, Carefree, Arizona, 1, 1852-1863.

Rassam, D. W., and Williams, D. J. (1999). "A relationship describing the shear strength of unsaturated soils." *Can. Geotech. J.*, 36, 363–368.

Richards, L.A. (1931). "Capillary conduction of liquids through porous mediums." Physics, NY, 1, 318-333.

Ridley, A.M., Dineen., K., Burland, J.B., and Vaughan, P.R. (2003). "Soil matrix suction: some examples of its measurement and application in geotechnical engineering." Geotechnique, 53(2), 241–253

Rahimi, A., Rahardjo, H., and Leong, E.C., (2011). "Effect of antecedent rainfall patterns on rainfall-induced slope failure." J. Geotech. And Geoenv. Eng., 137 (5), 483-491.

Rahardjo, H., Lim, T. T., Chang, M. F., and Fredlund, D. G. (1995). "Shear strength characteristics of a residual soil." Can. Geotech. J., 32, 60-77.

Rogers, L.E. and Wright, S.G. (1986) "The effect of Wetting and Drying on the Long-Term Shear Strength Parameters for Compacted Beaumont Clay." *Research Rep. 436-2F*, Center for Transportation Research, Univ. of Texas at Austin.

Rahardjo, H., Lee, T.T., Leong, E.C., and Rezaur, R.B. (2005). "Response of a residual soil slope to rainfall." Can. Geotech. J, 42, 340-351.

Sridharan, A., and Prakash, K., (2000). "Classification procedures for expansive soil." Proc. Instn. Civ. Engrs. Geotech. Engng. 143, 235-240.

Skempton, A.W. (1977) "Slope Stability of Cuttings in Brown London Clay." *Proc., Ninth Int. Conf. on Soil Mechanics and Foundation Engineering*, Tokyo, Vol. 3, 261-270.

Skemptom, A.W. (1985). "Residual strength of clays in landslides, folded strata, and the laboratory." Geotechnique, 35(1), 3-18.

Stark, T.D. and Duncan, J.M. (1991) "Mechanism of Strength Loss in Stiff Clays" *J. Geotech. Eng.,* 117(1), 139-154.

Stark, T.D., Hangseok, C., and McCone, S. (2005). "Drained shear strength parameters for analysis of landslides." Journal of Geotechnical and Geoenviromental Engineering, 131(5), 575-588.

Terzaghi, K. (1936). "The shearing resistance of saturated soils and the angle between the planes of shear." International Conference on Soil Mechanics and Foundations Engineering. Harvard University Press: Cambridge, MA, 54-56.

Tinjum, J.M., Benson, C.H., and Blotz, L.R. (1997) "Soil water characteristic curves for compacted clays." *J. Geotech. Geoenviron. Eng.,* 123(11), 1060-1069

Vanapalli, S.K., Fredlund, D.G., and Pufahl, D.E., (1999). "The influence of soil structure and stress history on the soil-water characteristics of a compacted till." Journal of Geptechnique, 49(2), 143-159.

Van Genuchten, M.T. (1980). "A closed-form equation for predicting the hydraulic conductivity of unsaturated soils." J. Soil Science, 44, 892-898.

Vanapalli, S.K., Fredlund, D.G., Pufahl, D.E. and Clifton, A.W. (1996). Model for the prediction of shear strength with respect to soil suction. Canadian Geotechnical Journal, 33(3), 379- 392.

Vanapalli, S. K., Fredlund, D G., and Pufahl, D. E. (1999). "The influence of soil structure and stress history on the soil-water characteristics of a compacted till." *Geotechnique,* 49(2), 143-159.

Vaunat, J., Amador, C., Romero, E., and Djeren-Maigre, I. (2006). "Residual strength of a low plasticity clay at high suctions." Proceedings of the Fourth International Conference of Unsaturated Soils, 1, 1279-1289.

Vaunat, J., Merchan, V., Romero, E., and Pineda, J. (2007). "Residual strength of clays at high suctions." Proceedings of the 2nd International Conference on Mechanics of Unsaturated Soils, Weimar, Germany, 2, 151–162.

Venkatarama, R.B., and Jagadish, K.S. (1993). The static compaction of soils. Géotechnique, 43(2): 337-341.

Vilar, O. M. (2006). "A simplified procedure to estimate the shear strength envelope of unsaturated soils." *Can. Geotech. J.*, 43, 1088–1095.

Zhan, T.L.T., Ng, C.W.W. (2004). "Analytical analysis of rainfall infiltration mechanism in unsaturated soils." Intrnational Journal of Geomechanics, 4(4), 273-284.

Zhan, T. L. T., Ng. C. W. W., and Fredlund, D. G. (2007). " Field study of rainfall infiltration into a grassed unsaturated expansive soil slope." *Can. Geotech. J.*, 44, 392-408.

Zhan, L. T., and Ng, C. W. W. (2006). "Shear strength characteristics of an unsaturated expansive clay." *Can. Geotech. J.*, 43, 751–763.

Zornberg, J.G., Kuhn, J., and Wright, S., (2007) "Determination of Field Suction Values, Hydraulic Properties and Shear Strength in High PI Clays" *Research Rep. 0-5202-1*, Center for Transportation Research, Univ. of Texas at Austin.

Zur, B. (1966). "Osmotic control of the matric soil-water potential." *Soil Sci.*, 102, 394–398.

BIOGRAPHICAL INFORMATION

Jubair Hossain graduated in Civil Engineering, Bangladesh University of Engineering and Technology, Dhaka, Bangladesh with a Bachelors degree in 2007 and later on started his graduate studies at The University of Texas at Arlington in 2008. He received his Master's degree in civil engineering with emphasis on goetechnical engineering in August 2009. In 2009, he was admitted to the doctoral program in the Civil Engineering Department at the University of Texas at Arlington. During his graduate program, he had an opportunity to work as a graduate research assistant and graduate teaching assistant under Dr. Sahadat Hossain in civil engineering department. He was awarded "University Scholar" in 2011 and also received NSF CMMI research and innovation student participation grant in 2011. He also received Dean Doctoral Fellowship from 2009 to 2012 during his study as a doctoral student. The author's main research interest includes Slope stability analyses and remedial measure, Site Investigation using Geophysical Method, Unsaturated Soil, Field Instrumentation, Non-destructive Testing, Numerical Modeling using PLAXIS and Geographic Information System (GIS).